الجـــــــــــــــــــــــمهوريــــة الجــــــــــــــزائرية الديمـــــقراطيـة الشــــــــــعبيـة

DEMOCRATIC AND POPULAR ALGERIAN REPUBLIC

وزارة التـــــــــــــــــــــــــــــعليــم العـــــالي و البـــــــحث العــلـمـــي

Ministry of Higher Education and Scientific Research

جـــــــــــامعة أبي بكــر بـلـقـايـد – تــلمســـــــــــان –

Aboubakr Belkaïd Universiy – Tlemcen –
Faculty of TECHNOLOGY

THESIS

Presented for obtaining the **3rd Cycle DOCTORATE degree**

In : Biomedical Engineering

Specialty: Medical Imaging

By: **Belmokeddem Mohamed**

Subject

Analysis of surgical artifacts of laparoscopic images as part of the 3D modeling of an automated optic cleaning device

Publicly supported, on 15 / 05 /2025, before the jury composed of :

Mr Hadj Slimane Zine-Eddine	Professor	Univ. Tlemcen, Faculty of Technology	President
M KHEMIS Kamila	MCA	Univ. Tlemcen, Faculty of Technology	Thesis director
Mr OMARI Tahar	MCA	Univ. Ain Temouchent, Faculty of Technology	Examinateur 1
Mr BENGANA Abdelfatih	MCA	Univ. Tlemcen, Faculty de Technology	Examinateur 2
Mr LOUDJEDI Salim	Professor	Univ. Tlemcen, Faculty of Medicine	Invited

Abstract

During minimally invasive surgery, the laparoscope lens is often contaminated by surgical artifacts such as blood, smoke, and fog. This project aims to develop a software solution for automatically detecting these artifacts to trigger the cleaning of the laparoscope's optical surface and propose a hardware solution for optimal cleaning.

Concerning the software, two artificial intelligence-based models are developed: a machine-learning method using a cascaded support vector machine and a deep learning model with ResNet-50. The Laparoscopic Video Quality database is used for training, testing, and validating the results. The deep-learning approach demonstrates superior accuracy, achieving detection rates of 97.5% for defocus blur, 97.5% for motion blur, and 85% for smoke. However, the machine-learning approach excels in inference speed, reaching 37 frame by second (FPS), making it better suited for real-time applications on low-cost systems.

For the hardware component, we used Computer-Aided Design (CAD) to develop a 3D model of the laparoscopic lens-cleaning device; featuring four nozzles arranged in two pairs positioned 120 degrees apart around the lens. Each pair includes two side-by-side nozzles, one for a physiological saline-based cleaning liquid and the other for a CO_2-based drying gas. A 2D cleaning simulation confirms the efficiency of the proposed prototype.

Keywords: Minimally invasive surgery; Surgical artifacts; Artificial intelligence; Machine learning; Deep learning; Lens contamination; Lens cleaning system; Computer-Aided Design, 3D modeling.

Résumé

En chirurgie mini-invasive, la lentille du laparoscope est souvent contaminée par les artéfacts chirurgicaux tel que le sang, la fumée et la buée. Ce projet vise à développer une solution logicielle pour la détection automatique de ces artéfacts, pour déclencher un mécanisme de nettoyage de la surface optique du laparoscope et propose une solution matérielle pour un nettoyage optimal.

Concernant le logiciel, deux modèles basés sur l'intelligence artificielle sont développés : une méthode d'apprentissage automatique utilisant une machine à vecteurs de support en cascade et un modèle d'apprentissage profond avec ResNet-50. La base de données «Laparoscopic Video Quality » est utilisée pour l'entraînement, les tests et la validation des résultats.

La méthode d'apprentissage profond démontre une précision supérieure, atteignant des taux de détection de 97,5 % pour le flou de défocalisation, de 97,5 % pour le flou de mouvement et de 85 % pour la fumée. Cependant, l'approche d'apprentissage automatique est plus performante en termes de vitesse d'inférence, atteignant 37 image par second (IPS), ce qui la rend mieux adaptée aux applications en temps réel sur des systèmes à faible coût.

Pour le composant matériel, nous avons utilisé la conception assistée par ordinateur (CAO) pour développer un modèle 3D du dispositif de nettoyage laparoscopique des lentilles. Ce modèle comprend quatre buses disposées en deux paires, espacées de 120 degrés autour de la lentille. Chaque paire comprend deux buses côte à côte, l'une pour un liquide de nettoyage à base de sérum physiologique, l'autre pour un gaz de séchage à base de CO_2. Une simulation de nettoyage 2D confirme l'efficacité du prototype proposé.

Mots-clés : Chirurgie mini-invasive ; Artefacts chirurgicaux ; Intelligence artificielle ; Apprentissage automatique ; Apprentissage profond ; Contamination des lentilles ; Système de nettoyage des lentilles ; Conception assistée par ordinateur, Modélisation 3D.

الملخص

في الجراحة طفيفة التوغل (MIS) تتعرض عدسة المنظار للتلوث بشكل متكرر وهو ما يُعرف بـ "تشوه الصور الطبية أثناء العمليات الجراحية" بسبب الدم، والدخان، والضباب.

يهدف هذا المشروع إلى تطوير برنامج للكشف التلقائي عن تشوه الصور الطبية أثناء العمليات الجراحية، مما يؤدي إلى تفعيل جهاز تنظيف عدسة المنظار حيث تم اقتراح نموذج له من اجل تنظيف مثالي.

فيما يتعلق بالبرمجيات، تم تطوير نموذجين يعتمدان على الذكاء الاصطناعي: طريقة للتعلم الآلي تعتمد على خوارزمية التصنيف (SVM) بالتتالي وطريقة التعلم العميق بالاعتماد على (ResNet-50) حيث تم استخدام قاعدة بيانات (Laparoscopic Video Quality) للتدريب والاختبار والتحقق من صحة النتائج.

أظهرت طريقة التعلم العميق دقة عالية، حيث حققت معدلات كشف بلغت 97.5% عن ضباب الصورة الناتج عن عدم مطابقة مصدر الضوء للمركز البؤري للصورة، و97.5% لضباب الحركة، و85% للدخان. ومع ذلك فإن طريقة التعلم الآلي تميزت بسرعة الكشف، حيث وصلت إلى 37 صورة في الثانية(FPS) ، مما يجعلها أكثر ملاءمة للتطبيقات التي تعتمد على الوقت الحقيقي والأنظمة ذات التكلفة المنخفضة.

بالنسبة لالة التنظيف، استخدمنا التصميم بمساعدة الحاسوب (CAD) لتطوير نموذج ثلاثي الأبعاد لجهاز تنظيف العدسات بالمنظار؛ يتميز بأربع فوهات مرتبة في زوجين، كل منهما بزاوية 120 درجة حول العدسة. يحتوي كل زوج على فوهتين متجاورتين، إحداهما لسائل تنظيف فسيولوجي قائم على محلول ملحي، والأخرى لغاز تجفيف قائم على ثاني أكسيد الكربون. تؤكد محاكاة التنظيف ثنائية الأبعاد كفاءة النموذج المقترح.

الكلمات المفتاحية: الجراحة قليلة التدخل؛ تشوه الصور الطبية أثناء العمليات الجراحية؛ الذكاء الاصطناعي؛ التعلم الآلي؛ التعلم العميق؛ تلوث العدسات؛ نظام تنظيف العدسات؛ التصميم بمساعدة الكمبيوتر؛ النمذجة ثلاثية الأبعاد.

General introduction

Laparoscopy, derived from the Greek term that means "looking at the wall," is a medical procedure that involves visualizing the inside of the abdominal cavity, uterus, ovaries, and fallopian tubes. It is known as minimum invasive surgery, referring to "looking at the stomach." This technique employs an endoscope, a flexible device with optical components, a light source, and a camera. Additionally, the endoscope can be equipped with surgical instruments, allowing for simultaneous surgery and examination.

The surgical team views the operative field on a screen using a combination of high-quality optics inserted through the abdominal wall and a camera connected to a light source. To create a working space known as pneumoperitoneum, laparoscopy involves introducing gas into the peritoneal cavity. The procedures utilize specialized instruments, also inserted through the abdominal wall using trocars, which typically range in size from 5 to 12 mm in diameter (figure 1) [1].

However, the clarity of the laparoscopic view can be compromised by factors like fogging, temperature fluctuations, and liquid buildup on the optics, causing the image to become blurred. The conventional solution to this problem involves the surgeon removing the camera, cleaning it repeatedly with a solution, and reinserting it into the abdominal cavity. This process not only increases the risk of infection but also extends the duration of the surgery.

To address this issue, we aim to develop an automated module that detects the parameters causing image blurring and controls a flow of cleaning liquid, effectively making the lens of the laparoscopy to become self-cleaning. This system could significantly reduce the need for manual camera cleaning during surgery, enhancing both safety and efficiency.

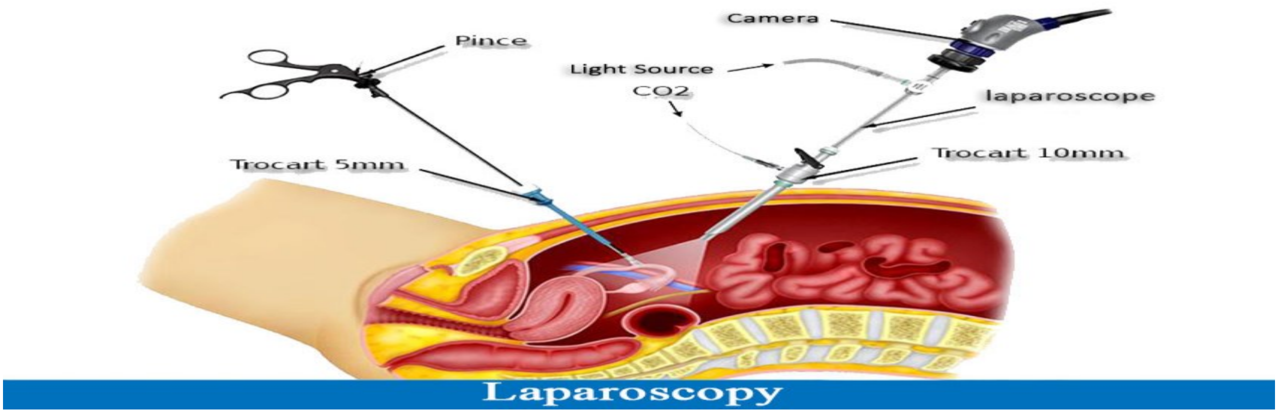

Figure 1. Schematization of laparoscopy [2]

The thesis is structured into several chapters, each addressing a specific aspect of the research:

- **Chapter 1**: Provides a definition and overview of laparoscopy, introducing the foundational concepts.
- **Chapter 2**: This chapter offers a literature review focused on patents related to in-situ cleaning of laparoscopic lenses. It details the state-of-the-art solutions proposed to address lens contamination during laparoscopic procedures.
- **Chapter 3**: Introduces the machine learning-based method developed to classify distortions caused by laparoscopic lens contamination.
- **Chapter 4**: Presents the development of a new framework based on a deep learning approach for classifying five types of distortions in laparoscopic videos: noise, defocus blur, motion blur, smoke, and uneven illumination.
- **Chapter 5**: Proposes a new prototype for an in vivo lens-cleaning device designed to address the identified challenges.
- **Chapter 6**: Concludes the thesis by summarizing the findings and offering perspectives for future research and improvements.

List of Publications

The research work presented in this thesis has led to the publication and submission of several papers in international journals and conferences, as outlined below:

Journal papers:

1)- **Mohamed, Belmokeddem**, Khemis Kamila, and Loudjedi Salim. " Automatic detection of laparoscopic videos distortion using machine learning classification." Frontiers Biomed Technol. 2025;12(2).

Conference papers:

1)- **Mohamed, Belmokeddem**, Khemis Kamila, and Loudjedi Salim. "Transfer learning and Machine Learning Classification for Laparoscopic Video Distortion Detection." 8th International Conference on Image and Signal Processing and their Applications (ISPA), Biskra, Avril 2024, IEEE, pp. 1-5.

2)- **Mohamed, Belmokeddem**, Khemis Kamila, and Loudjedi Salim. "Enhanced Classification of Laparoscopic Video Distortions with ResNet-18 Architecture." Innovations in Intelligent Systems and Applications Conference (ASYU), Ankara, October 2024, IEEE, pp. 1-6.

3)- **Mohamed, Belmokeddem**, Khemis Kamila, and Loudjedi Salim. “A review of patents for achieving laparoscopic len cleaning during minimally invasive surgery.” In Proceedings of the 1st International Online Conference on Bioengineering, Basel, October 2024, MDPI.

4)- **Mohamed, Belmokeddem**, Khemis Kamila, and Loudjedi Salim. “Automatic Laparoscopic Lens Contamination Detection Based on ResNet18 and Corresponding Cleaning Device Prototype.”

In Proceedings of the 1st International Online Conference on Bioengineering, Basel, October 2024, MDPI.

5)- **Mohamed, Belmokeddem**, Khemis Kamila, and Loudjedi Salim. "Automatic Laparoscopic Lens Contamination Detection using ResNet18 coupled with an innovative cleaning device prototype." 10th Journée doctoral de génie biologique et medical JD-GBM'2024, Tlemcen, November 2024, pp. 1-4.

6)- **Mohamed, Belmokeddem**, Khemis Kamila, and Loudjedi Salim. "Residual network (ResNet-18) for laparoscopic distortion classification." 1st National Conference on Artificial Intelligence and its Applications, Tlemcen, December 2023, No. 11575. EasyChair, pp. 1-4.

7)- **Mohamed, Belmokeddem**, Khemis Kamila, and Loudjedi Salim. "A Robust Approach for Classifying Laparoscopic Video Distortions using ResNet-50." Sixth IEEE International Conference on Image Processing Applications and Systems (IPAS 6), Lyon, January 2025, IEEE, pp. 1-6.

The key contributions of this research is summarized as follows:

- **Systematic Review:** Conducted a systematic review following the Preferred Reporting Items for Systematic Reviews and Meta-Analyses (PRISMA) guidelines to address the question: "What is the most effective category of patents for in-situ cleaning of laparoscopic lenses to achieve a successful patent?" This involved a comprehensive literature search using the ESPACENET electronic database.
- **Cascaded SVM Framework:** Developed a novel framework utilizing a cascaded support vector machine (SVM) classifier consisting of three sequentially interconnected SVMs. The objective of this machine learning-based approach is the automatic detection of distortions in laparoscopic videos.
- **Deep Learning-Based Detection:** Employed a deep learning method using Residual Networks (ResNet50) to detect and classify five distortion categories in laparoscopic videos: noise, defocus blur, motion blur, smoke, and uneven illumination. The computational framework was trained on the LVQ Challenge dataset.
- **Prototype for In vivo Lens-Cleaning Device:** Proposed a new prototype for an in vivo lens-cleaning device that operates in real-time. This integrated system is designed to detect distortions in live laparoscopic videos and automatically initiate the lens-cleaning process.

Contents

List of Tables

List of Figures

Chap1: Context and motivation

1. Introduction

Laparoscopy is a minimally invasive surgical procedure that differs from traditional surgery by utilizing small incisions to insert trocars and various surgical instruments, including an endoscope. This procedure is performed in a hospital or clinic setting under general anesthesia [1].

The main goal of laparoscopy is to inspect the internal organs within the abdomen, which are otherwise invisible to the naked eye. This method aids in accurate diagnosis and can also be used to perform surgery on a pre-existing condition, such as ectopic pregnancy, ovarian cysts, certain types of intestinal blockages, and appendicitis [1].

Laparoscopy allows intervention in all organs of the abdominal cavity:

- In visceral surgery: gallbladder, appendix, stomach, liver, spleen, small intestine, colon;
- In gynecology: uterus, ovaries, tubes;
- In urology: bladder, kidney, prostate, ureter [3].

This chapter highlights the benefits of laparoscopy, discusses the instruments involved, and examines the challenges associated with this specialized surgical technique.

2. The advantages of laparoscopy

- Minimally invasive surgical procedure
- Reduction in postoperative morbidity
- Aesthetic benefit
- Enhanced visualization of the surgical site
- Increased surgical precision and efficiency

3. Laparoscopy instrument trolley

Typically, most instrument trolleys consist of:

- The insufflator stack
- The light source
- The camera
- The screen positioned at the top of the tower (Fig. 2)
- Occasionally, a washing-suction system is included.

The patient is linked to the cart via the CO2 cable, the light cable, the camera cable, and sometimes a washing cable and a suction cable.

1. Monitor
2. Electronic insufflator
3. Light source
4. Electronic hydraulic pump
5. Digital Video Recorder
6. Screen for photo management
7. Carbon dioxide bottle
8. Generator for electrosurgery.

Figure 2. Laparoscopy instrument trolley [4]

4. The aspiration and washing or irrigation system

It facilitates the injection and removal of fluids into the pneumoperitoneum at the dissection site. This aids in cleaning the area, improving visibility for the surgeon, safeguarding tissues, ensuring hemostasis, and reducing the risk of adhesions. Typically, the device operates with an injection pressure of about 1 bar and a suction pressure of approximately -0.6 bar [4].

5. Vision system

The quality of the image obtained relies solely on the amount of light available at each stage of the optical and electronic chain. This chain can be categorized into three main sectors (Fig. 3):

- Light production: handled by the light source.
- Image acquisition: managed by the camera.
- Light transmission: facilitated by the endoscope and cable.

5.1. Light source

The main types are halogen and xenon. They vary in color temperature, with halogen emitting yellow-white light, whereas xenon leans slightly towards blue in color rendering. This light source is referred to as "cold" because it generates light while minimizing heat production, thus reducing the risk of tissue burns.

5.2. Video camera

The camera is characterized by the following specifications:

Sensor Type: Modern cameras use charge-coupled device (CCD) sensors. These sensors are electronic systems that convert the captured image into an electronic signal, to display them on a screen.

Sensitivity, measured in lux: The sensitivity of a camera is inversely related to the number of lux it requires. In simpler terms, the lower the lux rating, the less light the camera needs to produce a clear image [4].

Camera Resolution: Is measured in pixels—the higher the number of pixels, the sharper the image quality. Cameras can have different types of image sensors: a "tri-CCD" camera uses three separate sensors to capture red, green, and blue colors independently, leading to more accurate color reproduction, while a "mono-CCD" camera captures all three colors on a single sensor [3].

Signal-to-Noise Ratio: The quality of the video signal produced by a camera can be affected by "noise," which tends to be more prominent in darker areas or where there's a lot of red, such as in laparoscopy. The signal-to-noise ratio is measured in decibels (dB) [4].

Lens/Optics: Most cameras are equipped with panoramic optics, offering a wide field of view with straight and axial vision. An endoscope, often used in medical applications, consists of a metal tube that ranges from 5 to 10 millimeters in diameter and 15 to 30 centimeters in length. It uses fiber optics to illuminate the interior of a cavity and a set of lenses to transmit the image back. As with any optical system, light attenuation is a factor, and it is inversely proportional to the square of the lens diameter—meaning that smaller diameter lenses require more light to produce a clear image [4]. Optics are categorized into two main types: **direct vision at 0 degrees** and **adjustable aiming direction**. The direction of vision is determined by the angle formed between the central beam and the optical system's axis. Surgeons can adjust this parameter based on the specific requirements of a surgical procedure.

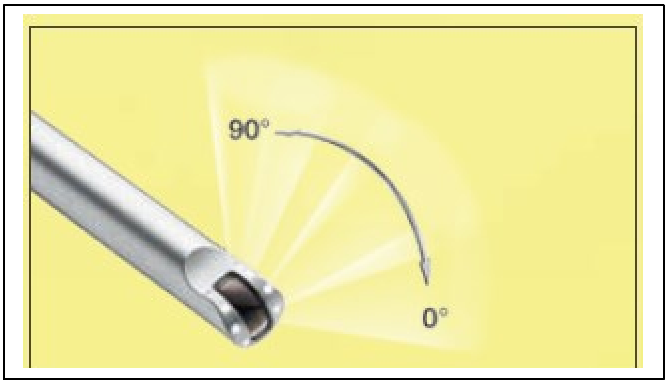

Figure 3. Aiming direction adjustable from 0° to 90° (HOPKINS KARL STORS) [5]

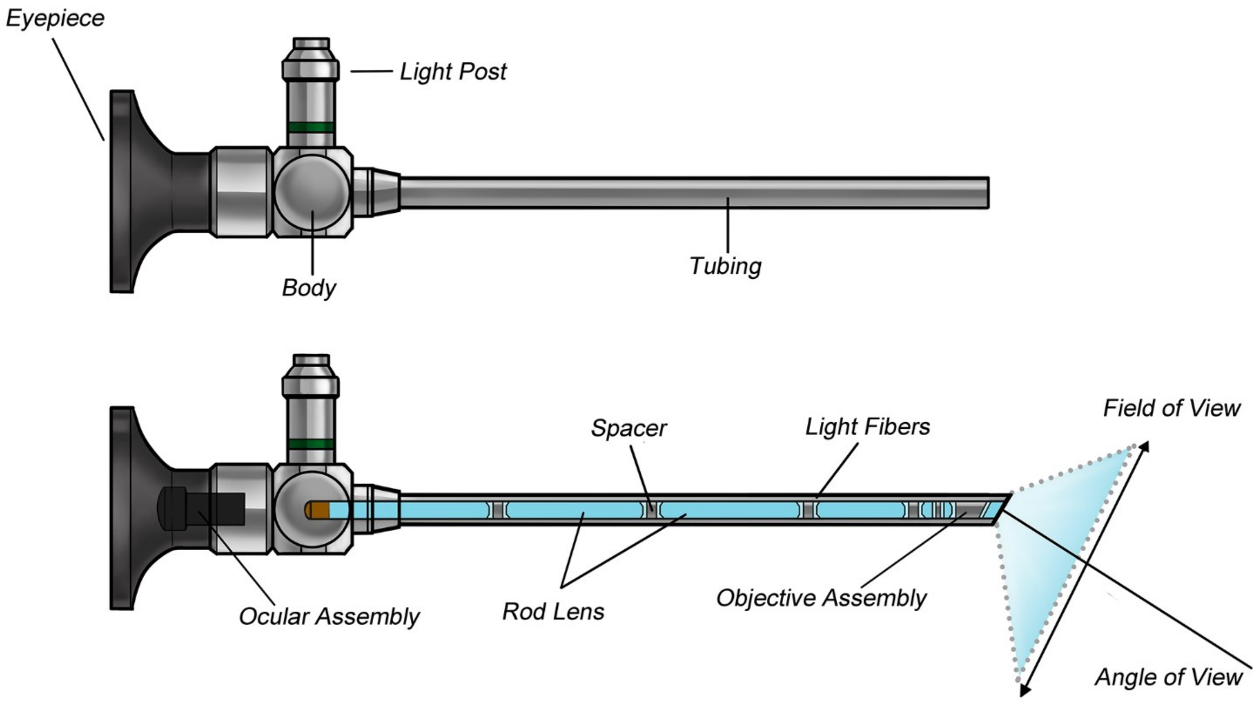

Figure 4. Parts of a rigid laparoscope [6]

5.3. Monitor

The monitor plays a crucial role in the imaging chain. It's essential to have a monitor that can accurately reproduce the resolution provided by the camera which means that the monitor's horizontal line count must be at least as high as the camera's output [4].

6. Laparoscopy constraints

Laparoscopic surgery is subject to various constraints that can affect the safety and efficiency of the procedure. These constraints include [7]:

6.1. Pressure Constraints

Laparoscopy involves the introduction of gas (usually carbon dioxide) into the abdominal cavity to create space. This positive pressure serves multiple purposes, such as separating internal structures, providing a clear view, and controlling bleeding. However, excessive pressure can lead to complications like increased cardiovascular stress.

6.2. Vision Constraints

Although laparoscopy offers the advantage of magnification and a direct view of the surgical site, it also has limitations in peripheral vision and risks related to visual obstructions and unnoticed burns. Two main risks associated with limited vision are:

- If instruments are not properly monitored, they can be accidentally left behind in the abdominal cavity.

- Electrical burns may happen if an instrument's insulation is compromised or if it makes unintended contact with another conductive object without being noticed.

6.3. Manipulation Constraints (Trocars)

Trocars are utilized to create entry points for laparoscopic instruments. The fixed point established by the trocar can restrict motion range and require additional force when manipulating tissues. Therefore, it is crucial to control angles and manage pressure.

6.4. Constraints on Camera Optics Cleaning:

During laparoscopic surgery, the camera lens may become obscured by bodily fluids or fogging, reducing visibility. To clean the lens, the camera needs to be taken out, cleaned, and then reinserted. This process not only extends the duration of the surgery but also increases the patient's risk due to longer exposure to anesthesia.

Strategies to address optic cleaning constraints include:

- Using defogging solutions to reduce condensation on the lens.

- Implementing protocols for frequent lens cleaning to maintain optimal vision.

- Investing in camera systems with anti-fogging technology or lens-cleaning mechanisms.

7. Techniques for Cleaning Camera Optics in Laparoscopic Systems

During endoscopic surgical procedures, surgeons spend about 3% of their time cleaning the camera optics to maintain a clear view, as the lens often becomes contaminated by bodily fluids like blood, bone dust, or smoke from surgical cauterization [8]. This equates to roughly six cleaning instances per hour [9]. Schoofs and Gossot [10] noted that 68% of surgeons find endoscope lens contamination during thoracoscopic surgery particularly disruptive.

Two primary methods are commonly employed to clean the endoscope lens during surgery:

7.1. Manual Cleaning

This technique involves either rubbing the lens against a soft tissue structure or, more commonly, removing the endoscope entirely from the abdominal cavity to clean it with gauze or a clean cloth dampened with a defogging solution or distilled water. Before reinserting the endoscope, the lens is typically dried with dry gauze to prevent further fogging. However, condensation can occur upon reinsertion due to temperature differences between the patient's body and the operating room environment, requiring repeated cleaning during the procedure[11, 12].

Figure 5. Manual cleaning of the laparoscope[13]

7.2. Irrigation Method

This approach uses an irrigation (suction) channel to flow a washing liquid, typically saline or distilled water, across the distal lens of the endoscope to remove contaminants. Specialized systems like CLEARVISION II from KARL STORZ and InstaClear from OLYMPUS are designed for this purpose. The irrigation method also utilizes a pump to create negative pressure, effectively extracting any residual fluid after irrigation, and helping to maintain a clear view during surgery.

Figure 6. CLEARVISION II irrigation cleaning [14]

Figure 7. InstaClear irrigation cleaning [15]

This cleaning method often doesn't achieve satisfactory results for lens clarity [16]. Additionally, irrigation can lead to unwanted fluid accumulation at the surgical site, which can obscure the field of view and disrupt the surgical process. Another common issue is the formation of bubbles or fluid droplets on the endoscope lens after irrigation, which further hampers visibility [17].

8. Conclusion

In this chapter, we presented the benefits of laparoscopy, explored the instruments used, examined the components of the vision system, discussed the various constraints of laparoscopic procedures, and reviewed different techniques for cleaning camera optics in laparoscopic systems with the associated challenges.

In laparoscopic surgery, keeping the operative field clearly visible is essential for precision and patient safety. However, endoscope lens frequently get covered with blood, tissue fragments, and other debris, which compromises visibility during surgery. Although manual wiping and lens irrigation systems are often employed to address this issue, they do not always provide consistent or effective results.

Therefore, in the following chapter, a comprehensive literature review is conducted to identify solutions that can be integrated into endoscopic instruments, aiming to keep the lens surface clean and ensure clear vision for the surgeon. This approach seeks to enhance visual acuity during surgery, reducing the risk of errors and improving overall surgical outcomes.

Chap2: A Patent Review on Laparoscopic Lens Cleaning Solutions for Minimally Invasive Surgery (State-of-the-Art)

Abstract

Objective: During minimally invasive surgery, laparoscopic lenses often become contaminated by condensation, smoke, blood, and debris, impairing the surgeon's visibility and complicating the procedure. This systematic review evaluates patents addressing this challenge, focusing on innovative approaches for effective laparoscopic lens cleaning to ensure optimal visualization.

Materials and Methods: A structured methodology was implemented to identify, analyze, and classify patents related to laparoscopic lens cleaning technologies. Patent searches were conducted using the ESPACENET database, with additional descriptions and statuses retrieved from Google Patents and the United States Patent and Trademark Office (USPTO). Each patent was scored based on its status using a 3-point Likert scale: 2 points for granted, 1 point for pending, and 0 points for abandoned. Patents were grouped then into categories based on their cleaning mechanisms.

Results: A total of 61 patents were thoroughly reviewed and categorized into two primary cleaning mechanisms: mechanical interactions and chemical interactions. Further sub-classifications were made, including collision methods and brush/wipe-based methods. Scores were aggregated to facilitate comparative analysis. Among granted patents, 48% employed collision-based cleaning techniques, indicating their higher viability and effectiveness. Conversely, 56% of abandoned patents relied on brush/wipe-based methods, highlighting potential limitations or challenges associated with these approaches.

Conclusion: The findings underscore that the collision methods outperform other techniques in developing successful laparoscopic lens cleaning solutions. The review recommends that future patents prioritize integrating collision cleaning mechanisms with lens surfaces engineered for hydrophilic or hydrophobic properties to enhance performance and durability. This combined approach can set a new standard for effective laparoscopic lens cleaning in minimally invasive surgical procedures.

1. Introduction

Minimally invasive surgery (MIS) has become increasingly popular due to its numerous advantages over open surgery, including easy recovery for the patient, reduced cost and hospital stay, minimal surgical incisions, and a lower risk of surgical site infections. During MIS, the laparoscopy camera system is inserted with a standard trocar into the patient's abdominal cavity, and the video signal is processed in real time and projected onto an external monitor [18]. However, the laparoscopic lens is often contaminated during surgery by body fluids, smoke generated by electrosurgical devices, and condensation due to the temperature difference between the body cavity and the operation room.

Cleaning the lens requires halting the surgical procedure, removing the laparoscope from the abdomen, and wiping it with gauze or a clean cloth. This process is repeated multiple times throughout the procedure. Cassera et al. reported that this cleaning procedure consumes 3% of operative time [8], and such interruptions can lead to disruptions, distractions, and errors in judgment [19, 20].

The growing need to clean laparoscopic lenses has sparked considerable interest in exploring alternative cleaning methods within the patient's body. We have found three recent review articles discussing different laparoscopic lens cleaning techniques in the literature. In the initial study, Kreeft et al. [17] classified lens cleaning methods into two categories: mechanical and chemical. The mechanical category relies on physical forces, while the chemical category utilizes forces generated by chemical reactions. Both categories are further subdivided into removal and prevention techniques. Mechanical removal methods include Brush/Wipe, Centripetal Force, Collision, Suction, and Vibration, while mechanical prevention methods include lens film protection. Chemical removal methods encompass Dissolution, Evaporation/Sublimation, Photo (catalytic) Degradation, and Surface Tension, while chemical prevention methods involve Hydrophilicity/Lipophilicity, Hydrophobicity/Lipophobicity, Amphiphilicity, and Adhesion Resistance.

In the second review, Nabeel et al. [21] scrutinized ten evaluative studies on diverse lens cleaning techniques, encompassing the use of dry CO2 gas [22], Povidone-iodine surgical scrub solution [23], warm fluid or surfactant application [24-26], warm saline or chlorhexidine solution application [25-27], sterile water use [28], wiper application [8, 28, 29], and air and water flow utilization [30].

In the third review, Kumar et al. [31] assessed different methods for defogging laparoscopic lenses and identified four categories. The first category involves the application of antifogging solutions [32]. The second category comprises methods based on warming the laparoscopic lens surface, utilizing warm saline solution, a water bath [33], warmed gas, a thermo flask [12], or light energy [34]. The third category consists of electrical methods that convert electrical energy into heat to warm the lens tip; indium tin oxide (ITO) was used to coat the lens to make it electrically conductive [35]. The fourth category encompasses miscellaneous methods, such as using a flow of CO2 [22] and an antifogging solution mixed with humidified CO2 [36]. An additional approach for defogging laparoscopic lens involved the application of superhydrophobic coatings, which was explored. A range of organic, inorganic, and hybrid materials underwent investigation for the production of superhydrophobic glass.

In this chapter, we aim to identify, categorize, and explore laparoscopic lens cleaning patents during surgical procedures and determine the final status of each patent (granted, pending, or abandoned). Ultimately, we will compare lens-cleaning methods based on patent status, utilizing the categorization suggested by Kreeft et al., to guide future inventors to focus on a promising category of laparoscopic lens cleaning and develop efficient and universal devices.

2. Search strategy

We have conducted a systematic review following the Preferred Reporting Items for Systematic Reviews and Meta-Analyses (PRISMA) guidelines to address the research question: What is the best category of patents for in-situ cleaning of laparoscopic lens to realize a successful patent?

We commenced by investigating the patents referenced in the review by Kreeft et al. for each method category outlined in Figure 8. Utilizing Google Patents and USPTO, we determined the final status of each patent, reviewing a total of 31 patents. In June 2022, we conducted a literature search for patents pertinent to our research question, employing the ESPACENET electronic database. Table 1 outlines the key terms and relevant syntax utilized for the database search.

Afterward, we conducted a secondary selection manually, categorizing the patents into their respective groups based on the abstract descriptions of each patent. Full-text patent descriptions and statuses were obtained using Google Patents and USPTO.

g

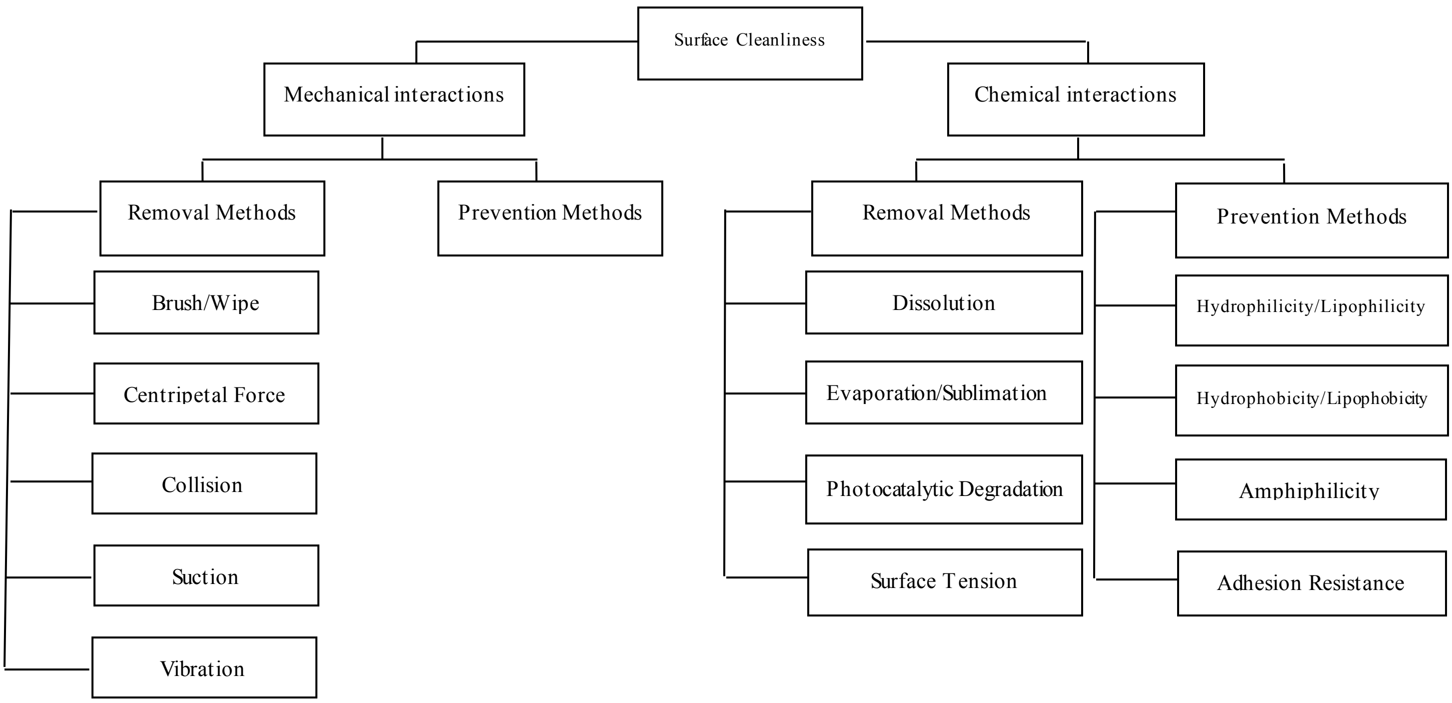

Figure 8. Schematic showing the Kreeft et al. optical surface cleanliness methods categorization[17].

Table 1. Search strategy

Electronic database	ESPACENET
Initial search terms/syntax	(endoscop* OR laparoscop*) AND ((eye* OR lens*) OR (glass* OR vision*)) AND (clean* OR wash* OR foul* OR rins* OR clear* OR defog*)
Filter terms of the first results	clean*, to filter the first results by searching title and abstract, in the under-classes A61B1/0008, A61B1/00121and A61B2017/00296
Publication date	01/12/ 2015-16/6/2022

2.1. The inclusion criteria

We included patents published in English language after 01/12/2015 (the date of Kreeft et al. research), in-situ lens cleaning patents.

2.2. The exclusion criteria

We excluded: patents published before December 2015, duplicate patents, external lens cleaning patents, non- English full text (Table 2).

2.3. Patents potential application score

Table 2. Inclusion and exclusion criteria

Inclusion criteria	Exclusion criteria
Date of publication between 01/12/ 2015 and 16/6/2022	Before December 2015
English full-text	Non-English full-text
Minimally invasive surgery	Open surgery
Under patient cavity lens cleaning patents	External lens cleaning patents

We attributed a score to each patent status using a 3-point Likert scale: (0) point for abandoned, (1) point for pending, and (2) points for application granted. We calculated the scores for each category of patents.

3. Results

3.1. Search results

After querying ESPACENET, we obtained 84 patents. After eliminating five duplicates, we found one additional patent through manual search, adding to the 31 patents identified in the Kreeft et al. review, totaling 111 patents. Subsequently, we screened the titles and abstracts of these patents, applying inclusion and exclusion criteria, resulting in the exclusion of 40 patents. We then conducted a full-text review of the remaining 71 patents, excluding ten (10) due to non-English text.

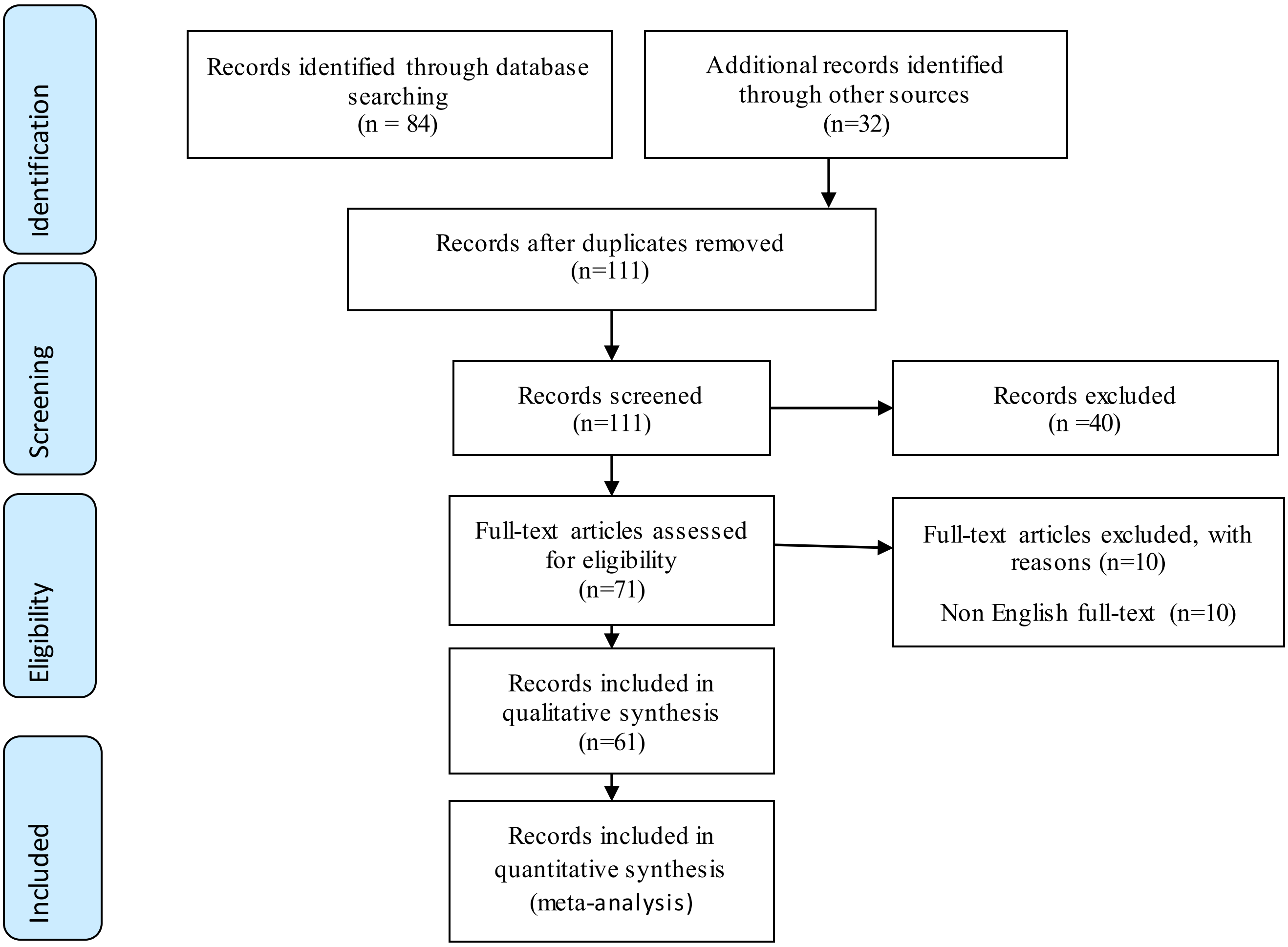

Figure 9. PRISMA (Preferred Reporting Items for Systematic Meta-Analyses) flow diagram of included and excluded patents of Endoscopic/laparoscopic lens in situ cleaning.

3.2. Results presentation

Table 3 and Table 6 describe the (31) patents found in the Kreeft et al review and classified into the categories of Figure 8. The (01) patent found in the manual search was added to the (29) patents found in our search, resulting in a total of (30) patents described in Table 7 and classified into either the mechanical interactions category (Table 4) or the chemical interactions category (Table 5).

Table 3. Lens-cleaning patents cited in Kreeft et al.

Category	Type	Methods	Patent number	Year	Status
Mechanical Interactions	Removal Methods	Brush/Wipe	US5514084A	1996	Abandoned
			US20090105543 A1	2008	Abandoned
			WO2014145063 A1	2014	**Application granted**
			US2009/0240111A1	2009	Abandoned
			AU2011236022	2011	Abandoned
			US8460180B1	2013	**Application granted**
			US5274874A	1994	**Application granted**
			US20140215736A1	2014	Abandoned
			US20140246051	2013	Abandoned
			US20130150670A1	2013	Abandoned
			US20090250081	2009	**Application granted**
		Centripetal Force	US6258025B1	2001	**Application granted**
		Collision	EP0664101	1994	Abandoned
			US6447446B1	2002	**Application granted**
			US20060293559A1	2005	Abandoned
			US6354992B1	1999	**Application granted**
			US20150005582A1	2015	**Application granted**
			US8047215B1	2008	**Application granted**
			US20070225566A1	2007	Abandoned
			US20080188715A1	2007	**Application granted**
			US20130204088A1	2013	Abandoned
			US20040220452A1	2001	**Application granted**
			GB2481727A	2009	**Application granted**
			US6409657B1	2002	**Application granted**
			US20130217970A1	2012	**Application granted**
			US5337730A	1994	**Application granted**
		Suction	US8133052B1	2012	**Application granted**
		Vibration	US20080188714A1	2008	Abandoned
			WO0053341A1	2000	**Application granted**
	Prevention Methods		US20120178995A1	2012	Abandoned
			US20150216401A1	2015	**Application granted**

Table 4. Mechanical interactions lens cleaning patents cited in our study

Category	Type	Methods	Patent number	Year	Status
Mechanical Interactions	Removal Methods	Brush/Wipe	US20220061646A1	2022	Pending
			US11058291B2	2021	**Application granted**
			WO2019226855A1	2019	**Application granted**
			US20220047354A1	2022	Pending
			US 20220039912A1	2022	Pending
			US 20210100444A1	2022	Pending
			US 20190231183A1	2019	Abandoned
			US 20180344141A1	2018	Abandoned
			US 20190110674A1	2019	Abandoned
			US11172813B2	2021	**Application granted**
			US10993609B1	2021	**Application granted**
			US2021033854A1	2021	Pending
		Centripetal Force	US10709321B2	2020	**Application granted**
		Collision	US20190110675A1	2019	Abandoned
			US11123152B2	2021	**Application granted**
			US20210219832A1	2021	Pending
			US20210177249A1	2021	Pending
			US11042020B2	2021	**Application granted**
			US 20220104696A1	2022	Pending
			WO2021219826A1	2021	Pending
			US 20200367736 A1	2020	Abandoned
			US 20220125288A1	2022	Pending
			WO2021179249A1	2021	**Application granted**
			WO2019227018A1	2019	**Application granted**
			US 20210228069A1	2021	Pending
			US 20200375444A1	2020	Pending
		Suction	/	/	/
		Vibration	US 20210369098A1	2021	Pending
		Hybrid (wipe+ collision)	US 10806337B2	2020	**Application granted**
	Prevention Methods		US 9241610B2	2016	**Application granted**

Table 5. Chemical interactions lens cleaning patents cited in our study

Category	Type	Methods	Patent number	Year	Status
Chemical interactions	Prevention Methods	Hydrophobicity/ Lipophobicity	US 20210315441A1	2021	Pending

Table 6. Description of patents cited in Kreeft et al review

Patent number	Brief description
US5514084A	Cannula having a retractable wipe at the distal end [37].
US20090105543 A1	Cannula with element expandable by passing fluid through, to contact the endoscope lens and clean it [38].
WO2014145063 A1	A shaft including a head having multiple prongs with cleaning cloths disposed between, deployed by an actuator [39].
US 2009/0240111A1	A hollow tube receive an endoscope and have a wiper near the lens manually disposed for cleaning [40].
AU2011236022	A wiper mechanism adjusted to contact and translate across a surface of the lens commanded by an actuator [41].
US8460180B1	Wiper assembly commanded by electromagnet to glide along the lens to clean it [42].
US5274874A	A sponge impregnated attached onto a trocar cannula, in contacted by the endoscope when is inserted [43].
US20140215736A1	A hollow tube receive an endoscope and have a multiple of cleaning elements disposed across, the lens is cleaned when it passes therethrough [44].
US20140246051	Cannula with scrubbing elements inside, condensation and debris are removed when the lens passed therethrough [45].
US20130150670A1	An elongated sheath configured to receive the scope therein, with cleaning portion includes a membrane [46].
US20090250081	Device fixed to the interior abdominal wall, to clean the endoscope lens in situ [47].
US6258025B1	A ring-shaped sleeve covers the optical device provided with a crown of turbine blades against which a pressurized air jets from nozzles are directed in order to turn it in rotation to remove impurities [48].
EP0664101	A hollow tubular is mounted to endoscope with a passage for flowing a fluid against the lens to clean it [49].
US6447446B1	A pump for delivering irrigation fluid with pressure over the lens through a sheath adjusted to receive the endoscope [50].
US20060293559A1	A disposable scope cleaner include a system for rinsing the lens with an irrigation fluid [51].
US6354992B1	A hollow sheath for endoscope has two channels, one for irrigation with cleaning fluid directed onto the lens. The other channel is for suction [52].
US20150005582A1	A flow of CO2 through the lumens forms a vortex to prevent the laparoscope lens fog and contamination [53].
US8047215B1	An elongated sheath for laparoscopic lens cleaning, having conduit and discharge fluid nozzle, a conduit and gas discharge nozzle [54].
US20070225566A1	A cleaning device having a nozzle to spray selectively cleaning liquid and a pressurized CO2 gas over the lens [55].
US20080188715A1	An endoscope with two supply channels for liquid and gas, which are mixed and ejected against the lens [56].
US20130204088A1	Apparatus with a nozzle that jets a gas/liquid mixture toward the endoscope lens [57].
US20040220452A1	Device with a gas nozzle providing a gas jet against the optical surface under high pressure, having a suction pump and a gas jet catcher [58].
GB2481727A	Apparatus having a flow guide for directing a fluid flow across a surface of an endoscope [59].
US6409657B1	Endoscope having a spray nozzle with a drain port in the opposite functioning as a suction channel [60].
US20130217970A1	Apparatus having a conduit attached to the endoscope for the passage of fluid therethrough and a suction device [61].
US5337730A	A cleansing catheter with a hollow shaft having an inflatable balloon with a multitude of small holes when it is filled, the liquid will escape to clean the endoscope lens [62].
US8133052B1	A dental mirror with Suction ports on the periphery, the cleaning is made by drawing air across the mirror [63].
US20080188714A1	Device having vibrating elements selectively activated during the application of a washing liquid over the lens to improve the cleaning [64].
WO0053341A1	Apparatus for the ultrasonic cleaning with a wire ultrasonic resonator inserted around the instrument to be cleaned [65].
US20120178995A1	A sheath to receive the endoscope having in the distal end a clear film strip to prevent the endoscope lens contamination [66].
US20150216401A1	Multitude of superposed films covered the optic lens, each removal of an individual film; remove lens contamination [67].

Table 7. Description of mechanical interactions lens-cleaning patents cited in our study

Patent number	Brief description
US20220061646A1	A rod with a curved spring structure having an element projecting at the end, containing an open cavity where a sponge is attached. The spring returns to its original curvature after insertion, to position the sponge in contact with an endoscope lens [68].
US11058291B2	A tubular member adapted for having a laparoscope, with a cleaning member attached to the distal end, the cleaning components can use a deformable, flexible, and/or absorbent material (rubber, sponges) [69]69].
WO2019226855A1	A longitudinal member extends along a laparoscope having a transverse member with a cleaning material, such as a cloth, sponge [70].
US20220047354A1	Cleaning device mounted to an endoscope having a wiper selectively displaced across the lens [71].
US 20220039912A1	A cleaning material disposed on an elongate shaft of a surgical instrument; against it, a lens of an endoscope is cleaned [72].
US 20210100444A1	An apparatus adapted to mount on endoscope, having a wiper or sponge incorporated to clean the lens with a control system configured to detect a deposit on a lens by analyzing the one or more images [73].
US 20190231183A1	A cleaning device having at the distal end a loop with a cleaning member formed of a biocompatible fabric or a microfiber pad. [74]
US 20180344141A1	A longitudinal element extends along of a laparoscope having at the distal portion a cleaning element, movable between a first position and a second position [75].
US 20190110674A1	An elongated cannula receive an endoscope, and having a wipe assembly to clean a lens [76].
US11172813B2	Apparatus adapted to mount on an endoscope having cleaning member (e.g., a resilient polymeric wiper) for cleaning the lens [77].
US10993609B1	Apparatus adapted to mount on an endoscope, having a clearing member, selectively rotated to contact the lens [78] .
US2021033854A1	A housing shaped to fit over an end of a camera lens, having a wiper movably between the first position and the second position to remove contamination [79].
US10709321B2	A housing having a shaft longitudinally extended, configured to rotate the lens protector, generate the centrifugal force and throwing debris [80].
US20190110675A1	An apparatus having a channel for receiving a flow of cleaning fluid and a multitude of nozzles aligned to direct cleaning fluid toward the optical element of the imaging system [81].
US11123152B2	Device having a nozzle for directing against the lens of the laparoscopy, a saline fluid for irrigation and a CO2 gas for drying [82]
US20210219832A1	A cannula that can receive an endoscope with manifold of the cleaning device positioned around of it distal end and includes fluid inlets [83].
US20210177249A1	An endoscope with an air supply/water supply nozzle for injecting a cleaning fluid toward the lens [84].
US11042020B2	An endoscope including a cleaning nozzle with an inclined opening through which liquid cleaning is ejected toward the lens [85].
US 20220104696A1	A multitude of nozzles and/or channels to direct a cleaning flow toward an endoscope lens [86].
WO2021219826A1	A house encapsulate a single use endoscope, having a fluid spray nozzle toward the viewing window [87].
US 20200367736 A1	An endoscope encompassed by an outer cylinder, having a lens cleaning system with one or more fluid delivery channels [88].
US 20220125288A1	A sheath with a fluid delivery system for cleaning a lens scope [89].
WO2021179249A1	A system for monitoring and cleaning a lens of a laparoscope having a software to provide a feedback signal to a cleaning system to activate when the image clarity is under a threshold, using a pressurized liquid , a compressed air , and a suction [90].
WO2019227018A1	An optical trocar that has self-cleaning capabilities by spraying irrigation liquid towards the laparoscopy lens [91].
US 20210228069A1	A cannula for covering an endoscope having a tubular member, through which a cleaning fluid to be supplied to the lens [92].
US 20200375444A1	A control system receive one or more images of a surgical field ,detect a deposit on a lens scope, and send a command for providing a fluid to clean the lens [93].
US 20210369098A1	An ultrasonic generator providing an ultrasonic signal to a transducer coupled to the lens in order to generate vibration thereto, to clean it [94].
US 10806337B2	An endoscope-cleaning device that combines fluid flow (collision) and wiping in order to clean the lens [95].
US 9241610B2	An endoscope having a flexible lens cover film, systematically unrolled from a first spool to provide a clean and clear cover, the end of the film is captured and wound onto on a second spool [96].
US 20210315441A1	A laparoscope with lens having a hydrophobic surface, treated with laser, that avoids the need for cleaning during use [97].

3.3. Categories scores' and evaluation

The score for each category was calculated and represented by the number of patents in Table 8 and Figure 10. The distribution of granted and abandoned patents by category is illustrated in Figure 11 and Figure 12.

Table 8. Patents potential application score

Category	Type	Methods	Number of Patents	Granted	Pending	Abandoned	Score
Mechanical Interactions	Removal Methods	Collision	27	14	7	6	35
		Brush/Wipe	23	8	5	10	21
		Centripetal Force	2	2	0	0	4
		Vibration	3	1	1	1	3
		Suction	1	1	0	0	2
		Hybrid (Collision +Wipe)	1	1	0	0	2
	Prevention Methods		3	2	0	1	4
Chemical interactions	Removal Methods	All	-	-	-	-	-
	Prevention Methods	Hydrophobicity/ Lipophobicity	1	0	1	0	1

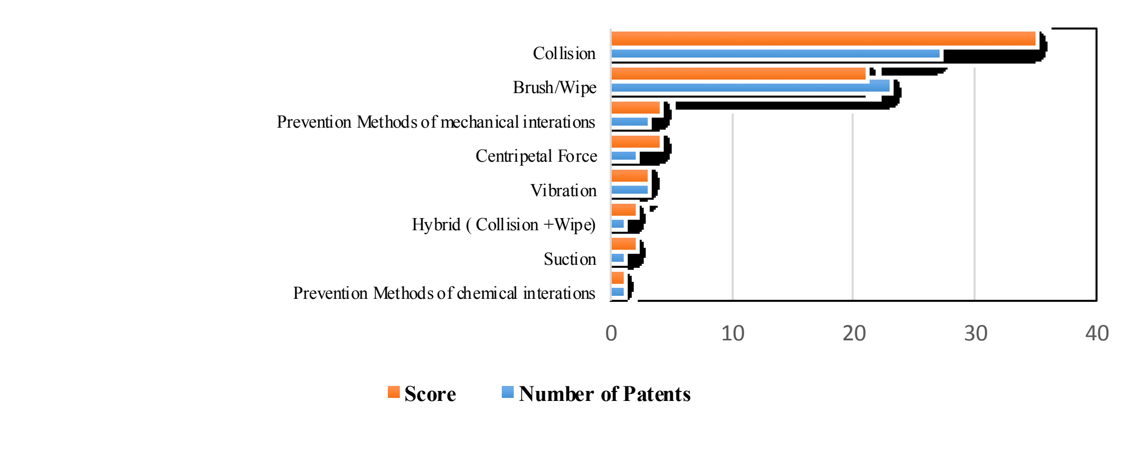

Figure 10. Number of patents and score by category

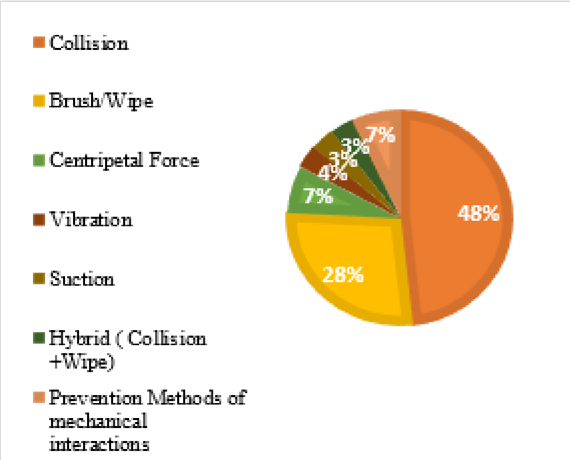

Figure 11. Granted patents by category

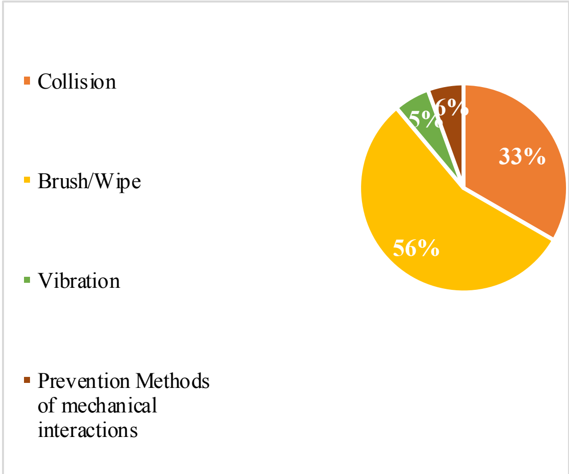

Figure 12. Abandoned patents by category

3.4. Laparoscopic lens cleaning devices

Table 9 shows the patents finished by commercial solutions, represented by the category of lens cleaning methods.

Table 9. Patents finished by commercialized products

	Type	Methods	Patent number	Device name	The commercial company	Year
Mechanical Interactions	Removal Methods	Brush/ Wipe	US20090250081	EndoClear	VIRTUAL PORTS LTD.	2009
			US11172813B2, US10993609B1	Kelling™ Device	ClearCam Inc	2021
		Collision	US20150005582A1	FloShield Air	MINIMALLY INVASIVE DEVICES, INC	2017
	Prevention Methods		US9241 610B2	ClickClean	MEDEON BIOSURGICAL, INC.	2016

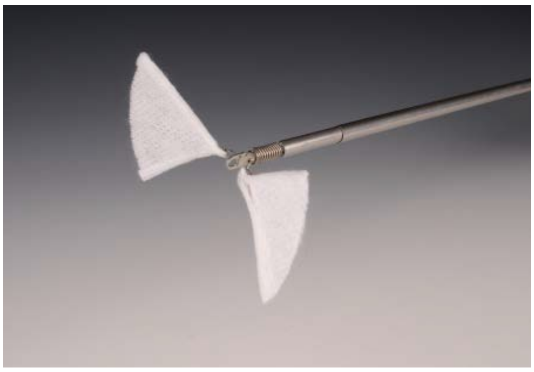

Figure 13. The EndoClear lens cleaner [8]

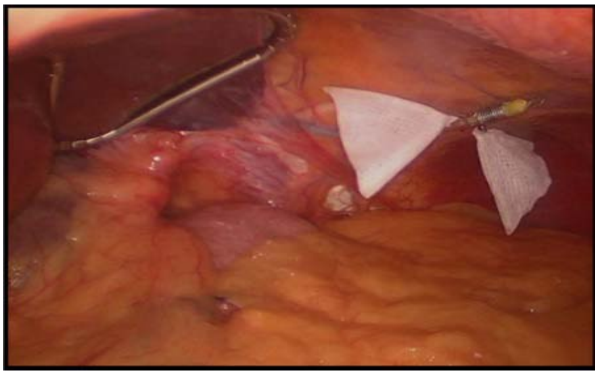

Figure 14. EndoClear on the internal abdominal wall[8]

Figure 15. Kelling™ Device device [98]

[99]

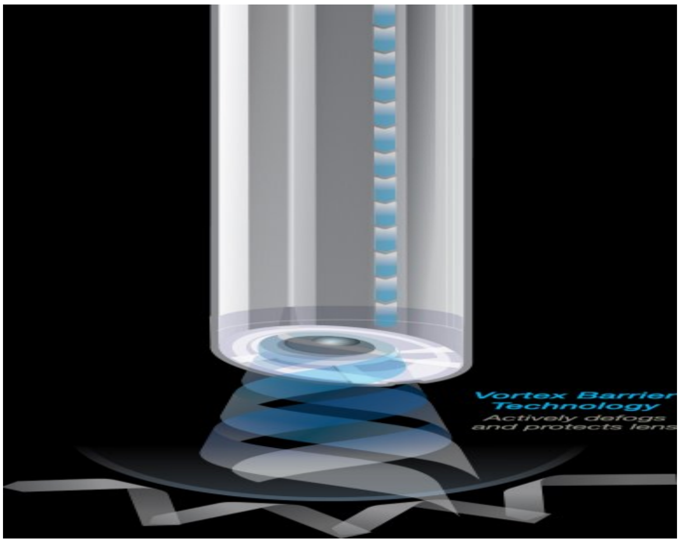

[100]

Figure 16. FloShield Air device

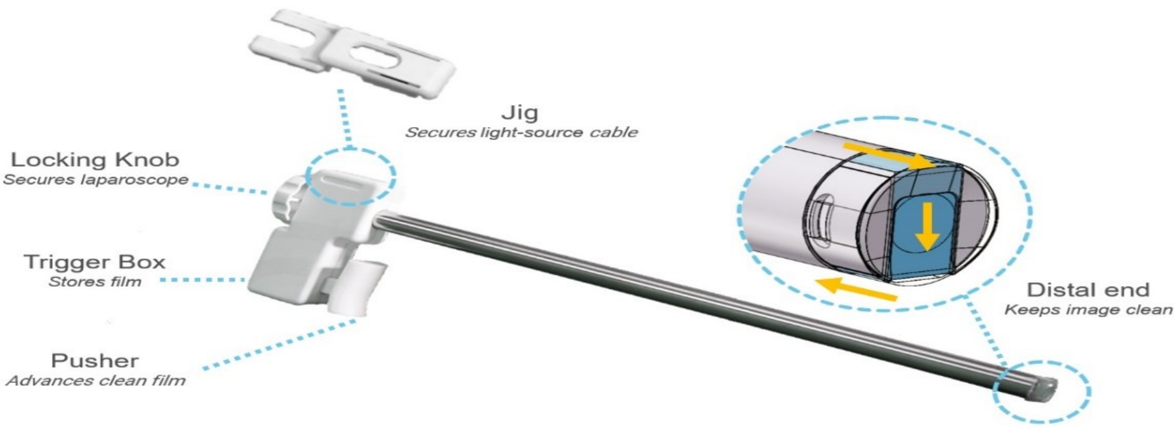

Figure 17. ClickClean device [101]

4. Discussion

Ensuring successful outcomes in laparoscopic procedures relies heavily on maintaining a clear view of the surgical field. However, the laparoscopic lens is susceptible to obstruction from condensation, debris, blood, and smoke. Typically, clearing the lens involves removing the laparoscope from the body, which interrupts the procedure and raises risks of errors. Alternative in-body cleaning methods have been proposed to address this challenge, with some protected by patents that offer innovative solutions.

Our systematic review aims to assess, summarize, and determine the current status of each patent (granted, pending, or abandoned). Specifically, our focus is to evaluate methods for cleaning laparoscopic lens based on their overall score across various categories. As far as we know, this study is the first to categorize and compare these patents based on their ultimate status.

We have found three recent review articles in the literature. The first review by Kreeft et al. analyzed various devices, patents, and laparoscopic lens cleaning techniques, proposing a new categorization of lens cleaning methods. However, this review is now outdated, and there is a need for a new review that includes recent data and patents. Nabeel et al.'s second review focused on statistical studies assessing cleaning methods and devices through prospective randomized controlled trials or experiments. However, it did not delve into lens cleaning techniques and patents. The third review by Kumar et al. highlighted various antifogging methods; particularly those based on superhydrophobic techniques, but did not cite associated patents and devices.

In this study, we started with 30 patents from our research, to which we added 31 patents found in the Kreeft et al. review. We then used the categorization of Figure 8 to group the patents by the type of lens cleaning method. Next, we found the final status of each patent and attributed a score using a 3-point LIKERT scale: (02) points for granted, (01) points for pending, and (0) points for abandoned. We then compared the categories according to their total scores. As shown in Tables 3, 4, and 5, there was a concentration of patents in two methods: brush/wipe (23 patents) and collision (27 patents), representing 89% of the patents found. Additionally, in the Kreeft et al. review, the category of chemical interactions did not contain any patents. (Table 3).

In this study, we only identified one patent in the chemical interactions category (Table 5), underscoring the challenges associated with implementing chemical methods inside the patient due to health risks. These risks include solvent toxicity, organ damage, respiratory impairment, dermatitis contamination, injury, and thermal burns. The sole patent found in this category was a preventive method based on modifying the lens surface to minimize the need for cleaning. In contrast, patents employing collision methods garnered a high score and were associated with a significant number of patents (Figure 10), which we can attribute to the biocompatibility of the cleaning fluids used inside the human body. Interestingly, patents employing brush/wipe methods ranked second, with a similar number of patents compared to those using collision methods but with a lower score (half of the collision patents' score). These results highlight the challenges associated with using devices equipped with wipers inside the patient cavity, which adds to the laparoscopic dimensions, imposes constraints on the limited surgical site, and compromises the success of the patents.

In the last position, we found patents using other methods, having a limited number (under 3) and a low score (under 4). This result highlights the difficulty of using centripetal force, vibration, or suction methods inside the cavity with a high risk of injury or organ damage. Additionally, as described in Table 7, among the 61 patents studied, only two patents included an automatic detection system of laparoscopic lens contamination using laparoscopic video analysis software.

As shown in Figure 11, 48% of the granted patents are in the collision methods category. Consequently, devices using these techniques have a good chance of being terminated by industrial applications. In contrast, 56% Of the abandoned patents are in the brush/wipe methods category (Figure 12), demonstrating the high failure rate of patents using these methods.

Regarding the patents associated with commercialized products, four devices were identified: EndoClear by Virtual Ports Ltd (Figure 13 &14), Kelling™ Device by ClearCam Inc. (Figure 15), FloShield Air by Minimally Invasive Devices, Inc. (Figure 16), and ClickClean by Medeon Biosurgical, Inc (Figure 17).

EndoClear is anchored to the intra-abdominal wall inside the body. The Kelling™ Device is designed as a windshield wiper specifically for the laparoscopic lens, providing effective cleaning. ClickClean attempts to cover the lens with a clear film, and when the film becomes dirty, a ratchet mechanism drags the film across the lens for cleaning. FloShield utilizes a vortex of CO_2 flowing in front of the lens to prevent visual obscurity, primarily addressing the issue of fog accumulation.

Cassera et al. [8] noted that EndoClear, priced at $110 per device, was a straightforward and relatively inexpensive solution that decreased the time required for laparoscopic lens cleaning. However, its utilization necessitates setup and repositioning time, and surgeons must remember to remove the device at the procedure's conclusion.

Bendifallah et al. [102] observed that FloShield Air decreased the need for laparoscope removals for cleaning. Nonetheless, the device came with a relatively high cost of $70.00 per unit.

Golestani et al. [103] found that the Kelling™ Device, with a total cost of $97.50, was easily constructed and reduced operative time and interruptions for lens cleaning, leading to smoother operations with fewer distractions.

Martin reported that ClickClean reduced the duration of bariatric surgery and provided surgeons with uninterrupted and continuously clear visualization [104]. However, information regarding the device's cost is currently unavailable.

In conclusion, our study underscores the superiority of the collision category in laparoscopic in-situ lens cleaning compared to other categories. Additionally, we highlight the limited exploration of preventative methods and advocate for their consideration in future patent applications. However, it is essential to acknowledge certain limitations. Firstly, we were unable to ascertain the final status (grant or abandonment) of pending patents. Secondly, despite implementing a comprehensive search strategy to identify all relevant patents, there remains a possibility that some pertinent patents were excluded based on the criteria used. This inherent risk cannot be entirely mitigated [21].

5. Conclusion

Ensuring clear visualization of the surgical field with minimal interruptions during laparoscopic procedures is crucial for safe and efficient minimally invasive surgery. However, the lens of the laparoscope is often obstructed by condensation, debris, blood, and smoke. In tackling this challenge, many patents have been developed, with many of them being discussed in this systematic review and categorized based on different cleaning methods for laparoscopic lenses. The goal is to identify effective strategies to prevent patent failure and abandonment. Our analysis indicates that the collision method is the most effective among other lens cleaning methods for achieving successful patents.

In summary, collision cleaner techniques combined with hydrophilic or hydrophobic lens surfaces show promise in developing high-performance devices, which we recommend for future laparoscopic lens cleaning patents.

Chap 3: Machine Learning Classification for the Automated Detection of Distortions in Laparoscopic Videos

Abstract

Purpose: High-quality video is crucial for the success of minimally invasive surgical procedures, as it ensures a smooth workflow and precision during operations. However, real-time laparoscopic video often faces challenges such as blurring and smoke, primarily due to lens contamination. Automatically detecting these visual distortions is essential for supporting surgeons, enhancing operational efficiency, reducing procedure duration, and minimizing patient risks.

Materials and Methods: This paper employs the Laparoscopic Video Quality (LVQ) database, developed by Khan et al., to train and validate a model that classifies common distortions in laparoscopic videos, including defocus blur, motion blur, and smoke. We propose an innovative-cascaded support vector machine (SVM) classification framework that integrates decisions from three binary classifiers. The first classifier separates videos into two categories: good quality and distorted. The second classifier distinguishes between smoke and blur distortions, while the third classifier further differentiates between defocus blur and motion blur, ensuring a precise and structured classification approach.

Results: In this study, we calculated various performance metrics, including accuracy rate, precision, recall, F1 score, and execution time, which are crucial for evaluating the quality of detection results. The machine learning classification exhibited impressive performance, achieving an accuracy rate of 96.55% with the first classifier, 100% with the second classifier, and 99.67% with the third classifier. Furthermore, the classification process achieved a high inference speed of 37 frames per second (fps).

Conclusion: The experimental results presented in this paper highlight the effectiveness of the proposed approach for automatically detecting distortions in laparoscopic videos. The method demonstrates high performance, excelling in both accuracy and processing speed. Notably, one of its advantages is its simplicity and the fact that it does not require high-performance computer hardware.

1. Introduction

High-quality video is essential for the success of minimally invasive surgical procedures, as it ensures a seamless workflow and precision during operations [105]. However, laparoscopic videos are susceptible to various distortions, including noise, smoke, uneven illumination, defocus blur, and motion blur, which are recognized as the five primary categories of laparoscopic video distortion [105]. These impairments not only hinder the surgeon's visibility but also degrade the performance of computational tasks critical to robot-assisted surgery and image-guided navigation systems [106, 107]. Such tasks include segmentation [108-111], instrument tracking [112-115], and augmented reality applications [116, 117]. Research has demonstrated that a decline in image quality caused by factors like blur, noise, or resolution loss significantly reduces the accuracy of these tasks [118].

To address these challenges, various approaches have been developed, primarily focusing on detecting and mitigating specific distortions. Early methods emphasized identifying and classifying smoke distortions using techniques such as support vector machines (SVM) [119] and convolutional neural networks (CNN) [120-123].

Researchers have explored alternative methods to address video distortions, such as analyzing the histogram of the saturation channel (S) in the HSV color space. These studies demonstrate that color saturation decreases when smoke obscures the field of view (FOV) [124].

To facilitate the classification of various distortions, a laparoscopic video quality database (LVQ) was developed, comprising 200 videos categorized into five types of distortions and four intensity levels [105]. Khan et al used specific methods to detect each distortion type:

- A fast noise variance estimator with a threshold for noise detection [125],
- A saturation analysis (SAN) classifier for smoke detection [120],
- Luminance statistics for uneven illumination [105], and
- A perceptual blur index (PBI) with a threshold for classifying motion and defocus blur [126].

Additionally, techniques such as Haar wavelet transform (HWT), fast Fourier transform (FFT), Laplacian operator, and Sobel operator are applied to assess image sharpness or blurriness [127, 128]. However, these methods are often limited to specific distortion types and are only applicable for single-distortion scenarios [129]. When multiple distortions coexist, detection complexity increases substantially, exacerbating masking effects between video frames [130].

Deep learning approaches have gained significant traction and are widely utilized in various domains, including both image and text classification. Architectures such as recurrent neural networks (RNNs) and bidirectional RNNs [131] have contributed to their adaptability and effectiveness.

In the context of laparoscopic image analysis, deep learning methods have been employed to detect and classify the five primary categories of video distortions. Some approaches use single-label classification with a single deep neural network (DNN) [132], while others leverage multi-label classification techniques. For instance, convolutional neural networks like ResNet50 have been utilized to extract features from laparoscopic frames for multi-label distortion classification [133]. More recently, a hybrid method combining ResNet with a fully connected neural network (FCNN) was introduced for multi-label classification, leveraging the LVQ database [105, 134].

Despite their promise, these approaches face several limitations. Training deep learning models is often computationally intensive and requires high-performance hardware [131]. Additionally, the medical field presents unique challenges, such as restricted data access due to privacy concerns and the need for high-quality, labeled datasets. The scarcity of large-scale datasets remains a significant obstacle in medical applications, hindering the broader adoption of deep learning models [132, 133].

To classify distortions, it is essential to differentiate between those caused by laparoscopic lens contamination and those arising from technical issues. During minimally invasive surgical procedures, the majority of distortions encountered by surgeons, such as blur and smoke, stem from lens contamination [135]. Consequently, our work focuses on detecting these specific types of distortions.

In this chapter, we introduce an alternative approach that employs a cascaded framework of three SVM classifiers for the automatic detection and classification of defocus blur, motion blur, and smoke in laparoscopic videos. The proposed framework operates in three stages:

1. **Quality Assessment:** The first classifier evaluates video quality, categorizing it as high or low.
2. **Distortion Identification:** The second classifier identifies whether the distortion is caused by smoke or blur.
3. **Blur Differentiation:** The third classifier distinguishes between defocus blur and motion blur.

The first two classifiers utilize features such as the variance and maximum values of the Laplacian and Sobel operators, along with the Saturation Analysis (SAN) classifier. The third classifier focuses on the Laplacian and Sobel operator features to differentiate between the two types of blur.

This three-stage computational framework enables precise, real-time detection of defocus blur, which can be further applied to activate an automatic in-situ lens cleaning system, ensuring uninterrupted surgical procedures.

This chapter presents several key contributions:

- **Innovative Distortion Classification System:** A novel framework for identifying distortions, specifically those resulting from laparoscopic lens contamination.
- **Real-Time Detection:** A solution designed for real-time identification of distortions in live-captured videos, enhancing its practical applicability in surgical settings.
- **Resource-Efficient Approach:** A straightforward, machine-learning-based classification method that operates without requiring high-performance computational resources, thereby addressing the challenge of limited large-scale medical datasets.
- **Pioneering Study:** To the best of our knowledge, this is the first study to utilize a cascaded SVM approach for detecting distortions caused by laparoscopic lens contamination.

The structure of this chapter is as follows: Section II, Materials and Methods, provides an overview of the datasets and a detailed description of the method employed. Section III, Results, delves into the experimental setup and results. Section IV, Discussion, provides an analysis and discussion of the results. Lastly, Section V, Conclusion, summarizes the outcomes and significance of this work, offering insights into potential future improvements.

2. Dataset overview

In this chapter, we utilize the LVQ database created by Khan et al. [105]. The database contains 10 reference videos, each 10 seconds long, extracted from the Cholec80 dataset [136]. The Cholec80 dataset includes 10 distinct scene categories: bleeding (BL), grasping and burning (GB), multiple instruments (MI), irrigation (IR), clipping (CL), stretching away (SA), cutting (CU), stretching forward (SF), organ extraction (OE), and burning (BU).
Each reference video was subjected to five types of distortions, each with four levels of severity, as detailed in Tables 10 and 11. This result in a total of 200 videos, each annotated with subjective scores obtained from expert and non-expert observers. Khan et al. [105] used these severity rankings to study how both experts and non-experts perceive different distortion types. The distortions include smoke, noise, uneven illumination, defocus blur, and motion blur, as illustrated in Figure18.

(a) Smoke

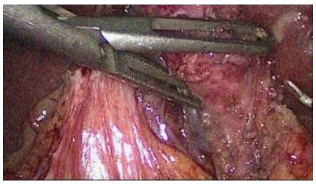

(b) Noise

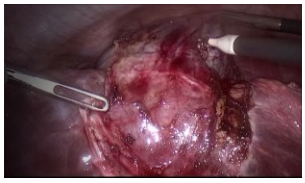

(c) Uneven illumination

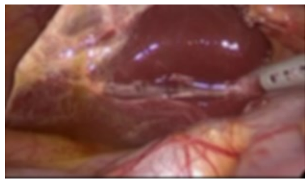

(d) Defocus blur

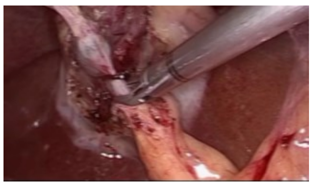

(e) Motion blur

Figure 18. Different distorted images extracted from the LVQ database.

Table 10. Dataset description

Resolution of each video	Frame rate	Number of distortions	Number of levels
512 X 288	25 fps	5	4

Table 11. Dataset summary

Distortions categories	Number of distorted videos	Number of videos by level	Number of level of severity
Smoke	40	10	4
Noise	40	10	4
Uneven illumination	40	10	4
Defocus blur	40	10	4
Motion blur	40	10	4
Total	200	50	/

To validate our method, we used an extended version of the LVQ database, known as the ICIP LVQ Challenge dataset, introduced at the International Conference on Image Processing (ICIP 2020) [136]. The ICIP_LVQ_test dataset consists of 200 laparoscopic videos, encompassing both single and multiple distortions. Specifically, it includes 60 videos with noise, 50 videos with defocus blur, 45 videos with motion blur, 95 videos with smoke, and 95 videos with uneven illumination.

3. The proposed method

In this chapter, we present a novel approach that uses a cascade of three SVM classifiers for the automatic detection and classification of defocus blur, motion blur, and smoke in laparoscopic videos. The first classifier evaluates the video quality, categorizing it into two classes: 'Degraded Image' and 'Good Image.' The second classifier detects the presence of blur or smoke, while the third classifier distinguishes between defocus blur and motion blur.

To create degraded frames for training, we exclude frames that exhibit the first level of defocus blur, motion blur, and smoke distortions. These exclusions are based on expert evaluations, where good scores range from 0.8 to 1, as described in [105]. As a result, the second, third, and fourth levels of distortion are used to form the training dataset, which includes three classes: 'Defocus Blurred Image,' 'Motion Blurred Image,' and 'Smoked Image.'

For training, 90 videos are selected and converted into frames at a rate of 5 frames per second (fps), as shown in Table 12. These three classes are consolidated into a single class labeled 'Degraded Image.' Note that the 'Noise' and 'Uneven Illumination' classes are not considered in this work, as it focuses on detecting blur and smoke.

Additionally, frames from 10 reference videos in the LVQ database are extracted at a rate of 25 fps, and these frames are labeled as 'Good Image.'

To address the issue of imbalanced class distribution in the dataset, we chose a data-level approach [137]. Specifically, we applied oversampling to the 'Good Image' class, which is the minority class, by vertically flipping the extracted frames. This resampling technique helped balance the training dataset, as shown in Table 12.

For the second classifier, the 'Defocus Blurred Image' and 'Motion Blurred Image' classes are merged into a single class called 'Blurred Image.' To balance this class with the 'Smoked Image' class, data augmentation is applied by vertically flipping the extracted frames, as illustrated in Table 13.

For the third classifier, we utilize two classes: 'Defocus Blurred Image' and 'Motion Blurred Image' as shown in Table 14.

Table 12. Overview of Training Data for the Initial Classifier

Dataset	Number of frames
Defocus blurred frames	1548
Motion blurred frames	1548
Smoked frames	1548
Total of degraded frames	4644
Reference frames	2561
Reference frames after data augmentation	4644
Total frames	9288

Video frames are resized to 224x224 pixels before being applied to the SVM classifiers.

Table 13. Overview of training data for the second classifier

Dataset	Number of frames
Blurred frames (defocus and motion)	3096
Smoked frames	1548
Smoked frames after data augmentation	3096
Total frames	6192

Table 14. Overview of training data for the third classifier

Dataset	Number of frames
Defocus blurred frames	1548
Motion blurred frames	1548
Total frames	3096

4. Features extraction

-Blur features: To detect blur in laparoscopic videos, we employ two pixel-based edge detection algorithms: the Laplacian, a second derivative operator, and the Sobel operator, a first derivative operator. These methods were chosen based on the observation that sharp images typically exhibit clearer, more defined edges compared to blurred images [128].

The Laplacian highlights areas with rapid intensity changes. By calculating the variance of the Laplacian of an image, we can distinguish between blurred and sharp images. A high variance indicates significant edge responses, suggesting a sharp image, while a low variance signals a more uniform response, characteristic of a blurred image [138]. Additionally, we use the Sobel operator for edge detection because it is less sensitive to noise and operates with a relatively small mask, making it effective in detecting edges in noisy images [139].

In this study, we extract the variance and maximum values from each operator as image features for the SVM classifier. These features are crucial for distinguishing between blurred and non-blurred frames [128, 139]. For blurred images, both the variance and maximum values of the Laplacian and Sobel operators fall below a threshold automatically determined by the SVM classifier.

-Smoke features: For smoke detection, we use the SAN classifier, which operates based on the histogram of the saturation channel in the HSV color space. Images containing smoke typically exhibit reduced color saturation, making the saturation channel in the HSV space a reliable indicator of smoke presence [120]. Leibetseder et al. utilized saturation peak analysis (SPA) to evaluate the saturation of a frame by converting it into the HSV color space. This technique isolates the S-channel and generates an intensity histogram. It has been observed that images with low color saturation or those containing smoke tend to have a higher number of low-saturation pixels, resulting in histograms with increased values in the lower bins and decreased values in the higher bins [140]. If most of the bin values in the histogram fall below a threshold of tc=0.35, as proposed in [120], the frame is classified as containing smoke. The probability of an image containing smoke is then defined as:

$$Preds(H) = \frac{1}{|H|} \sum_{\substack{i=0 \\ b \in H \\ i \leq tc}} b_i \qquad (1)$$

Where: bi is the i-th bin value of histogram H, with |H|=256, and t_c the threshold (t_c = 0.35) [120].

Detecting smoke using saturation histograms involves determining an appropriate concentration point for the bin values in non-smoke samples, known as the classification threshold (tc). This threshold acts as a reference for smoke samples, which generally exhibit a lower concentration of saturation values [120].

5. The proposed work

Machine Learning (ML) is a powerful tool used in various fields, such as computer vision, bioinformatics, and healthcare. It analyzes large datasets to identify patterns and make predictions with minimal human intervention. ML algorithms are commonly used in research to classify and predict outcomes accurately. In the medical field, ML shows promise in improving disease diagnosis and aiding clinical decision-making [141]. Among the various ML techniques, Support Vector Machine (SVM) is a widely recognized and effective algorithm known for its robust performance in classification tasks. It can handle linear and non-linear data through diverse kernel functions, such as linear, polynomial, and radial basis function (RBF) kernels [142]. SVMs also have robust predictive performance and resistance to overfitting [143], which made it the algorithm of choice for this work. The input to the SVM consists of feature vectors extracted from frames in the dataset discussed earlier. The primary objective of the SVM is to separate these feature vectors by maximizing the margin between them.

While dimensionality reduction techniques like linear discriminant analysis (LDA) and principal component analysis (PCA) are commonly used to reduce computational complexity during training [141], they were not employed in this work. Instead, the focus was on identifying the optimal SVM kernel to achieve the best separation of feature vectors and maximize classification accuracy.

Through extensive evaluation of various SVM kernels, the Gaussian RBF kernel emerged as the most effective, providing the highest accuracy. The optimal hyperparameters were determined to be C=100 and Gamma=0.01.

In this work, SVM is trained to map the extracted features to their respective classes. The approach employs three binary SVM classifiers arranged in a cascade, as illustrated in Figure 19. This configuration enables a step-by-step refinement of the classification process, enhancing overall accuracy and performance.

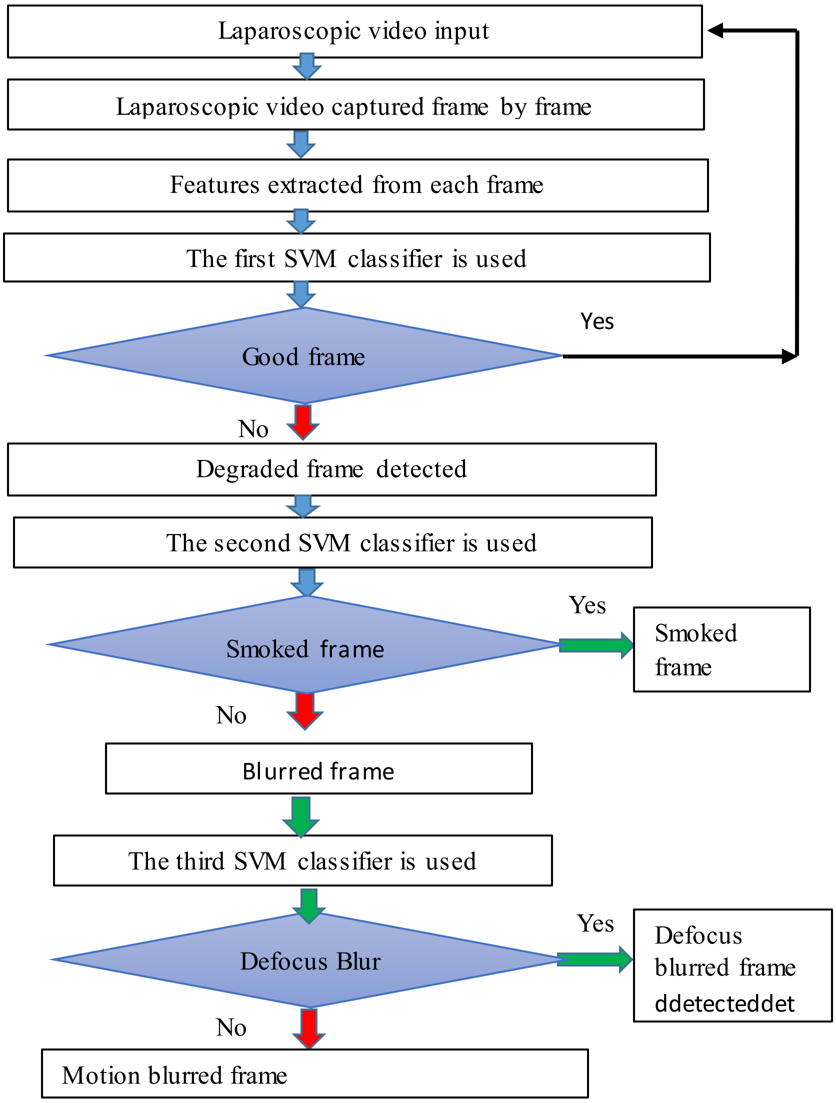

Figure 19. Diagram of the proposed framework for detecting distortions in laparoscopic videos.

5.1. First step - degraded image/good image classification

For the first classifier, the training dataset is prepared by combining frames from two categories: 'Degraded Image' and 'Good Image.' These frames are then stored in a dedicated data file for further processing. To optimize the classifier's performance, various feature combinations are evaluated, including:

- The variance and maximum value of the Laplacian operator and SAN classifier.
- The variance and maximum value of the Sobel operator and SAN classifier.
- The variance and maximum value of the Laplacian and Sobel operators and the SAN classifier.

The performance of these feature combinations is assessed using Scikit-learn's confusion matrices, which provide detailed insights into the classifier's output. Key metrics, such as accuracy, precision, recall, and F1-score, are computed to identify the optimal feature set. The bestperforming feature combination is selected, and the corresponding prediction model is saved for use in subsequent steps.

5.2. Second step - blurred image/ smoked image classification

In the second stage, the training process involves frames categorized into two classes: 'Blurred Image' and 'Smoked Image.' The feature set for training includes the variance and maximum values of the Laplacian and Sobel operators, and the SAN classifier.

Once the training is complete, the resulting prediction model is saved for deployment. This classifier specifically comes into play when the first classifier identifies a degraded frame.

5.3. Third step - defocus blurred image/ motion blurred image classification

In the third stage, the training dataset consists of frames classified into two categories: 'Defocus Blurred Image' and 'Motion Blurred Image.' The image features utilized for training include the variance and maximum values of the Laplacian and Sobel operators. Upon completing the training process, the resulting prediction model is saved for future use. This model is specifically activated when the second classifier identifies a blurred image, enabling precise differentiation between defocus blur and motion blur distortions.

6. Results

6.1. Experimental setup

The experiments were conducted on a desktop computer with the following specifications: an Intel Core i3-2365M CPU operating at 1.40 GHz, Intel HD Graphics 3000 GPU, and 4 GB of RAM. The system runs on a 64-bit Windows 7 operating system. The implementation utilized various frameworks, including OpenCV (CV2) version 4.5.5, Scikit-Learn version 1.1.2, and Scikit-Image version 0.19.2, all executed in a Python 3.8 environment.

6.2. Performance metrics

To train and evaluate the proposed methodology, each dataset was randomly split into two non-overlapping subsets: 80% allocated for training and 20% reserved for testing. The distribution of data for each classifier is outlined as follows:

- First Classifier: 7430 frames for training and 1858 frames for testing.
- Second Classifier: 4953 frames for training and 1239 frames for testing.
- Third Classifier: 2476 frames for training and 620 frames for testing.
- The proposed method is evaluated using 200 videos from the testing dataset [135], with results compared against the dataset's ground truth. Performance metrics, including accuracy, precision, recall, F1 score, and execution time, are calculated to assess the effectiveness of the quality detection approach. A detailed summary of these performance metrics is presented below:

- **Accuracy** measures the proportion of correctly predicted frames relative to the total number of frames in the test dataset.

$$\text{Accuracy} = \frac{TP+TN}{TP+TN+FP+FN} \qquad (2)$$

Where TP is true positive, TN is true negative, FP is false positive, and FN is false negative.

- Precision refers to the accuracy of positive predictions .

$$\text{Precision} = \frac{TP}{TP+FP} \qquad (3)$$

- **Recall (Sensitivity)** quantifies the proportion of actual positive instances that were accurately identified by the model .

$$\text{Recall} = \frac{TP}{TP+FN} \qquad (4)$$

- **F1 Score** combines both recall and precision into a single metric, with a perfect score of 1.0 indicating the best performance .

$$\text{F1\_score} = \frac{2*\text{precision}*\text{recall}}{\text{precision}+\text{recall}} \qquad (5)$$

- **CPU Execution Time** refers to the amount of time the CPU spends running the framework and classifying the frames.

- **Frame Rate**, expressed in frames per second (fps), indicates the speed at which video frames are processed to detect distortions in real-time laparoscopic videos.

6.3. Experimental results

This section presents the evaluation results of the proposed method for each classifier, focusing on key performance metrics such as accuracy, precision, recall, F1 score, and the confusion matrix.

6.3.1 The first classifier

For the first classifier, we performed a comparative analysis of various methods for detecting blur and smoke in images. Different feature combinations, as outlined in the methodology section, were evaluated. The confusion matrix for each method is presented in Figure 20.

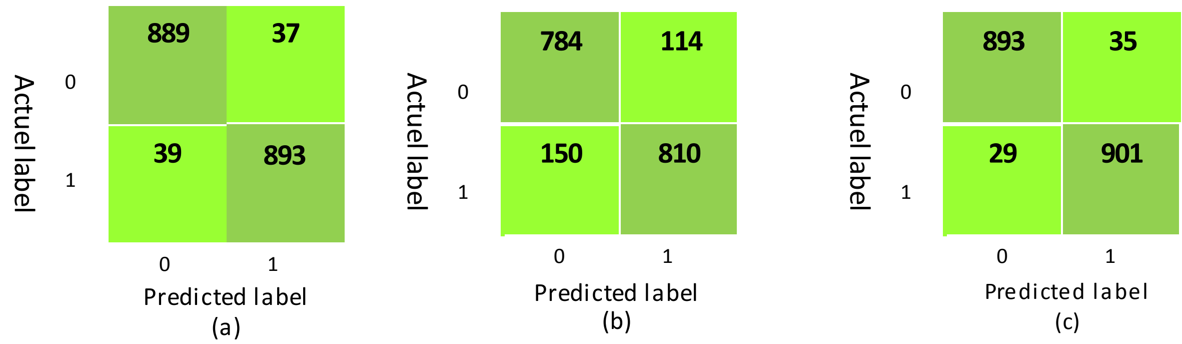

Figure 20. Confusion Matrix for the First Classifier in the Proposed Solution, Evaluated with Each Feature Configuration: (a) The variance and the maximum value of the Laplacian operator and SAN classifier; (b) The variance and the maximum value of the Sobel operator and SAN classifier; (c) The variance and the maximum value of the Laplacian and Sobel operators and SAN classifier.

Figure 20 shows the confusion matrices for each feature combination. In each matrix, the rows correspond to the true (actual) classes: 'Degraded Image' (class 0) and 'Good Image' (class 1). The columns represent the predicted classes for each feature combination (a, b, and c). Each element (i, j) in the matrix indicates the number of frames that belong to the true class i and were predicted to be in class j.

Table 15. Performance metrics of the first classifier for different feature configuration

Methods	Accuracy %	Recall %	Precision %	F1-Score %	CPU execution time (s)
The variance and the maximum value of the Laplacian operator and the SAN classifier	95.90	95.81	96.02	95.91	0.93
The variance and the maximum value of the Sobel operator and the SAN classifier	85.79	84.37	87.66	85.98	2.18
The variance and the maximum value of the Laplacian, the Sobel operators, and the SAN classifier	96.55	96.88	96.26	96.56	0.78

Table 15 shows accuracy, recall, precision, F1 score, and CPU execution time.

6.3.2 The second and the third classifier

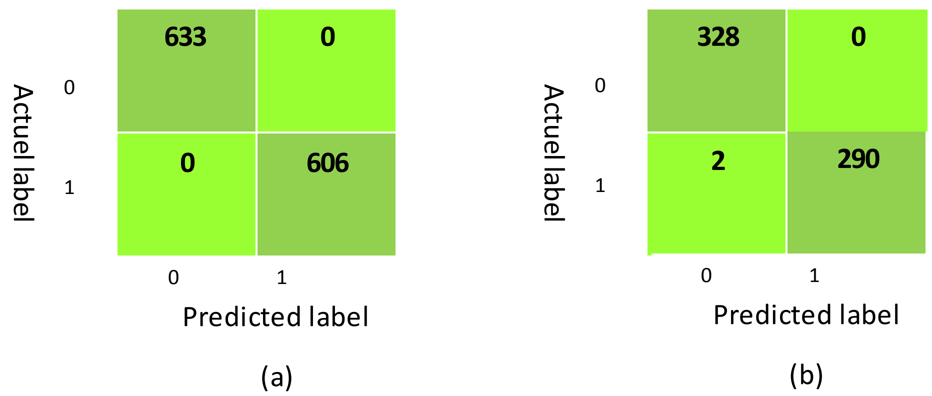

Figure 21. Confusion matrix for the second and third classifiers in the proposed solution: (a) The second classifier with the maximum value and the variance of the Laplacian, the Sobel operators, and the SAN classifier; (b) The third classifier with the maximum value and the variance of both the Laplacian and the Sobel operators.

Figure 21 presents the confusion matrices for the second and third classifiers. In panel (a), the confusion matrix for the second classifier distinguishes between 'Blurred Image' (class 0) and 'Smoked Image' (class 1). Panel (b) displays the confusion matrix for the third classifier, which differentiates between 'Defocus Blurred Image' (class 0) and 'Motion Blurred Image' (class 1).

Table 16 displays the accuracy, recall, precision, F1 score, and CPU execution time for the second and third classifiers.

Table 16. Evaluation metrics for the second and third classifiers

Methods	Accuracy %	Recall %	Precision %	F1-Score %	CPU execution time (s)
The second classifier (the maximum value and the variance of the Laplacian and Sobel operators, and the SAN classifier)	100	100	100	100	0.24
The third classifier (the maximum value and the variance of both the Laplacian and Sobel operators)	99.67	99.31	100	99.65	0.14

6.4. The proposed method tested on the ICIP2020 dataset

Our method was evaluated using the 200 videos from the ICIP2020 testing dataset [136]. The distortion classification results obtained with our approach were compared to the ground truth of the ICIP2020 testing dataset. The outcomes are visualized through confusion matrices, as shown in Figure 22. These matrices are organized by distortion types: defocus blur (a), motion blur (b), and smoke (c).

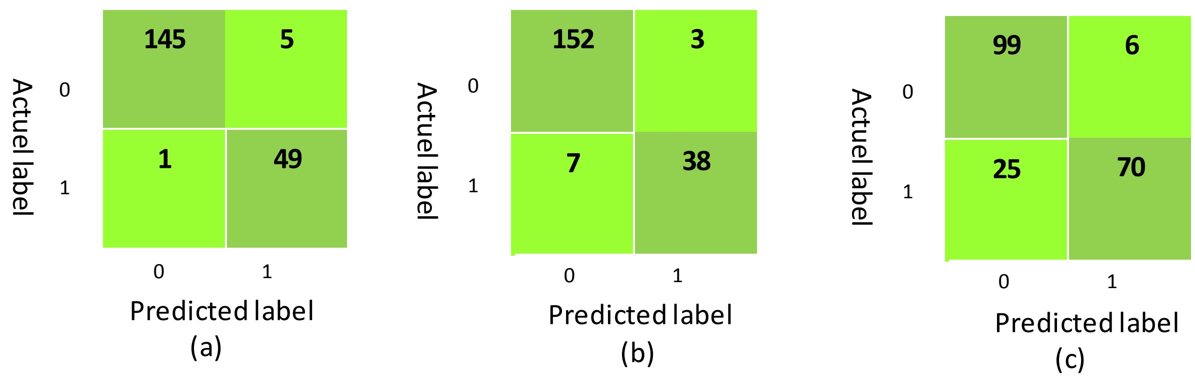

Figure 22. The confusion matrix of the proposed solution for each distortion tested on the ICIP testing dataset: (a) defocus blur, (b) motion blur, and (c) smoke.

Table 17 summarizes the performance metrics (accuracy, recall, precision, and F1 score) of our method when tested on 200 distorted videos from the ICIP2020 testing dataset. The results are presented for each distortion type: defocus blur, motion blur, and smoke.

6.5. Comparison of methods

To demonstrate the effectiveness of our approach in classifying defocus blur, motion blur, and smoke distortions in single-label classification, we compare its performance to the methods proposed by Aldahoul et al. [133] and Khan et al.[105]. Both studies also utilized the ICIP2020 dataset for their evaluations. Aldahoul et al. used ResNet-50 for feature extraction and an SVM for classification, while Khan et al. employed specialized methods for detecting each distortion: a fast noise variance estimator for noise, a saturation analysis (SAN) classifier for smoke, luminance statistics for uneven illumination, and a perceptual blur index (PBI) for both motion and defocus blur.

Table 17. Evaluation Metrics of the proposed method tested on the ICIP testing dataset

Distortions	Accuracy %	Recall %	Precision %	F1-Score %
Defocus blur	97	98	90.74	94.23
Motion blur	95	84.44	92.68	88.36
Smoke	84.5	73.68	92.10	81.86

Table 18. Comparison of the performance metrics: our method vs. Aldahoul et al. and Khan et al. for defocus blur.

Distortions	Accuracy %	Recall %	Precision %	F1-Score %
Our method	97	98	90.74	94.23
Aldahoul et al. method	100	100	100	100
Khan et al. method	91	77.5	77.5	77.5

Table 19. Comparison of the performance metrics: our method vs. Aldahoul et al. and Khan et al. for motion blur.

Distortions	Accuracy %	Recall %	Precision %	F1-Score %
Our method	95	84.44	92.68	88.36
Aldahoul et al. method	90	55.55	100	71.42
Khan et al. method	89.5	75	73.17	74.07

Table 20. Comparison of the performance metrics: our method vs. Aldahoul et al. and Khan et al. for smoke.

Distortions	Accuracy %	Recall %	Precision %	F1-Score %
Our method	84.5	73.68	92.10	81.86
Aldahoul et al. method	95.5	90.53	100	95.03
Khan et al. method	86.2	95	58.46	72.37

Tables 18, 19, and 20 summarize the performance metrics (accuracy, recall, precision, and F1 score) of our proposed method in comparison with those of Aldahoul et al. [133] and Khan et al.[105]. The metrics are presented for each distortion type: defocus blur, motion blur, and smoke. The evaluation was conducted on 200 distorted videos from the ICIP2020 testing dataset. Results for Khan et al.'s method were derived from their thesis [144].

The inference time for our solution was 0.027 seconds, measured from the moment a video frame was input to the point where the distortion type was output. This performance translates to a frame processing speed of 37 frames per second (FPS). In comparison, Aldahoul et al.'s method achieved a speed of 20 FPS, while Khan et al. did not report the frame rate of their approach.

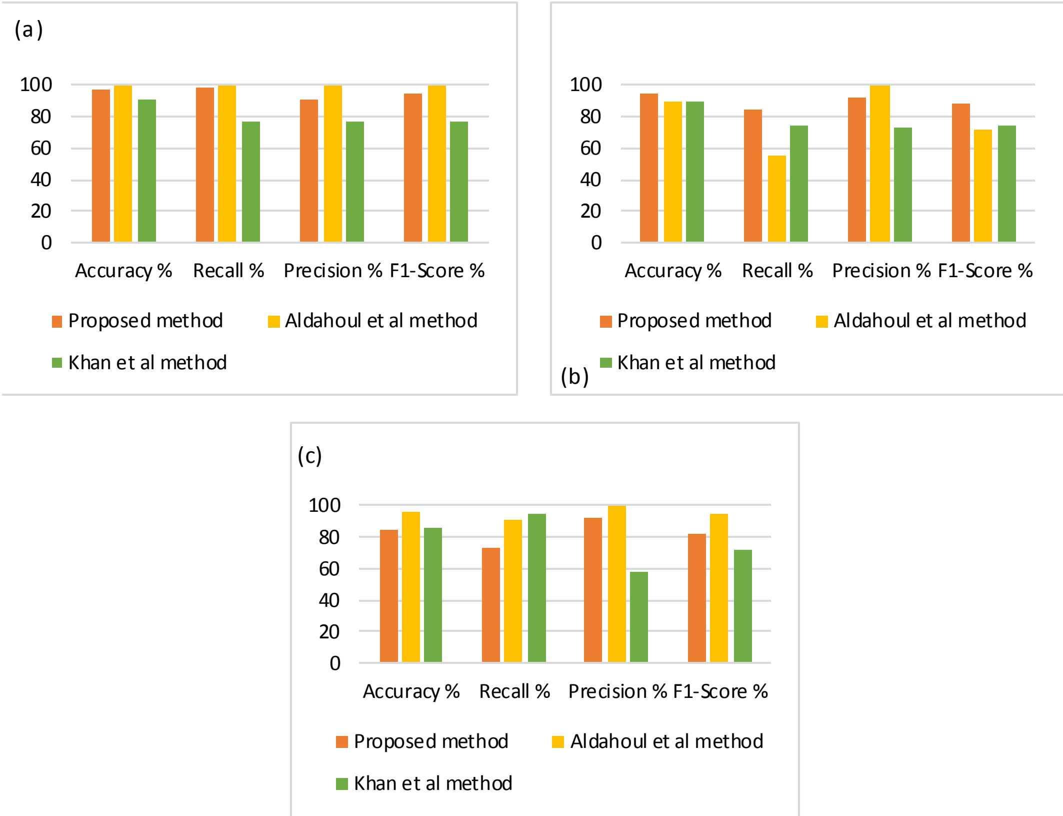

Figure 23. Visual Comparison of Performance: Proposed Method vs. Aldahoul et al. [133] and Khan et al. Methods [144] on the ICIP testing dataset for each distortion: (a) defocus blur; (b) motion blur; (c) smoke.

Figure 23 provides a graphical comparison of the three methods (our approach, Aldahoul et al.'s method, and Khan et al.'s method) for each distortion type: defocus blur (a), motion blur (b), and smoke (c). The comparison evaluates performance metrics, including accuracy, recall, precision, and F1 score.

7. Discussion

The primary goal of this study was to develop a real-time solution for detecting and classifying defocus blur and smoke distortions in laparoscopic video, which often result from lens contamination and can significantly impair surgical visibility. Given the critical importance of processing speed in aiding surgeons, we propose an innovative cascaded framework of support vector machine (SVM) classifiers. This framework consists of three sequentially interconnected SVMs designed to address the unique challenges of real-time distortion detection and classification in laparoscopic videos.

The first SVM classifier determines whether the video is of good quality or degraded. If a distortion is detected, the second classifier identifies the specific type of distortion: either blur or smoke. For videos identified as blurred, the third classifier further distinguishes between defocus blur and motion blur.

To train and validate the proposed framework, we utilized the LVQ database developed by Khan et al.[105]. This comprehensive approach demonstrates the potential for improving surgical visibility and ensuring real-time support for laparoscopic procedures.

In Section 3.3.1, we observe that the first classifier performs optimally when using a combination of the variance and maximum values of the Laplacian and Sobel operators, alongside the SAN classifier as image features. This configuration achieves an accuracy of 96.55%, an F1-score of 96.56%, and a CPU execution time of 0.78 seconds, as illustrated in Figure 20 and summarized in Table 15. The second-best performance is achieved when utilizing the variance and maximum values of the Laplacian operator in conjunction with the SAN classifier, yielding an accuracy of 95.90%, an F1-score of 95.91%, and a CPU execution time of 0.93 seconds. These results highlight the significant influence of feature extraction methods on the evaluation metrics and, ultimately, on the overall classification performance.

In Section 3.3.2, we observe that the second classifier achieves perfect performance, with an accuracy and F1-score of 100% and a CPU execution time of 0.24 seconds. This demonstrates its exceptional ability to identify blurred and smoked frames, as shown in Figure 21 and Table 16. The third classifier, on the other hand, achieves an accuracy of 99.67%, an F1-score of 99.65%, and a CPU execution time of 0.14 seconds, indicating its strong capability in distinguishing between defocus-blurred and motion-blurred frames.

In Section 3.3.3, the evaluation of our method on the 200 videos from the testing dataset demonstrates its strong ability to detect defocus-blurred videos and other distortions. The method achieves an accuracy of 97% and an F1-Score of 94.23%, as shown in Figure 22 and Table 17. The method performs effectively in detecting motion-blurred videos, achieving an accuracy of 95% and an F1-Score of 88.36%. The few misclassified videos involve combinations of motion blur with uneven illumination or smoke. Regarding smoke detection, the method achieves a reasonable accuracy of 84.5% and an F1-Score of 81.86%. However, the lower performance in smoke detection is primarily due to 25 false negatives, many of which are videos with a combination of smoke and defocus blur. This highlights a limitation of the method in accurately detecting smoke when accompanied by defocus blur.

In Section 3.3.4, the performance analysis of the evaluated methods reveals that for defocus blur classification (Table 18), our method achieves an accuracy of 97%, outperforming Khan et al. (91%) but falling short of Aldahoul et al. (100%). The F1 score for our method is 94.23%, which is higher than Khan et al.'s 77.5% but lower than Aldahoul et al.'s 100%, as shown in Table 19. For motion blur classification, our method attains an accuracy of 95%, surpassing both Aldahoul et al. (90%) and Khan et al. (89.5%). Moreover, our method achieves the highest F1 score of 88.36%, compared to 74.07% for Khan et al. and 71.42% for Aldahoul et al. These results underscore the effectiveness of our model, not only in accurately detecting blur but also in distinguishing between defocus blur and motion blur.

In smoke classification (Table 20), the Aldahoul et al. method achieves the highest accuracy at 95.5%, outperforming both the Khan et al. method (86.2%) and our method (84.5%). The F1 score for Aldahoul et al. is 95.03%, which is the highest, compared to 81.86% for our method and 72.37% for Khan et al., further reinforcing the findings from the previous section.

In terms of processing speed, our method operates at 37 frames per second (fps), outperforming the Aldahoul et al. approach, which operates at 20 fps. This significant difference highlights the practical advantage of our method for real-time systems, even on low-cost computers. With a frame rate of 37 fps, our algorithm is capable of detecting distortions in live-captured laparoscopic videos effectively and efficiently, making it a suitable solution for real-time applications.

8. Conclusion

During laparoscopic procedures, the visual field can be impaired by condensation, debris, blood, and smoke, leading to distortions such as defocus blur and smoke in the real-time video feed. Ensuring rapid processing is essential to assist surgeons in detecting and resolving lens contamination efficiently.

Our proposed method offers the advantage of simplicity and low computational requirements, making it feasible for use on standard hardware. By employing machine learning-based classification, we successfully achieved automated detection of video distortions with high accuracy and processing speed.

However, the current approach has a limitation: its reliance on manually crafted features. Future advancements could address this limitation by adopting deep learning techniques. Deep learning offers several key benefits over traditional machine learning, such as automatic feature extraction, superior handling of complex and large-scale datasets, enhanced performance, and the ability to model non-linear relationships effectively. Additionally, deep learning algorithms can process both structured and unstructured data seamlessly and excel in predictive modeling tasks. Platforms like Google Colab and Kaggle further facilitate the development and implementation of these advanced methods, opening new possibilities for improving laparoscopic video distortion detection.

Chap 4: A ResNet-50-Based Framework for Accurate Classification of Laparoscopic Video Distortions

Abstract

During minimally invasive surgery, the laparoscopic lens is prone to contamination from condensation, smoke, blood, and debris, which can severely impair the surgeon's visibility and degrade the quality of the laparoscopic video feed. Numerous methods have been developed to detect and classify various types of distortions in laparoscopic videos to solve these problems.

Our approach aims to automate the identification and classification of five key distortion types outlined in Khan et al.'s Laparoscopic Video Quality (LVQ) database. These include noise ('NO'), smoke ('SM'), uneven illumination ('UI'), defocus blur ('DB'), and motion blur ('MB').

Leveraging the power of Residual Networks (ResNet-50), our system demonstrates exceptional accuracy in detecting and categorizing these distortions: 100% for 'SM' and 'NO, 99.82% for 'UI, 99.92% for 'DB,' and 99.87% for 'MB.' These results underscore the robustness and precision of the model, showcasing its capability to generalize effectively across diverse distortion categories and deliver reliable predictions in real-world scenarios.

1. Introduction

Laparoscopy, or minimally invasive surgery (MIS), has revolutionized surgical procedures by offering significant advantages over traditional open surgery. These benefits include reduced recovery time for patients, lower healthcare costs, and shorter hospital stays [18]. The technique involves the insertion of a laparoscopic camera into the patient's abdominal cavity through a small incision using a trocar. This camera captures real-time video, which is processed and displayed on a monitor, enabling the surgeon to perform precise interventions [8].

Despite its advantages, laparoscopic video quality is frequently compromised by various distortions. These include noise, defocus blur, motion blur, smoke, and uneven illumination, all of which can hinder the surgeon's visibility and affect the accuracy and safety of the procedure. Developing robust solutions to address these challenges is essential for improving the overall effectiveness of laparoscopic surgeries.

To support these efforts, the Laparoscopic Video Quality (LVQ) database challenge was introduced, offering a comprehensive dataset to advance research in this field. This database is an extended version of the LVQ database introduced in Chapter 3, featuring a significantly larger collection of videos (800 compared to 200 in the initial version). It includes both single and multiple distortions, allowing for more accurate model training. The dataset is evenly divided into two categories: 400 videos with single distortions and 400 with multiple distortions. These videos cover five distortion types: noise, defocus blur, motion blur, smoke, and uneven illumination, each assessed at four distinct intensity levels.

In contrast to Chapter 3, where machine learning techniques were employed, this chapter leverages the larger dataset of 800 videos to improve the classification accuracy of various distortions using deep learning methods. Several deep-learning approaches have been explored. Some rely on a single Deep Neural Network (DNN) for end-to-end classification [132], while others utilize ResNet50, a convolutional neural network, as a feature extractor for processing laparoscopic video frames. An advanced strategy integrates ResNet50 with a Fully Connected Neural Network (FCNN) to further enhance classification performance [134].

Despite these advancements, existing methods have struggled to achieve significant and consistent improvements in overall classification accuracy. Additionally, when dealing with multi-class classification tasks, these models often fail to maintain balanced performance across all distortion categories, highlighting a critical limitation in their generalizability and robustness [145].

In this chapter, we have developed a novel computational framework designed to detect and classify distortions in laparoscopic videos. The framework is initially trained on the LVQ Challenge dataset, leveraging the powerful capabilities of Residual Networks (ResNet50) for feature extraction and classification.

This chapter introduces several contributions:

- A novel distortions classification system used to identify distortions in laparoscopic video.
- A deep-learning, classification-based method using Resnet50 for the identification and the classification of the different laparoscopic video distortions.

The structure of this chapter is as follows: Section II, Materials and Methods, provides an overview of the datasets and a detailed description of the method employed. Section III, Results, delves into the experimental setup and results. Section IV, Discussion, provides an analysis and discussion of the results. Lastly, Section V, Conclusion, summarizes the outcomes and significance of this work, offering insights into potential future improvements.

2. Dataset description

This chapter leverages the LVQ Challenge database [105, 132], a comprehensive resource derived from the Cholec80 dataset [146]. The database consists of 20 reference videos, each lasting 10 seconds, which were systematically modified to include five distinct distortion types at four intensity levels.

The dataset encompasses 800 videos: 400 with single distortions and 400 featuring multiple distortions. The five primary distortion categories: noise, defocus blur, motion blur, smoke, and uneven illumination.

For training, our model utilizes videos from both single and multiple distortion categories. Each single-distortion class comprises 80 videos, ensuring a balanced representation. The multiple-distortion dataset includes various combinations:

- **Defocus_uneven (80 videos)**
- **Noise_smoke (80 videos)**
- **Noise_smoke_uneven (35 videos)**
- **Noise_uneven (80 videos)**
- **Smoke_uneven (60 videos)**

Our primary focus is on mixed distortion classes, such as defocus_uneven, noise_smoke, noise_smoke_uneven, and smoke_uneven, as these combinations reflect the complex distortions encountered in real laparoscopic videos. Training on these mixed distortions enhances the model's ability to identify and classify overlapping distortions within the same frame.

To address the challenges of imbalanced learning, we employed a data-level balancing approach [141]. The dataset was resampled by oversampling underrepresented classes, such as smoke_uneven and noise_smoke_uneven, using frame augmentation techniques like vertical flipping. These strategies ensured a balanced class distribution in the training dataset, as summarized in Table 21.

For validation, we utilized the ICIP_LVQ_test dataset presented at the International Conference on Image Processing (ICIP). This testing set comprises 200 videos, offering a mix of single and multiple distortions [105, 132]:

- **Noise** (60 videos)
- **Defocus blur** (50 videos)
- **Motion blur** (45 videos)
- **Smoke** (95 videos)

• **Uneven illumination** (95 videos)

This rigorous validation process ensures the model's robustness in handling both individual and mixed distortions in real-world laparoscopic video scenarios.

3. Methods

Deep convolutional neural networks (CNNs) often face challenges like gradient vanishing as their depth increases, which can hinder learning and reduce accuracy [147]. To address this issue, the Residual Network (ResNet) incorporates skip connections, allowing gradients to flow more effectively through the network layers and mitigating the limitations of purely stacked architectures [147]. ResNet has become a cornerstone in deep learning and is renowned for its strong generalization capabilities across image recognition tasks. Among its variants, ResNet50 stands out with its 50-layer architecture and over 23 million trainable parameters, offering a powerful tool for complex classification problems [147].

3.1. ResNet-50 Architecture

ResNet-50 is a deep convolutional neural network with 50 layers organized into five stages, each consisting of residual blocks. These blocks focus on learning the residual (the difference) between input and desired output, addressing vanishing gradient issues, and enabling the training of deeper networks. ResNet-50 uses Bottleneck Residual Blocks to improve efficiency and reduce computational costs. These blocks feature 1×1 convolutions to create a bottleneck structure, minimizing parameters and matrix multiplications while maintaining learning capabilities.

Each bottleneck block includes three convolutional layers [147]:

- 1×1 Convolution reduces channels.
- 3×3 Convolution extracts features.
- another 1×1 Convolution restores dimensionality.

The residual connection adds input to the output, enhancing learning through ReLU activation (Figure 24).

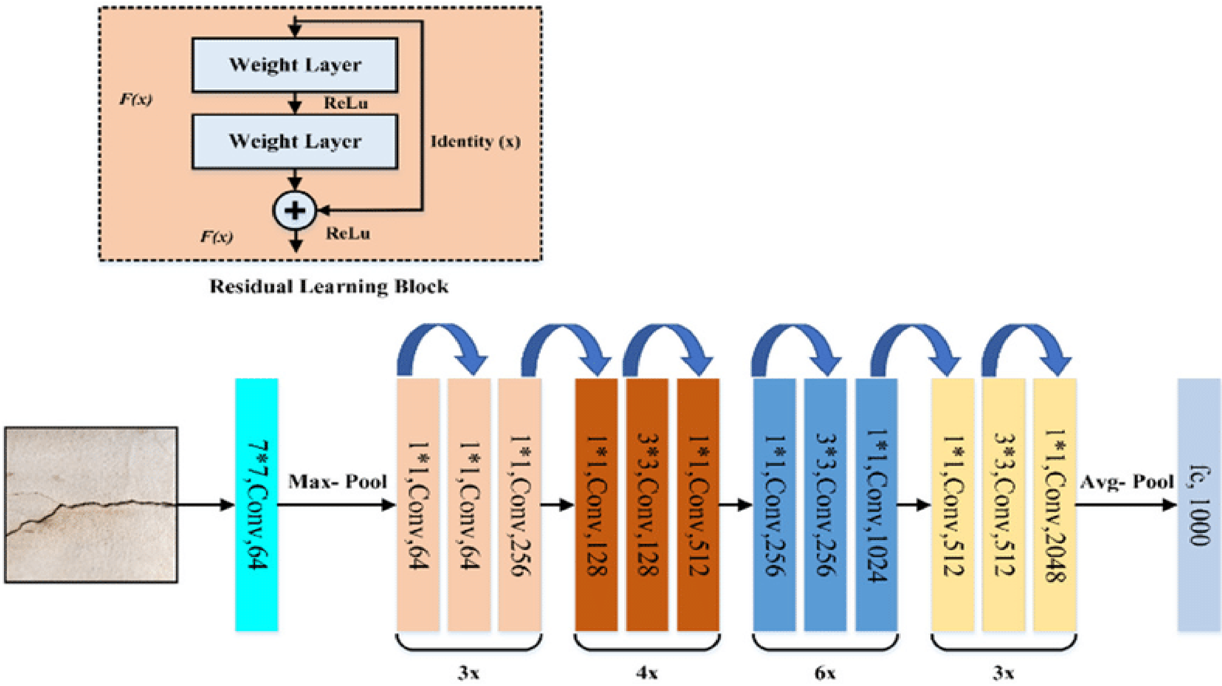

Figure. 24. ResNet-50 architecture [148]

3.2. The proposed method

In this study, we adopt ResNet50, customizing its architecture to suit our dataset. Specifically, we modify the output fully connected layer to include ten units corresponding to the ten classes in our laparoscopic video dataset. The final layer employs the Softmax activation function, transforming the outputs into a vector of probabilities across these classes (Figure 25).

Training our model relies on the laparoscopic video dataset introduced earlier. To optimize learning, we use the cross-entropy loss function, a widely adopted metric for classification tasks. This function measures the divergence between predicted probabilities and actual labels, guiding the model to make accurate predictions. The training process seeks to minimize this loss, which is mathematically expressed as follows:

$$L = -\sum_{n=1}^{10} y_n \log(p_n) \quad [132] \qquad (6)$$

In this setup, yn is a binary indicator, taking the value of 1 if the class label n is the correct classification and 0 otherwise. On the other hand, pn denotes the predicted probability assigned by the model for class n.

To optimize our model, we employ the Adam optimizer with a learning rate of 0.0001. The training is carried out using the PyTorch framework and executed on an NVIDIA T1000 GPU with 12 GB of memory. We use mini-batches of size 100 and train the model for a total of 5 epochs.

Table 21. Overview of Training Data

Class	Number of images
Defocus blurred frames	4132
Motion blurred frames	4132
Smoked frames	4132
Uneven illumination frames	4132
Noised frames	4132
Noise_smoke frames	4132
Defocus_uneven illumination frames	4132
Noise_uneven illumination frames	4132
Smoke_uneven illumination frames	2785
Smoke_uneven illumination frames after data augmentation	4132
Noise_smoke_uneven illumination frames	1646
Noise_smoke_uneven illumination frames after data augmentation	4132
Number of total frames	41320

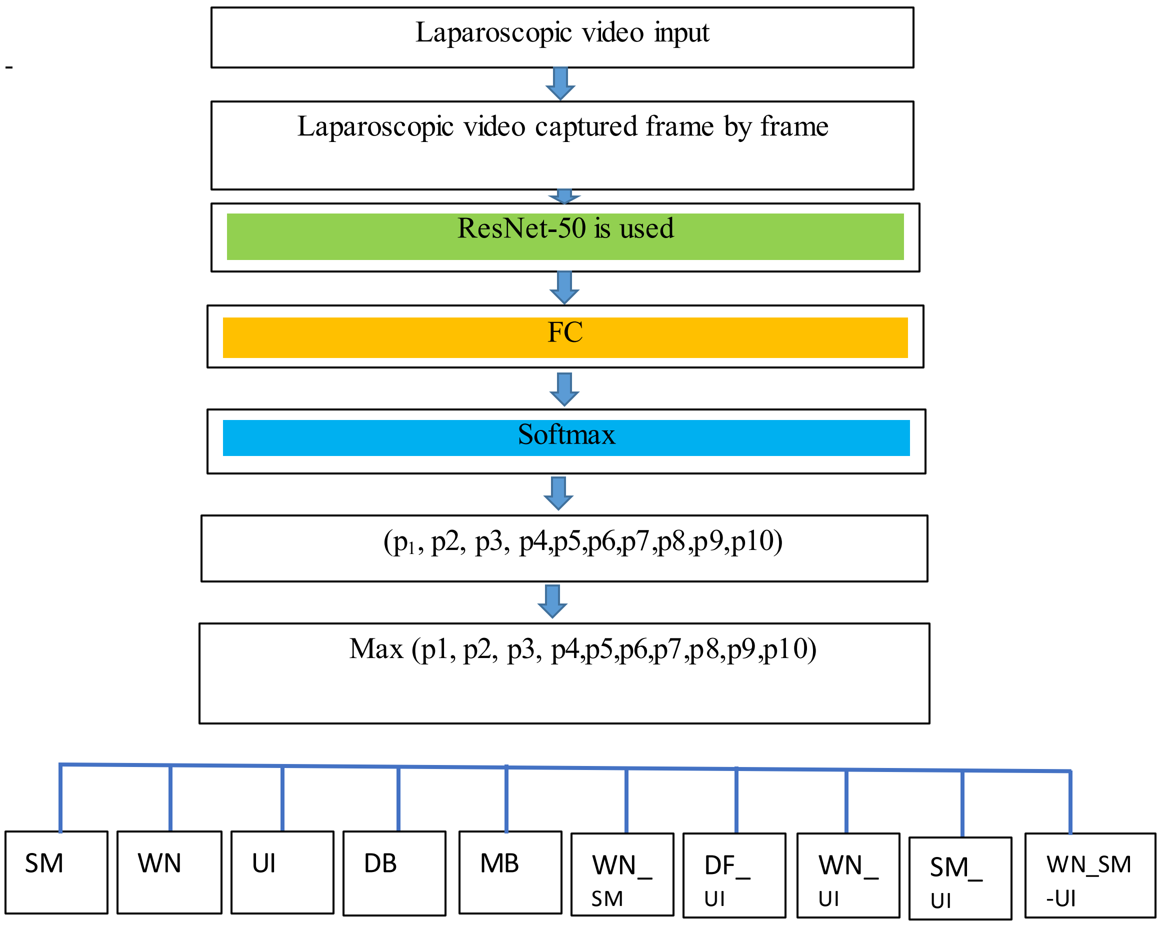

Figure. 25. Schematic representation of the proposed approach for laparoscopic video distortion detection

As shown in Figure 25, a video is considered to have a distortion if at least one of its frames exhibits the specific distortion.

4. Results

4.1. Experimental results

In this chapter, frames were extracted from the ten distortion classes in the LVQ dataset challenge. ResNet-50, with a modified output layer consisting of ten units, was then trained on 80% of the dataset.

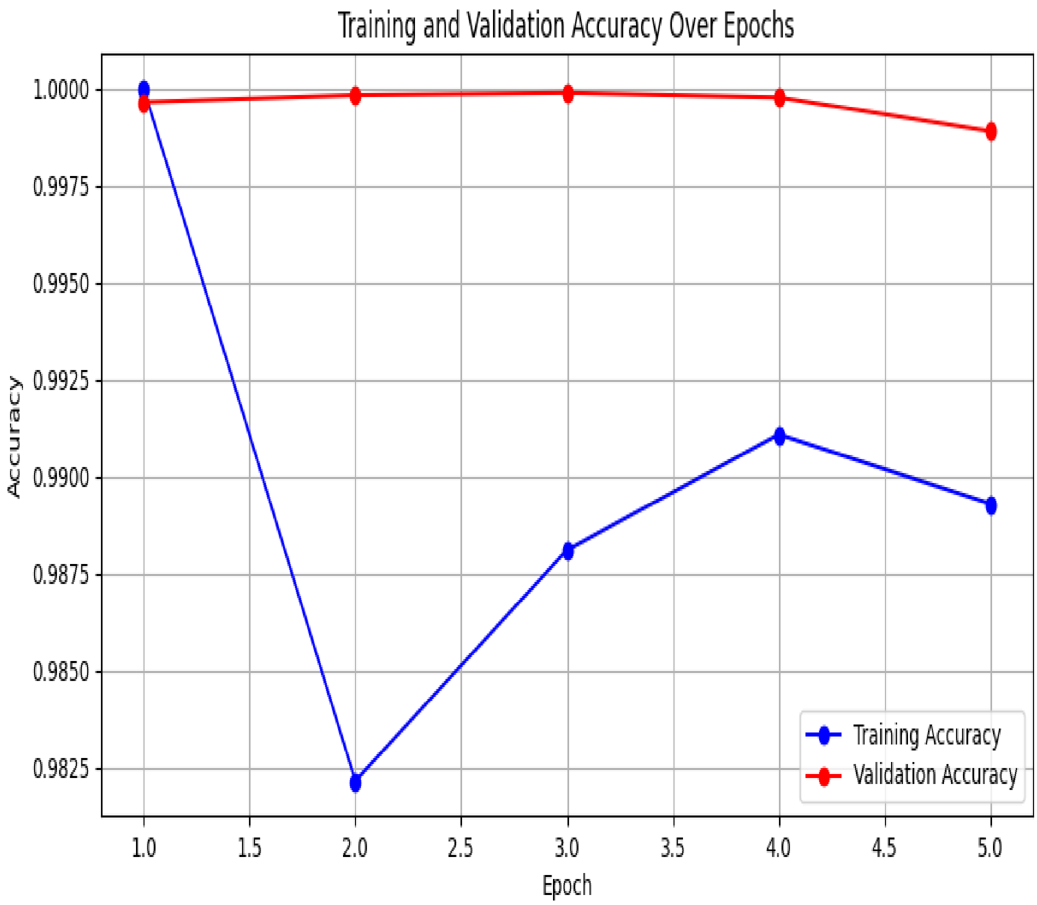

Figure. 26. Training and validation accuracy progression across epochs.

As depicted in Figure 26, the accuracy metric plot compares the training and validation accuracy achieved during the training process. The plot reveals a consistent upward trend in both accuracy curves as training progresses, with the training accuracy peaking notably after two epochs for ResNet-50. By the conclusion of three epochs, the training accuracy reached 98.87%, and the validation accuracy stood at 100%. At epoch=5 a rapid decline in validation accuracy to 99.90%

was observed. Based on these findings, it was determined that extending training beyond three epochs was unnecessary for our model.

Additionally, Figure 27 presents the loss plot, highlighting a sharp decline in training loss, which stabilizes at 0.008 after two epochs and further decreases to 0.005 by the fourth epoch before increasing to 0.01 in the fifth epoch. Similarly, the validation loss decreases, reaching its lowest value of 0 at the third epoch but rising to 0.015 by the fifth epoch. These observations indicate that the third epoch is the optimal training point, as it achieves a balanced performance between training and validation.

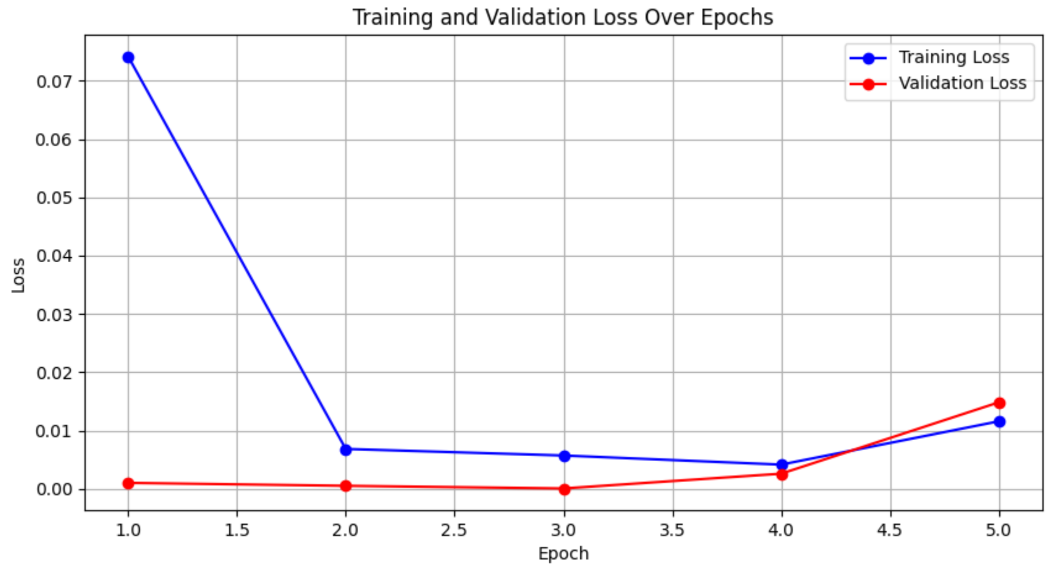

Figure. 27. Training and validation lose across epochs.

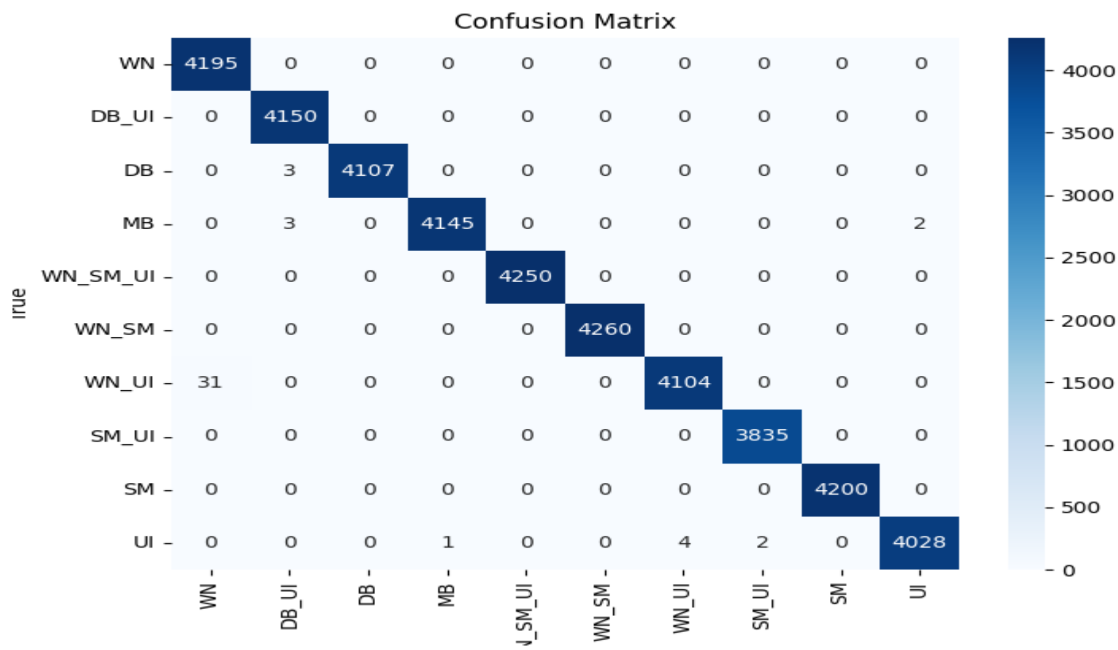

Figure. 28. The confusion matrix of the proposed solution.

Figure 28 showcases the confusion matrix, illustrating the classification performance for each distortion type and their combinations. The distortion types are abbreviated as follows: **SM** (smoke), **WN** (noise), **UI** (uneven illumination), **DB** (defocus blur), and **MB** (motion blur). For mixed distortions, the abbreviations are **DB_UI** (defocus blur and uneven illumination), **WN_SM_UI** (noise, smoke, and uneven illumination), **WN_SM** (noise and smoke), **WN_UI** (noise and uneven illumination), and **SM_UI** (smoke and uneven illumination). This matrix provides a comprehensive breakdown of how accurately each distortion and its combinations were classified.

Table 22. Classification prediction rate across different distortion categories

Class	SM	WN	UI	DB	MB	DB_UI	WN_SM_UI	WN_SM	WN_UI	SM_UI
Prediction rate %	100	100	99.82	99.92	99.87	100	100	100	99.25	100

Table 22 presents the prediction rate of the model for each class.

4.2. The proposed method tested on ICIP2020 dataset

We evaluated our proposed method using a testing dataset of 200 videos provided by the ICIP2020 challenge [140].

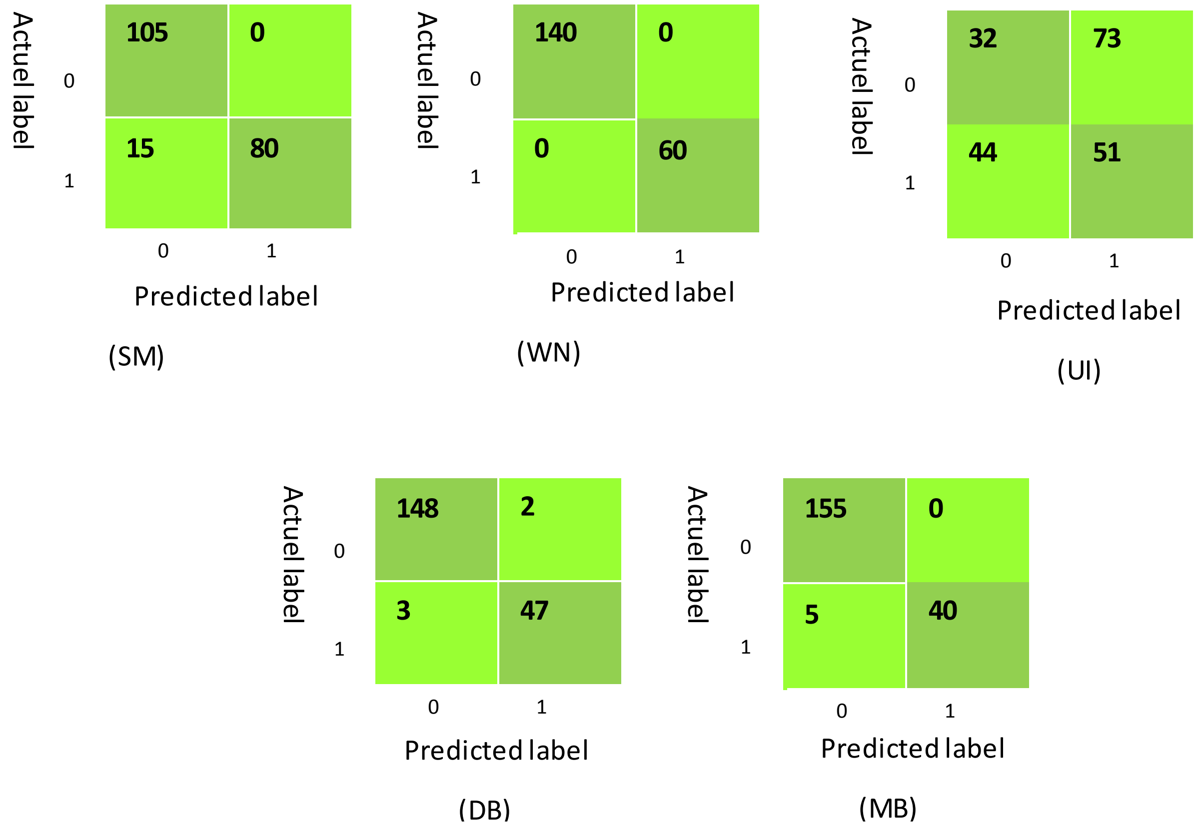

Figure. 29. Confusion matrix for each distortion category tested on ICIP testing dataset.

The distortion classification results of the proposed method are assessed by comparing them with the ground truth from the ICIP 2020 testing dataset. The outcomes are visualized through confusion matrices, as shown in Figure 29, highlighting the model's performance across each distortion type.

Table 23. Evaluation metrics of the proposed method on the ICIP testing dataset

Distortions	Accuracy %	Recall %	Precision %	F1-Score %
WN	100	100	100	100
DB	97.5	94	95.91	94.94
MB	97.5	88.88	100	94.11
SM	85	84.21	100	91.42
UI	41	53.68	41.12	46.57

Table 23 summarizes the performance metrics, including accuracy, recall, precision, and F1 score, of our method evaluated on the ICIP 2020 testing dataset.

4.3. Comparison of methods

To evaluate the effectiveness of our approach in classifying distortions including noise, defocus blur, motion blur, smoke, and uneven illumination, we compare its performance against the methods proposed by Aldahoul et al. [133]and Konduri et al. [145], both of which were tested on the ICIP 2020 dataset. Konduri et al. used DenseNet-65 for feature extraction and the flow direction algorithm for classification, while Aldahoul et al. used transfer learning based on ResNet-50 and the SVM classifier.

Table 24. Evaluation metrics of Aldahoul et al.'s method

Distortions	Accuracy %	Recall %	Precision %	F1-Score %
WN	100	100	100	100
DB	100	100	100	100
MB	90	55.55	100	71.42
SM	95.5	90.53	100	95.03
UI	90	97.89	95.88	96.87

Table 24 summarizes the performance metrics (accuracy, recall, precision, and F1 score) achieved by Aldahoul et al.'s method [133].

Table 25. Evaluation metrics of Konduri et al.'s method [145]

Distortions	Accuracy %	Recall %	Precision %	F1-Score %
WN	**100**	100	100	100
DB	**98.65**	99.24	97.22	98.23
MB	**95.83**	95.96	92.42	94.19
SM	**97.8**	98.74	95.45	97.22
UI	**99.01**	98.74	98.74	98.74

Table 25 summarizes the performance metrics (accuracy, recall, precision, and F1 score) achieved by Konduri et al.'s method [145].

Table 26. Accuracy comparison of three methods: our approach, Aldahoul et al., and Konduri et al. tested on the ICIP dataset.

Metrics	Distortions	Our method	Aldahoul et al.	Konduri et al.
Accuracy%	Defocus blur	97.5	**100**	98.65
	Motion blur	**97.5**	90	95.83
	Smoke	85	95.5	**97.8**
	Noise	**100**	**100**	**100**
	Uneven illumination	41	90	**99.01**

Table 26 compares the accuracy performance of three methods(our approach, Aldahoul et al., and Konduri et al.) evaluated on the ICIP dataset.

Table 27. Comparison of our two methods: the first based on machine learning (Chapter 2) and the second based on deep learning (Chapter 4), both tested on the ICIP dataset.

Metrics	Distortions	Machine learning based method	Deep learning based method
Accuracy%	Defocus blur	97	97.50
	Motion blur	95	97.50
	Smoke	84.5	85
Inference speed (fps)		37	0.925

Table 27 compares the performance metrics (accuracy and inference speed) of our two proposed methods: the machine learning-based approach (Chapter 2) and the deep learning-based approach (Chapter 4). Both methods were tested on 200 distorted videos from the ICIP 2020 testing dataset, with results detailed for each distortion type: defocus blur, motion blur, and smoke.

5. Discussion

The primary goal of this study was to detect and classify various laparoscopic video distortions, including noise, defocus blur, motion blur, smoke, and uneven illumination. To enhance the model's ability to handle real-world scenarios, we included classes with combined distortions, such as noise with smoke, noise with uneven illumination, and smoke with uneven illumination. This comprehensive approach significantly improves the model's capacity to detect and classify individual distortions even when they appear alongside others. The results demonstrate the exceptional performance of the ResNet-50 model in accurately identifying and categorizing frames affected by these distortions.

Figure 26 illustrates the progression of training and validation accuracy across epochs, with the validation accuracy peaking at 100% by the third epoch. The high prediction rates across all distortion classes, detailed in Table 3, underscore the model's robustness and ability to generalize effectively. This conclusion is further supported by Figure 27, which shows the validation loss converging to zero by the third epoch, confirming that this is the optimal point for training.

Figure 28 offers a detailed analysis of classification errors across different distortion classes, while Table 22 highlights the model's exceptional prediction rates. Notably, the highest classification rates were achieved for smoke (100%), noise (100%), and combinations such as defocus blur with uneven illumination (100%) and noise with smoke (100%). Slightly lower rates were observed for defocus blur (99.92%), motion blur (99.87%), uneven illumination (99.82%), and noise with uneven illumination (99.25%). This consistent performance across all distortion types and combinations reflects the balanced distribution of training samples, with 4,132 images per class ensuring no model bias.

Table 23 evaluates the model's performance (accuracy, recall, precision, and F1-score) on the ICIP 2020 testing dataset. The results highlight the model's high accuracy for noise (100%), defocus blur (97.5%), and motion blur (97.5%). Smoke classification achieved 85%, while uneven illumination showed a reduced accuracy of 41%, attributed to a higher number of false positives where videos were incorrectly labeled as having uneven illumination.

When comparing the performance of our method to those of Aldahoul et al. [131] and Konduri et al. [145], several insights emerge. All methods achieved 100% accuracy for noise classification (Tables 24,25 and 26). For defocus blur, Aldahoul et al. led with 100% accuracy, compared to 98.65% for Konduri et al. and 97.5% for our method. In motion blur classification, our method excelled, achieving 97.5% accuracy versus 90% for Aldahoul et al. and 95.83% for Konduri et al. For smoke, Konduri et al. achieved the highest accuracy (97.8%), outperforming Aldahoul et al. (95.5%) and our method (84.5%). Similarly, in uneven illumination classification, Konduri et al. achieved 99.01%, followed by Aldahoul et al. at 90%, while our method lagged at 41%.

The reduced performance in classifying smoke and uneven illumination highlights specific challenges. The high false-negative rate in smoke detection (15 cases) is primarily due to its combination with defocus blur, while the high false-positive rate for uneven illumination (73 cases) is due to misclassification in videos that also contain smoke, defocus blur, or both. These findings emphasize our method's difficulty in handling overlapping distortions.

Finally, comparing our two proposed methods: machine learning (Chapter 2) and deep learning (Chapter 4), provides additional insights. While the deep-learning approach achieves higher accuracy for defocus blur (97.5% vs. 97%), motion blur (97.5% vs. 95%), and smoke (85% vs. 84.5%), the machine-learning method outperforms in the inference speed, achieving 37 FPS. This makes it more suitable for real-time applications on low-cost systems. Conversely, the deep-learning method, requiring high-performance hardware, is less practical for real-time use but offers superior accuracy in most distortion types. This trade-off highlights the importance of selecting the appropriate method based on the computational resources and real-time requirements of the application.

6. Conclusion

The primary objective of this research was to develop a system capable of accurately identifying distortions in laparoscopic videos using the ResNet50 model. The outcomes, particularly regarding classification accuracy, provide strong evidence of the model's potential for improving distortion detection in laparoscopic imaging. The incorporation of mixed distortion classes proved to be an effective strategy, allowing the model to maintain high performance even when multiple distortions were present in the same video.

Looking ahead, future research will aim to further optimize the model, with a particular focus on improving inference speed and enhancing the detection capabilities for distortions such as smoke and uneven illumination. To achieve this, we plan to explore advanced techniques such as fine-tuning hyperparameters or experimenting with deeper ResNet architectures, like ResNet101 or ResNet110, to further improve performance across all distortion types. These improvements will help create a more robust and efficient system, ensuring better reliability in real-world laparoscopic video applications.

Chap 5: The laparoscopic lens-cleaning device

1. Introduction

Minimally invasive surgery reduces patient trauma, shortens hospital stays, and speeds up recovery by employing small keyhole incisions. During laparoscopic procedures, the surgical team relies on a video signal generated by the camera to guide their actions [18]. This readily available video feed offers opportunities for automatic content analysis to support the surgical team. As a result, various research groups have developed techniques to process and analyze the video signal, either in real-time during the procedure or for later post-procedural analysis [149]. In both cases, image-processing techniques are used to preprocess individual video frames, either to enhance the effectiveness of subsequent analysis steps or to improve the video's visual quality [149]. Since laparoscopic lens is frequently contaminated during surgery by bodily fluids, smoke, or condensation, which can affect visibility, real-time video analysis can be helpful in the detection of these visibility issues in the first step, and then triggering an in-vitro cleaning system to address them in the next step. These techniques fall under the concept of Computer Integrated Surgery (CIS) [149]. For this kind of assistance, the system must track the progress of the procedure and, in the event of low visibility, automatically detect and clean the laparoscopic lens.

As noted in Chapter 2, out of 61 patents reviewed, only two patents were found that incorporate an automatic detection system for laparoscopic lens contamination using laparoscopic video analysis software. The first patent is a system for monitoring and cleaning a laparoscope lens, featuring software that provides a feedback signal to a cleaning system to activate when image clarity falls below a certain threshold. It uses pressurized liquid, compressed air, and suction for cleaning [90]. The second patent describes a control system that receives one or more images of a surgical field, detects deposits on the lens, and sends a command to initiate a fluid-based lens cleaning [93]. Further details about these systems are provided in the following section.

In this chapter, we aim to present a new prototype for an in vivo lens-cleaning device that can be operated using the real-time solution outlined in Chapter 2. The integrated system is designed to detect distortions in live-captured videos and automatically trigger the cleaning of the laparoscopic lens.

The structure of this chapter is as follows: Introduction, Computer-Controlled in vivo laparoscopic lens cleaning systems, the proposed model and conclusion.

2. Computer-Controlled In vivo Laparoscopic Lens Cleaning Systems

In this section, we describe two patents identified in our study of the state of the art. These patents feature an automatic detection system that uses laparoscopic video analysis to identify reduced visibility in the surgical field. Once low visibility is detected, these systems trigger an in vivo cleaning mechanism to address the problem.

2.1. Ding et al.'s patent: Methods and systems for real-time monitoring and cleaning of a laparoscopic lens

This patent is a device featuring software that evaluates the clarity of images generated by a laparoscope, connected to a cleaning mechanism that activates when it receives a feedback signal from the monitoring software as shown in figure 1. The cleaning strategy comprises a source of pressurized liquid, a source of compressed air, and a suction system, designed to work in tandem to ensure effective cleaning [90].

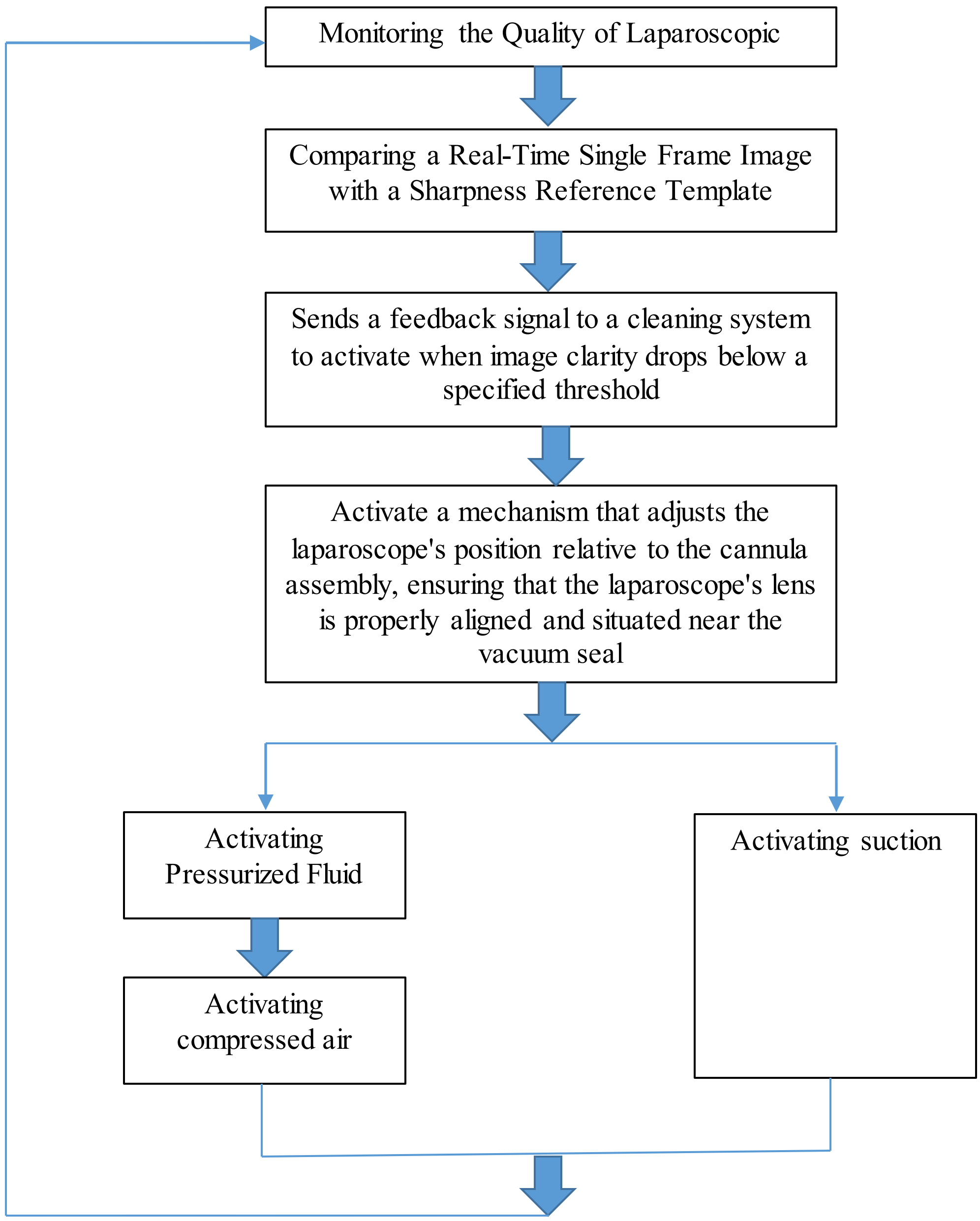

Figure 30. Diagrammatic Representation of the Detection and Cleaning Process of Ding et al.'s Patent [90].

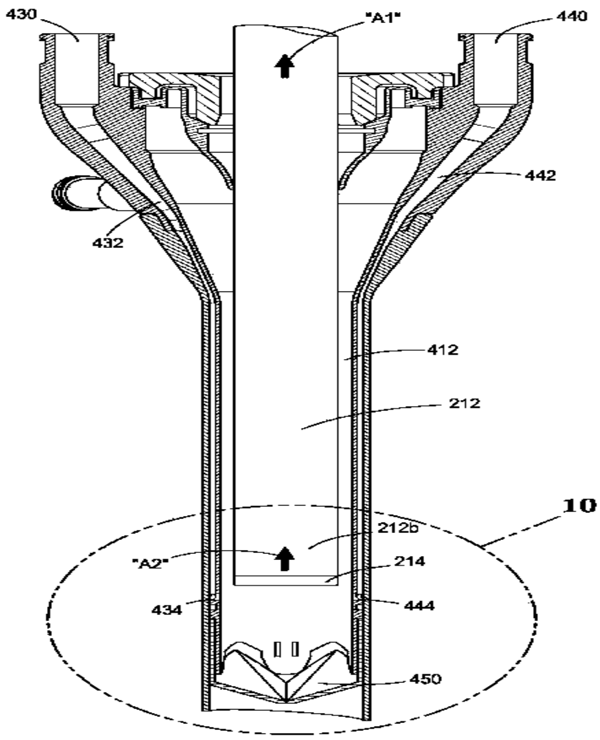

Figure 31. A cross-sectional side view of the cannula assembly illustrating the retraction of a laparoscope (image of Ding et al.'s Patent) [90].

In operation, as depicted in figure 30, the laparoscope 212 requiring cleaning is partially retracted within the cannula assembly (as indicated by the arrows "A1" and "A2" in FIG. 31), positioning the lens 214 of the laparoscope 212 just before the vacuum seal 450. A vacuum is created by connecting a suction source to the vacuum port 440, which pulls the vacuum seal tight, forming a secure closure. Liquids and/or gases are then introduced through the inlet port 430. The vacuum pulls the liquids and/or gases through the inlet tube 432 into the lens of the laparoscope via the entry opening 434, clearing away any condensation, tissue fragments, blood, or other bodily fluids. As the vacuum continues to draw, the liquids, gases, and any other removed materials exit through the exit opening 444, pass through the outlet tube 442, and leave the cannula assembly via the vacuum port 440 [90].

2.2. Coffeen et al.'s Patent : Systems and methods for intraoperative surgical scope cleaning

This patent uses an approach that includes a control procedure that communicates with a device responsible for delivering both liquid and gas flows to a surgical field for cleaning a laparoscope lens during a surgical operation. The control system receives images of the surgical field and detects lens contamination by analyzing these laparoscopic images. Upon receiving a command from the control system, the cleaning sequence initiates by supplying liquid flow for a designated first period, followed by a gas flow for a second period. The liquid and gas used in the cleaning process are saline and carbon dioxide; respectively saline is commonly used for flushing or irrigation during surgery, while carbon dioxide is used for insufflation in laparoscopic procedures.

Receives images of the surgical field from a laparoscopic source

Detecting contamination on a laparoscopic lens by analysing one or more images

The control system sends a command to a fluid management apparatus to deliver fluid to the surgical field for cleaning the laparoscopic lens

Figure 32. Diagrammatic Representation of the Detection and Cleaning Process of Coffeen et al.'s Patent [93].

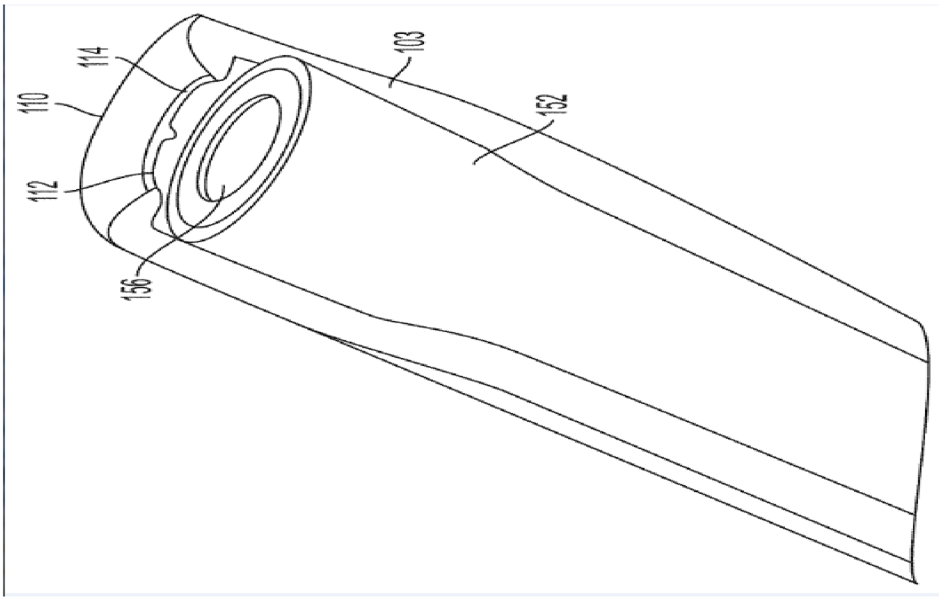

Figure 33. The cannula assembly depicting the laparoscopic cleaning system (image of Coffeen et al.'s Patent) [93].

As shown in figure 33, a sheath is designed to receive the laparoscope in the correct angular orientation, ensuring that the nozzle head 110 at the distal end 103 of the sheath is properly aligned with the lens of the laparoscope. The nozzle head features two nozzles positioned side-by-side the liquid nozzle 112 and the gas nozzle 114. These nozzles direct their respective flows onto the lens 156 at the distal end of the laparoscope's tube 152. The liquid and gas can be sprayed or blown from the nozzle head to clean the lens effectively. The liquid and gas are supplied through a supply line connected to the sheath.

The burst of gas can be used either after the liquid spray to dry the lens surface or simultaneously with the liquid spray to enhance its efficiency. The fluid management system controls the flow of both the liquid and the gas through an electromechanical valve [93].

2.3. Advantages and limits

In this section, we present the advantages and the limits of the two patents presented previously.

Table 28. The advantages and limits of Ding et al.'s and Coffeen et al.'s Patents

Patent	Advantages	Limits
Ding et al.'s Patent	- In vivo lens cleaning system. - Automatic detection of the laparoscopic lens contamination. - Efficient Cleaning strategy involves a combination of a pressurized liquid source, a compressed air source, and a suction system. - The vacuum seal provides secure sealing, creating a tight closure that prevents leakage and maintains a controlled environment for cleaning. - The system's vacuum seal and controlled flow of cleaning materials help reduce the risk of contamination, promoting a sterile environment.	- The mechanism's positioning operation not only increases the system's complexity but also adds additional time to the cleaning process, making it more time-consuming. - Add a vacuum seal to enclose the laparoscope during the cleaning process. - The system's reliance on multiple components such as vacuum, liquid, and gas flow adds complexity, which may necessitate additional maintenance or calibration. - Improper use of pressurized liquids or gases could lead to overpressure, which may damage the laparoscope or affect surrounding tissues. - The system requires specific configurations, limiting its adaptability to different laparoscopic instruments. - The current automatic detection technique is based on comparing a real-time single-frame image with a specified threshold. However, questions remain about how this threshold is determined. What type of distortion does it detect? What features are used to select this threshold?
Coffeen et al.'s Patent	- In vivo lens cleaning system. - Automatic detection of the laparoscopic lens contamination. - An effective cleaning strategy consists of supplying a liquid flow to clear away debris, followed by a gas flow to dry the lens surface, or applying the gas simultaneously with the liquid spray for enhanced cleaning efficiency. - The liquid and gas used in the cleaning process are saline and carbon dioxide. Both are used in laparoscopy and are considered safe and compatible with the human body. - The fluid management system enables precise control of liquid and gas flow through electromechanical valves, supporting automated cleaning processes.	- The sheath increases the size of the laparoscope, which is a concern given the limited space within the abdominal cavity. - This patent outlines a process for detecting contamination on a laparoscopic lens based on the analysis of one or more images. However, it doesn't specify how the system identifies low-quality images, or what method is used to make that determination.

3. The proposed model

Based on the advantages and limitations of the two patents discussed in the previous section, we determined that the second patent aligns more closely with our approach, though it requires some hardware modifications. However, for the software component, we believe that machine learning-based classification approach, can make the in vivo lens cleaning system more effective.

In this section, we propose a modified version of the lens cleaning mechanism described in Coffeen et al.'s patent, integrating the software developed with Python 3.8 (refer to Chapter 3 for more details). This combination aims to enhance the cleaning system's efficiency and accuracy.

3.1. The proposed in vivo lens cleaning mechanism

3.3.1. The hardware component

Chapter 2 emphasized that collision-based methods are more effective for in-situ laparoscopic lens cleaning compared to other techniques. As a result, the most common approach for cleaning the laparoscope lens in situ is to use an irrigation sheath that flushes liquid or gas across the lens [95]. This approach utilizes a cleaning nozzle to spray a cleaning fluid, like water, onto the viewing window to remove debris or dirt. One common drawback of cleaning nozzles is that the fluid flow tends to expand as it exits the nozzle, reducing cleaning effectiveness. To address this challenge, some nozzles have guiding elements on their side walls to channel the fluid along a specific path. However, these guiding elements lose their effectiveness once the fluid leaves the nozzle, leading to the spread of the fluid flow [87]. Additionally, the Coanda effect in a convex lens draws fluid toward its center when flowing along the curved surface. This concentration effect impedes effective cleaning when fluid is directed onto the lens from a single nozzle, preventing thorough cleaning on the opposite side [84]. Furthermore, the angular orientation of fluid or gas flow significantly impacts cleaning efficiency.

3.3.1.1 Modelling

In this work, we propose a new cleaning device prototype with a 45-degree angle for the fluid flow relative to the lens to optimize cleaning efficiency. Importantly, this angle prevents obstruction of the lens field of view by the nozzle head, a detail not addressed in Coffeen et al.'s patent.

Additionally, The nozzle head features four nozzles organized in pairs: one pair comprising a liquid nozzle beside a gas nozzle, and another pair (also with a liquid nozzle and a gas nozzle) positioned to create a 120-degree circumferential arc between the two pairs (figure 33, 34 and 35).

All bursts of liquid or gas are emitted in a fan-beam direction. There are multiple possible configurations: the two pairs of nozzles can be used either consecutively, simultaneously, or by combining one nozzle from each pair. The ultimate goal is to dry the lens surface and improve the effectiveness of the cleaning fluid.

The liquids used are warm saline and warm carbon dioxide, both heated to 37°C (body temperature) to prevent condensation caused by temperature differences between the liquid/gas and the laparoscopic lens within the patient's body.

As described in Coffeen et al.'s patent [93], the sheath includes conduits for liquid and gas that may be integrated into one side of the sheath wall. This design maintains a small diameter, allowing the sheath to fit through a standard-size trocar while being mounted to a standard-size scope.

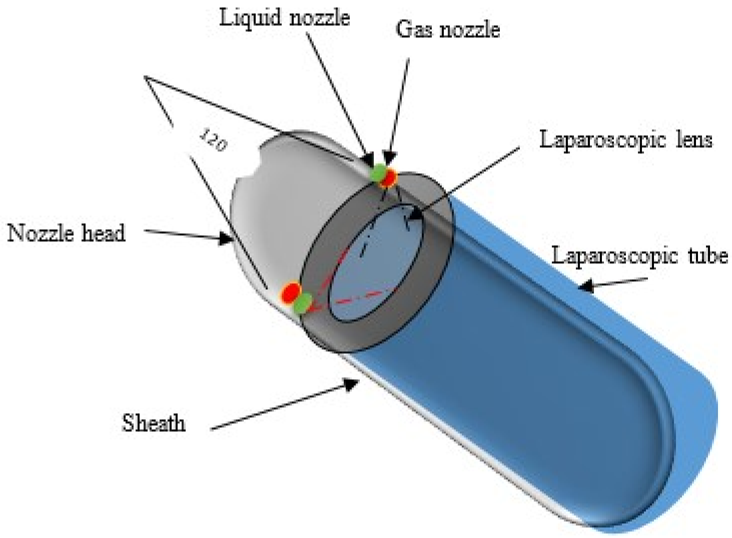

Figure 34. The proposed cannula assembly depicting the laparoscopic cleaning.

The cleaning device tailored for 10 mm diameter laparoscopes, encompassing variations with 0°, 30°, and 45° angles. The sheath has an inner diameter of 10 mm and an outer diameter of 12 mm. Consequently, the shaft thickness usually measures about 2 mm.

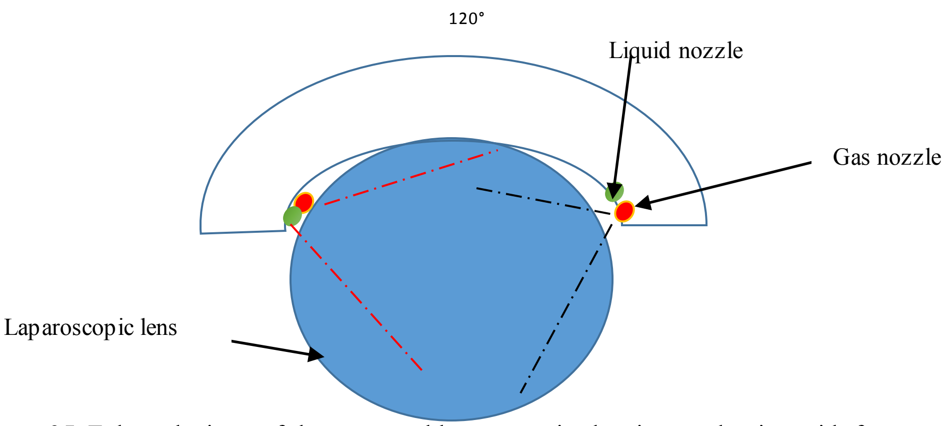

Figure 35. Enlarged views of the proposed laparoscopic cleaning mechanism with four nozzles.

- **Liquid and gas connector**

In Wayne L. et al.'s patent [53], the fluid supply apparatus includes three supplies connected to three ports of the connector: the first supplies gas for insufflating a surgical cavity, the second supplies liquid for cleaning, and the third supplies a second gas flow for clearing the liquid. In contrast, our model proposes two varieties:

- **First Solution (Personal contribution based on Coffeen et al.'s patent [93])**

  - For the additional air nozzle, we suggest using a Y-connector to split the anhydrous CO2 output from the third supply into two branches, directing them into two air nozzles.
  - For the additional liquid nozzle, we propose using a Y-connector to split the anhydrous liquid output from the second supply into two branches, directing them into two liquid nozzles (see figure 36).

- **Second Solution (Personal contribution based on Wayne L. et al.'s patent [53])**

  - This model features a Y-connector that splits the anhydrous CO2 output from the existing insufflation circuit into two branches: one directed to an insufflation trocar inserted into the body cavity and the other to the sheath for the cleaning system, as detailed in Wayne L. et al.'s patent [53].
  - The same system is used for the saline liquid by utilizing the existing saline source. This configuration eliminates the need for additional sources of liquid and carbon dioxide for lens cleaning (see figure 37).
  - For effective cleaning, it is essential to incorporate a heating instrument to obtain warmer gas and liquid.
  - To remove the solution and debris during and after cleaning, the surgeon uses the existing suction system.
  - Additionally, the mechanism should include two valves: the first for controlling the gas flow from the insufflator connection tube to the sheath, and the second for controlling the liquid flow from the liquid source connection tube to the sheath.

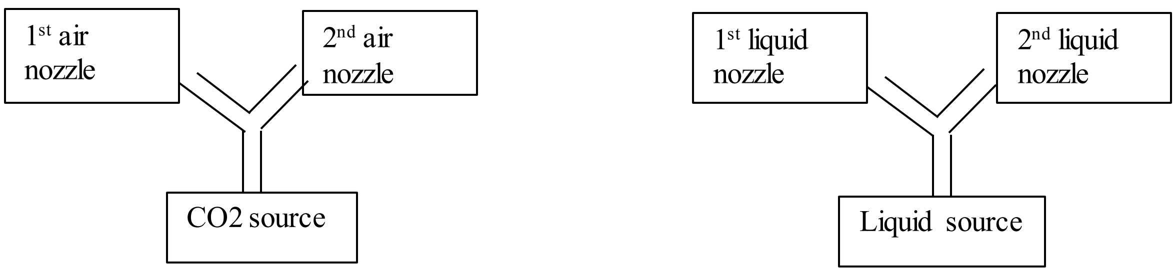

Figure 36. Schematic of the Fluid and Gas Conduits using Coffeen et al.'s supply apparatus

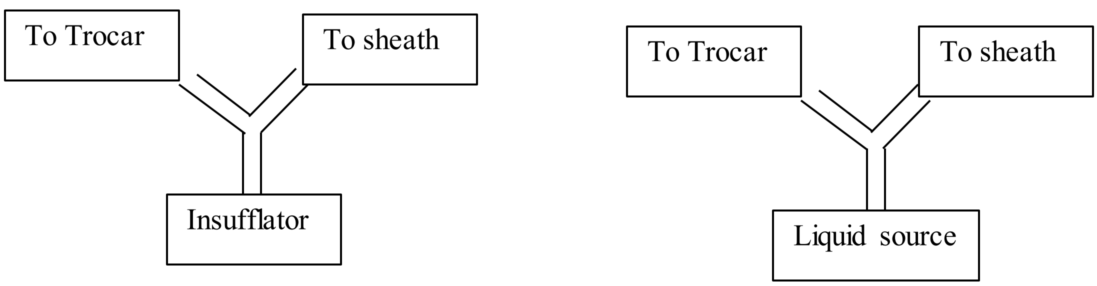

Figure 37. Schematic of the Fluid and Gas Conduits using an ordinary supply apparatus [53]

In laparoscopic lens cleaning, the delivery of cleaning fluids and gases, as well as the duration of nozzle activation, are controlled by electromechanical valves [93]. These valves consist of a magnetic coil and a valve body. The flow regulation of liquids or gases relies on electromagnetic force: when an electric current passes through the coil, it generates a magnetic field that moves the valve body. This movement opens or closes the valve [150].

3.3.1.2 Cleaning device prototype conception

For designing the in vivo laparoscopic lens-cleaning prototype, we utilized SolidWorks (figure 38), a widely used 3D CAD software in engineering fields. Developed by Dassault Systems, SolidWorks provides powerful tools for creating detailed 3D models, assemblies, and 2D drawings. It supports features like parametric design, finite element analysis (FEA), and motion simulation, making it well-suited for mechanical engineering, product development, and manufacturing. Its intuitive interface and compatibility with other engineering tools enhance efficiency throughout the design and development process [151].

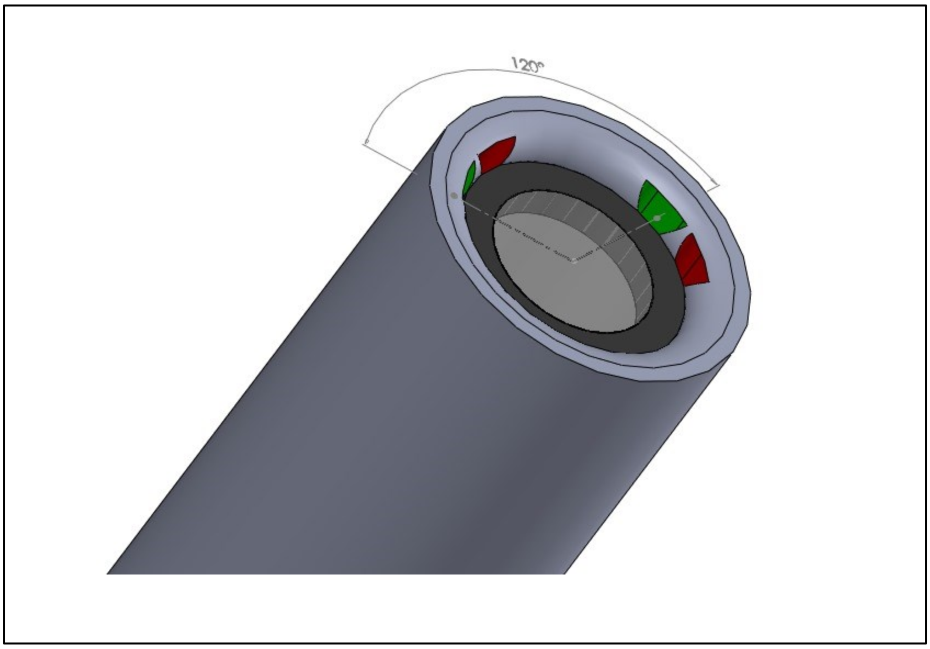

Figure 38. 3D conception of the proposed laparoscopic cleaning system

3.3.1.3 The laparoscopy lens cleaning simulation

To evaluate the effectiveness of lens cleaning of this prototype, we visualize the liquid flow coverage on the lens surface over time using the following approach:

- We divide the lens surface into a grid of small cells.
- We monitor the frequency or duration of the impact of liquid particles on each cell.
- We represent this data as a heatmap overlaid on the lens surface. This visualization allows us to identify which areas of the lens are being cleaned effectively and which areas may have insufficient coverage (figure 39 &40).
- We Count the number of grid cells with non-zero impacts.
- Finally, we calculate the percentage of lens coverage achieved.
- This simulation is implemented in Python 3.8 with a particle speed of 10 mm/s.

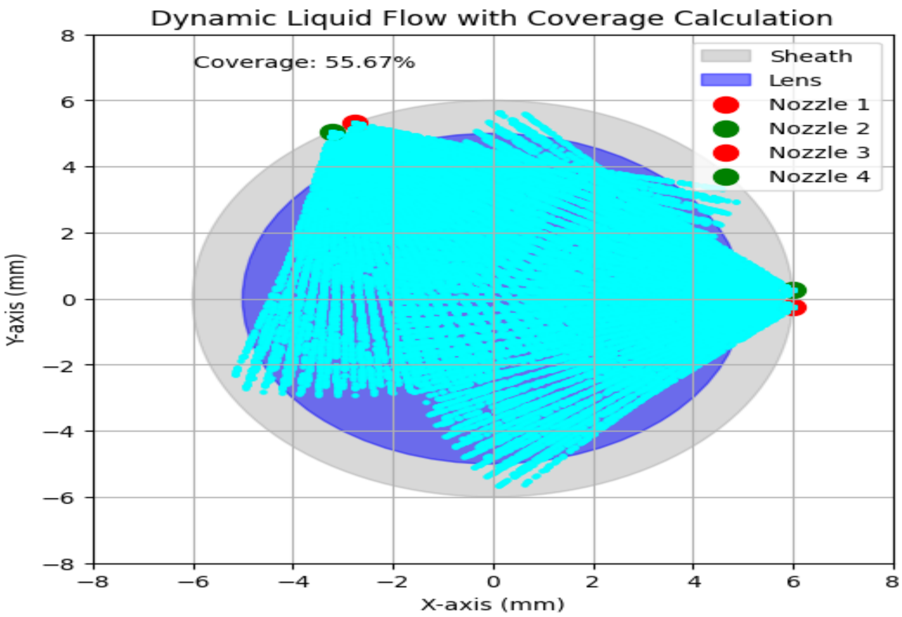

Figure 39. Liquid flow with coverage calculation of the proposed prototype

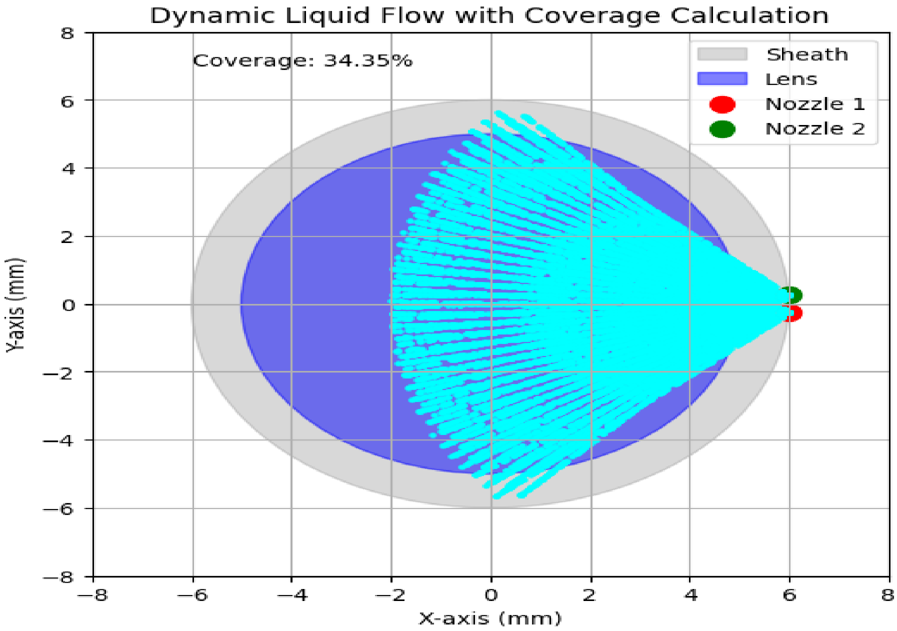

Figure 40. Liquid flow with coverage calculation of Coffeen et al.'s patent

The simulation of liquid flow during 10 seconds in two laparoscopic lens cleaning systems, Coffeen et al.'s patent, featuring a single pair of nozzles, and the proposed design with two pairs of nozzles, as illustrated in Figures 39 and 40, highlights the superior performance of our prototype. The proposed system achieves significantly greater lens liquid coverage (55.65%) than the single-pair nozzle system (34.35%). Moreover, it reduces cleaning time by efficiently covering a larger lens surface in less time.

3.3.2. The software component

The detection process includes image processing that analyzes real-time laparoscopic video frame by frame. The software for detecting laparoscopic lens contamination comprises a three-stage computational framework for automatic distortion detection. Real-time detection of defocus blur in laparoscopic video triggers an automatic in-situ lens cleaning system, detailed in the previous section. The framework employs three SVM classifiers in cascade. The first classifier assesses the video quality as high or low. The second classifier identifies the presence of blur or smoke. Finally, the third classifier distinguishes between defocus blur and motion blur (as detailed in the second paragraph). When contamination is detected, the control system sends a command to the fluid management apparatus to activate liquid and gas valves, delivering one or more fluids (liquid and gas) to the surgical field for cleaning the laparoscope lens. The control system includes one or more processors and memory, which store the program.

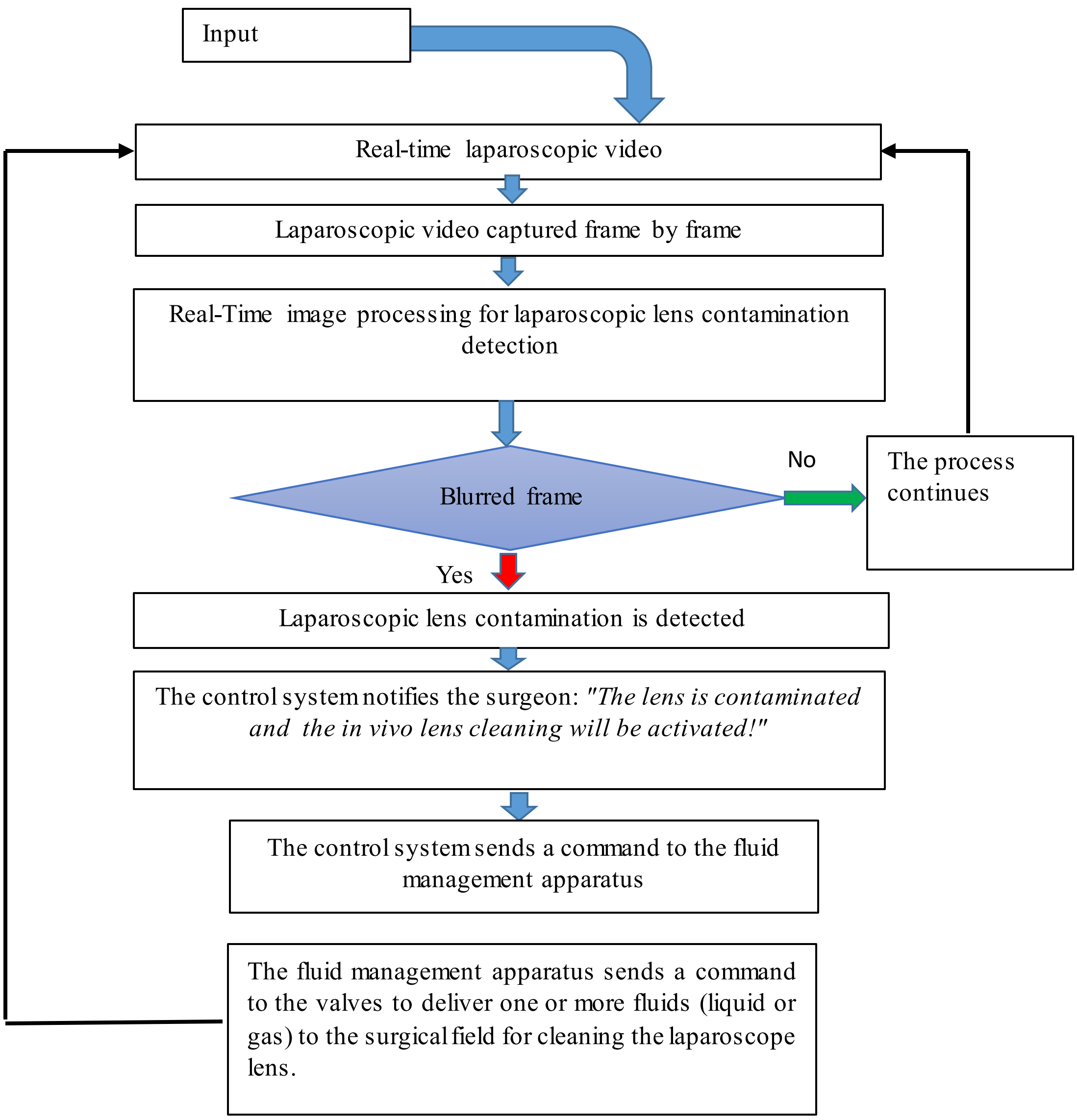

Figure 41. Flowchart of the Automated In vivo Laparoscopic Lens Cleaning System.

3.3.3. The program of detection

To develop the program for detecting laparoscopic lens contamination, we used Python 3.8 with several frameworks, including OpenCV (CV2) v4.5.5, Scikit-Learn 1.1.2, and Scikit-Image 0.19.2.3.2. For this goal we have followed these steps:

A. Generation of classes

In our program, we have used six classes organized into pairs, with each SVM classifier handling two classes (as detailed in the third chapter):

- 'DegradedImage' and 'GoodImage' classes for the first SVM classifier.
- 'BlurredImage' and 'SmokedImage' classes for the second SVM classifier.
- 'DefocusBlurImage' and 'MotionBlurImage' for the third SVM classifier.

These classes are generated by extracting frames from four video classes of the Laparoscopy Video Quality Database (LVQ) developed by Khan et al. [105]. The video classes used are:

- Reference video class: Frames extracted from this class are used to build the 'GoodImage' class.
- Defocus blur video class: Frames extracted from this class are used to build the 'DefocusBlurImage' class.
- Motion blur video class: Frames extracted from this class are used to build the 'MotionBlurImage' class.
- Smoke video class: Frames extracted from this class are used to build the SmokeImage' class.

The frames from the three previous video classes (Defocus Blur, Motion Blur, and Smoke) are merged to build the 'DegradedImage' class.

B. Detection Methods

- Blur Detection: We use the variance and maximum values derived from Laplacian and Sobel operators as image features for the SVM classifier, enabling the discrimination between blurred and non-blurred frames. For blurred images, the variance and maximum values of each operator fall below a threshold automatically determined by the SVM classifier.
- Smoke Detection: We use the SAN classifier, which relies on the histogram of the saturation channel from the HSV color space. Smoke-containing images typically exhibit reduced color, resulting in the saturation channel showing a notable correlation with the presence of smoke.
- Differentiating Good and Degraded Frames**:** We combine blur features and smoke features to distinguish between good and degraded frames.

3.3.4. Execution of the detection program

When the detection program is executed, it follows these steps:

1. **Capture video**: The program captures laparoscopic video frame by frame.
2. **Feature extraction**: It extracts features from each frame.
3. **Classification process** :

- **First Classifier**: The program combines blur features and smoke features and uses the first SVM classifier to distinguish between good and degraded frames.

- **Second classifier**: If a frame is classified as degraded, the second classifier is used to distinguish between smoke and blur.

- **Third classifier**: If a frame is classified as blurred, the third classifier differentiates between defocus blur and motion blur.

4. **Notification and cleaning starting** :

- Defocus Blur Detection: If a frame is classified as defocus blurred, the program sends a notification to the surgeon indicating that the lens is contaminated and the lens cleaning operation will be strated.

- Surgeon Response: If the surgeon allows the cleaning operation, the control system sends a command to the fluid management apparatus. (Note: This step is not implemented in this project as the cleaning device has not yet been developed).

3.3.5. Conversion of the python program to executable

Python does not convert its code directly into machine code that the hardware can understand. Instead, it compiles the code into bytecode (.pyc or .pyo files). The CPU cannot directly understand this bytecode. Therefore, an interpreter called the Python Virtual Machine (PVM) is needed to execute the bytecode [152].

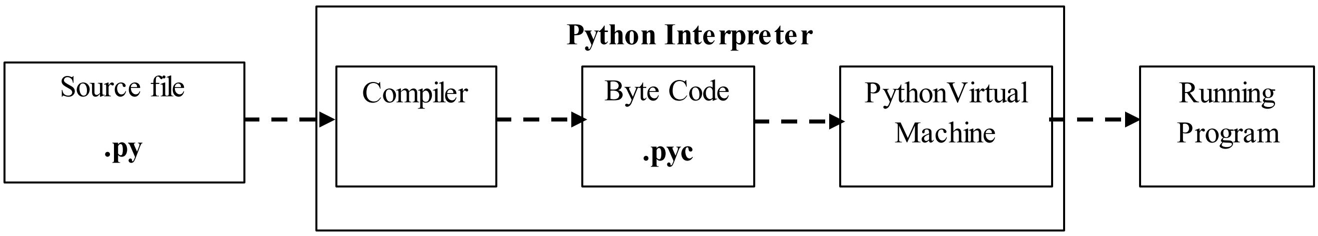

Figure 42. Python's Internal Processes [152]

Step 1: The Python compiler reads the Python source code in the code editor, which is then saved as a .py file on the system. This stage marks the beginning of code execution.

Step 2: During the compilation, the source code is converted into bytecode. The Python compiler checks for syntax errors and generates a .pyc file.

Step 3: The bytecode (.pyc file) is then sent to the Python Virtual Machine (PVM). The PVM converts the Python bytecode into machine-executable code, reading and executing the file line by line. If an error occurs during this interpretation, execution is stopped, and an error message is displayed.

Step 4: The PVM converts bytecode into machine code understandable by the system's CPU [152].

3.3.6. Running a Python program directly on a processor without operating system

As discussed in the previous section, Python typically relies on the services provided by an operating system (OS). Running a Python program directly on a processor without an OS can be accomplished using minimalistic runtime environments or specialized tools designed for such constrained environments.

In this project, the program of lens contamination detection can be integrated into the laparoscopic control system by incorporating it into a processor that can take the real-time laparoscopic video as input and send commands to the fluid management system as output (figure 41).

One approach to running a Python program on a processor without a traditional operating system is the use of MicroPython, which is an implementation of the Python 3 programming language that includes a small subset of the Python standard library and is optimized to run on microcontrollers and in constrained environments [153].

MicroPython comprises a Python compiler, a runtime interpreter, and a small subset of the Python standard library. It supports various microcontrollers such as ESP32, ESP8266 and boards such as Pyboard (Figure 44).

MicroPython can be used for implementing motor control, sensor processing, and decision-making logic in robotics projects [154].

The steps for using MicroPython are as follows:

- The Choosing of a Supported Microcontroller is based on the project's requirements.
- For the specific microcontroller, the MicroPython firmware is downloaded and flashed onto the device.
- Then Python scripts are uploaded to the microcontroller.
- The MicroPython interpreter will run the Python script on the microcontroller [154].

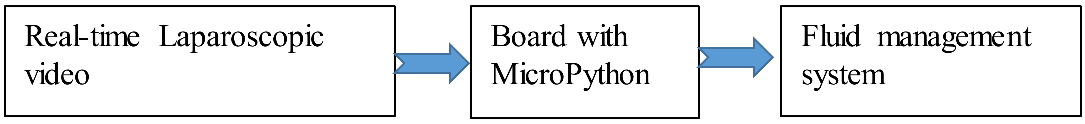

Figure 43. Schematization of the use of our Python script on MicroPython for automatic laparoscopic lens cleaning.

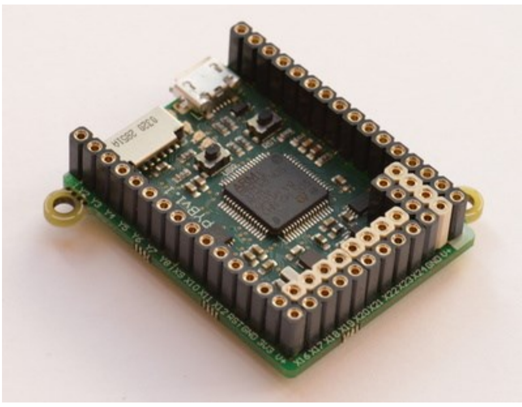

Figure 44. Example of a MicroPython microcontroller board (the pyboard) [153](STM32F405RG microcontroller, 168 MHz Cortex M4 CPU, 1048KB flash ROM and 196KB RAM)

4. Conclusion

During minimally invasive surgery, the laparoscopic lens can become contaminated by debris, blood, fog, and smoke, which obstruct the surgeon's visual field and distort the real-time video. It is crucial for supporting surgeons to have an effective system for detecting and eliminating this contamination in real time without interrupting the surgical procedure.

In this chapter, we utilized an existing patent and proposed a few hardware modifications for automatic laparoscopic lens cleaning contamination detection and cleaning. For the lens cleaning device prototype, we propose the following modifications: a 45-degree angle for the fluid flow relative to the lens to optimize cleaning efficiency and prevent obstruction of the lens field of view by the nozzle head, and the addition of two nozzles (a liquid nozzle and a gas nozzle). This configuration results in four nozzles organized in pairs, with one pair comprising a liquid nozzle beside a gas nozzle and another pair of nozzles positioned to create a 120-degree circumferential arc between the two pairs.

A 10-second liquid flow simulation demonstrates the superior performance of our prototype, achieving significantly greater liquid coverage on the lens compared to the single-pair nozzle system. Additionally, the proposed design efficiently reduces cleaning time by covering a larger lens surface more quickly.

Our goal is to enhance this mechanism by integrating our automatic lens contamination detection program. The Python script can also be used to command the modified in situ laparoscopic lens-cleaning device, taking advantage of the program's high accuracy and processing speed.

Chap 6: Summary and Future works

This chapter synthesizes the key findings of this thesis and explores potential avenues for future research. Section 1 offers a comprehensive overview of the accomplishments within the scope of the thesis, highlighting the primary conclusions drawn from the study. Section 2 proposes potential enhancements and expansions that could build upon the current work, suggesting areas where further investigation could be beneficial.

1. Conclusions

Laparoscopy, or minimally invasive surgery (MIS), allows for the internal examination of the abdominal cavity, uterus, ovaries, and fallopian tubes. MIS has gained widespread acceptance due to its significant benefits over traditional open surgery, such as quicker patient recovery, lower costs, shorter hospital stays, smaller incisions, and a reduced risk of surgical site infections.

In laparoscopic procedures, surgeons rely on real-time video feeds from a camera inserted into the body to guide their actions. This video stream presents valuable opportunities for automated content analysis, which can assist the surgical team by providing real-time or post-operative insights. Consequently, various research groups have developed techniques to process and analyze these video signals, leveraging image-processing methods to enhance the quality of individual video frames. These enhancements can improve the effectiveness of subsequent analysis or the visual clarity of the video.

One of the challenges during laparoscopy is maintaining clear visibility, as the lens is often obstructed by bodily fluids, smoke, or condensation.

Existing research addressing these issues has primarily focused on improving the quality of laparoscopic video by classifying various distortions. However, these approaches often do not differentiate between distortions caused by laparoscopic lens contamination and those resulting from technical issues. In minimally invasive surgical procedures, the majority of distortions encountered by surgeons, such as blurring and smoke, are due to contamination of the laparoscopic lens. Recognizing this, the work presented in this thesis has concentrated on overcoming these challenges by developing methods specifically aimed at detecting and addressing distortions caused by lens contamination.

The upcoming paragraphs offer a concise overview of the research conducted in this thesis, along with the conclusions drawn. Following this summary, the next section will outline potential perspectives for future research and development.

We began by introducing laparoscopy, detailing its definition, applications, instruments involved, as well as its benefits and limitations. Additionally, we reviewed the techniques currently employed for cleaning camera optics in laparoscopic systems, highlighting their limitations.

For our next contribution, we conducted a systematic review guided by the Preferred Reporting Items for Systematic Reviews and Meta-Analyses (PRISMA) guidelines. Our research focused on answering the question: "What is the most effective category of patents for in-situ cleaning of laparoscopic lenses to achieve a successful patent?" We performed a comprehensive literature search using the ESPACENET electronic database, including patents published in English after

December 1, 2015 (the date of Kreeft et al.'s research). We specifically targeted in-situ lens cleaning patents and excluded those published before December 2015, duplicate patents, external lens cleaning patents, and non-English texts.

Each patent's status was evaluated using a 3-point Likert scale: (0) points for abandoned, (1) points for pending, and (2) points for granted applications. The goal of our review was to assess, summarize, and determine the current status of each patent, focusing on their overall effectiveness across different categories. Our findings revealed that 48% of granted patents fall under the collision methods category, while 56% of abandoned patents are associated with brush/wipe methods. Among the patents linked to commercialized products, four devices were identified: EndoClear by Virtual Ports Ltd, Kelling™ Device by ClearCam Inc., FloShield Air by Minimally Invasive Devices, Inc., and ClickClean by Medeon Biosurgical, Inc.

As our third contribution, we developed a machine learning-based method for the automatic detection of distortions in laparoscopic videos. To accomplish this, we introduced a novel framework that utilizes a cascaded support vector machine (SVM) classifier, consisting of three sequentially interconnected SVMs. Our machine-learning model demonstrated impressive performance, achieving a high inference speed of 37 frames per second (fps). This result highlights the practicality of implementing our algorithm in real-time systems, including on low-cost computers, to detect distortions in live laparoscopic videos.

As our fourth contribution, we employed Residual Networks (ResNet50) to detect and classify five distortions in laparoscopic videos: noise, defocus blur, motion blur, smoke, and uneven illumination. Our computational framework was initially trained on the LVQ Challenge dataset.

The results, especially regarding accuracy, are promising, providing a strong basis for enhancing distortion detection in laparoscopic videos. Furthermore, the inclusion of mixed classes has significantly improved the model's ability to accurately identify individual distortions, even when multiple distortions occur simultaneously.

In the final chapter, we introduced a new prototype for an in vivo lens-cleaning device operating using a real-time solution. This integrated system is capable of detecting distortions in live laparoscopic videos and automatically initiating the cleaning of the lens.

The hardware design is based on modifications of Coffeen et al.'s patent, but we have enhanced the software component by incorporating our machine learning-based classification approach, which we believe will significantly improve the effectiveness of the lens cleaning system.

To achieve effective cleaning, we recommend angling the fluid flow at 45 degrees relative to the lens surface. The nozzle head in our design incorporates four nozzles arranged in pairs, an improvement over Coffeen et al.'s two-nozzle configuration. Each pair includes one liquid and one gas nozzle, designed to emit bursts in a fan-shaped pattern for enhanced coverage.

The cleaning process utilizes warm saline and warm carbon dioxide, both heated to 37°C (body temperature), to prevent condensation caused by temperature differences between the cleaning fluids and the laparoscopic lens within the patient's body. Simulation of the liquid flow highlights the superior performance of our prototype, achieving significantly better liquid coverage on the lens compared to the single-pair nozzle system. Furthermore, the proposed design reduces cleaning time by efficiently covering a larger lens area in a shorter duration.

2. Future Work

The research conducted in this thesis on developing a real-time video analysis system to detect low visibility during laparoscopy and trigger an automated lens cleaning system can be further refined and expanded in several ways. Key directions for future work include:

Incorporating Deep Learning Algorithms: Leveraging deep learning techniques offers numerous advantages over traditional machine learning methods, including automatic feature extraction, superior handling of large and complex datasets, enhanced performance, and better management of non-linear relationships.

Enhancing the ResNet50 Model: Improving the ResNet50-based model to address current limitations, particularly in terms of inference speed and the detection of smoke and uneven illumination. This could involve fine-tuning hyperparameters or upgrading to more advanced models like ResNet101 or ResNet110 to boost performance.

Fabricating and Integrating the Lens Cleaning Device: Moving forward with the fabrication of the lens cleaning device based on the prototype developed in this work. Once built, the device should be integrated with the software, and both components should be incorporated into a fully functional laparoscopic system. This will enable comprehensive testing and validation in real-world surgical environments.

References

1- Top Sante. Laparoscopie (cœlioscopie). [Online]. Available: https://www.topsante.com/medecine/examens-medicaux/laparoscopie-coelioscopie.

2- Zest de savoir. [Online]. Available: https://zestedesavoir.com/articles/4085/les-revers-de-la-chirurgie.

3- Humatem. (2024). Colonne de Coelioscopie [Online]. Available: https://www.humatem.org/telecharger_fiche_info/12.

4- UMVF. (2008). Coelioscopie et coeliochirurgie : principes généraux et instrumentation. [Online]. Available: https://archives.uness.fr/sites/campus-unf3s-2014/chirurgie-generale/enseignement/coelioscopie/site/html/cours.pdf.

5- Karl Storz. ENDOCAMELEON. [Online]. Available: https://www.karlstorz.com/cps/rde/xbcr/karlstorz_assets/ASSETS/3591906.pdf.

6- ScopeCare. (2024). Rigid and Semi-Rigid endoscopes. [Online]. Available: https://www.scopecare.com/rigid-and-semi-rigid-endoscopes/.

7- Lee Swanstrom. (2019). Evaluation of Safety and Efficacy of Using EndoClear-Endoscopic Lens Cleaning Device. [Online]. Available: https://ichgcp.net/clinical-trials-registry/NCT01197222.

8- Maria Cassera, Trudie Goers, Georg Spaun, and Lee Swanstrom, "Efficacy of Using a Novel Endoscopic Lens Cleaning Device: A Prospective Randomized Controlled Trial." *Surgical innovation,* Vol. 18pp. 150-5, 02/01 (2011).

9- Kyle Weld *et al.*, "Analysis of Surgical Smoke Produced by Various Energy-Based Instruments and Effect on Laparoscopic Visibility." *Journal of endourology / Endourological Society,* Vol. 21pp. 347-51, 03/01 (2007).

10- Neil Fleshner and Damien Bolton, "Laparoscopic Lens Fogging: A Review of Etiology and Methods to Maintain a Clear Visual Field." *Journal of endourology / Endourological Society,* Vol. 24pp. 905-13, 04/01 (2010).

11- Ivan Macia and Dominique Gossot, "Maintaining a clear vision during long-lasting thoracoscopic procedures." *Interactive cardiovascular and thoracic surgery,* Vol. 11pp. 522-4, 11/01 (2010).

12- Derek van Deurzen, G. Mannaerts, Jack Jakimowicz, and Alfred Cuschieri, "Prevention of lens condensation in laparoscopic surgery by lens heating with a thermos flask." *Surgical Endoscopy,* Vol. 19pp. 299-300, 03/01 (2005).

13- Toray Industries. (2024). Sterile optical lens cleaning cloth for endoscopic surgery. [Online]. Available: https://www.toray.com/global/lifeinnovation/medical/.

14- KARL STORZ. CLEARVISION® II. [Online]. Available: https://www.strattner.com.br/wp-content/uploads/2020/11/CLEARVISION-II.pdf.

15- Olympus. InstaClear. [Online]. Available: https://medical.olympusamerica.com/products/instaclear.

16- Yoshinori Komazawa *et al.*, "Oolong tea is useful for lens cleansing in transnasal small-caliber esophagogastroduodenoscopy." *Endoscopy,* Vol. 42pp. 104-8, 12/01 (2009).

17- D. Kreeft, E. A. Arkenbout, P. W. J. Henselmans, W. R. van Furth, and P. Breedveld, "Review of Techniques to Achieve Optical Surface Cleanliness and Their Potential Application to Surgical Endoscopes." *Surg Innov,* Vol. 24 (No. 5), pp. 509-27, Oct (2017).

18- Bruce Levy and Mohammad Mobasheri, "Principles of safe laparoscopic surgery." *Surgery (Oxford),* Vol. 35 (No. 4), pp. 216-19, (2017).

19- D. A. Wiegmann, A. W. ElBardissi, J. A. Dearani, R. C. Daly, and T. M. Sundt, 3rd, "Disruptions in surgical flow and their relationship to surgical errors: an exploratory investigation." *Surgery,* Vol. 142 (No. 5), pp. 658-65, Nov (2007).

20- E. Sutton *et al.*, "Gaze disruptions experienced by the laparoscopic operating surgeon." *Surg Endosc,* Vol. 24 (No. 6), pp. 1240-4, Jun (2010).

21- A. Nabeel, S. K. Al-Sabah, and H. Ashrafian, "Effective cleaning of endoscopic lenses to achieve visual clarity for minimally invasive abdominopelvic surgery: a systematic review." *Surg Endosc,* Vol. 36 (No. 4), pp. 2382-92, Apr (2022).

22- J. T. Calhoun and J. A. Redan, "Elimination of laparoscopic lens fogging using directional flow of CO2." *JSLS,* Vol. 18 (No. 1), pp. 55-61, Jan-Mar (2014).

23- B. Mohammadhosseini, "Povidone-iodine surgical scrub solution prevents fogging of the scope's lens during laparoscopic surgery." *Surg Endosc,* Vol. 24 (No. 6), pp. 1498-9; author reply 500, Jun (2010).

24- Austin Drysch, Kenneth Schmitt, Brittany Uribe, Renai Yoon, Zhamshid Okhunov, and Jaime Landman, "Comparative analysis of techniques to prevent laparoscopic fogging." *Minimally Invasive Therapy & Allied Technologies,* Vol. 25 (No. 6), pp. 319-22, 2016/11/01 (2016).

25- T. G. Manning *et al.*, "Laparoscopic lens fogging: solving a common surgical problem in standard and robotic laparoscopes via a scientific model." *Surg Endosc,* Vol. 32 (No. 3), pp. 1600-06, Mar (2018).

26- V. Palvia, A. J. H. Gonzalez, R. S. Vigh, and J. N. Anasti, "A Randomized Controlled Trial Comparing Laparoscopic Lens Defogging Techniques through Simulation Model." *Gynecol Minim Invasive Ther,* Vol. 7 (No. 4), pp. 156-60, Oct-Dec (2018).

27- T. Song and D. H. Lee, "A randomized Comparison of laparoscopic LEns defogging using Anti-fog solution, waRm saline, and chlorhexidine solution (CLEAR)." *Surg Endosc,* Vol. 34 (No. 2), pp. 940-45, Feb (2020).

28- Robin Merkx *et al.*, "Effectiveness of Heated Sterile Water vs ResoClear® for Prevention of Laparoscopic Lens Fogging in a Randomized Comparative Trial." *Journal of Endourology,* Vol. 32 (No. 1), pp. 54-58, 2018/01/01 (2017).
29- E. Kobayashi *et al.*, "A novel device for cleaning the camera port during laparoscopic surgery." *Surg Endosc,* Vol. 30 (No. 1), pp. 330-4, Jan (2016).
30- H. Tatsuki *et al.*, "A novel one-step lens cleaning device using air and water flow for endoscopic surgery." *PLoS One,* Vol. 13 (No. 7), p. e0200749, (2018).
31- Ravinder Kumar, Shaan Jallu, Kritika Pasricha, Bijit Basumatary, Bhanu Pratap Singh Parmar, and Ashish Kumar Sahani, "Laparoscopic Lens Defogging: a Review of Methods to Maintain a Clear Operating Field." *Indian Journal of Surgery,* Vol. 84 (No. 4), pp. 698-706, (2021).
32- Kenneth Buxey, S. Wong, and M. Pham, "Novel Technique for Defogging and Cleaning the Laparoscope Lens uring Minimally Invasive Surgery." *Hellenic Journal of Surgery,* Vol. 90pp. 321-22, 11/01 (2018).
33- James A. Brown, Michelle D. Inocencio, and Chandru P. Sundaram, "Use of a Warming Bath to Prevent Lens Fogging during Laparoscopy." *Journal of Endourology,* Vol. 22 (No. 11), pp. 2413-14, 2008/11/01 (2008).
34- D. Hashimoto and M. Shouji, "Development of a fogless scope and its analysis using infrared radiation pyrometer." *Surgical Endoscopy,* Vol. 11 (No. 8), pp. 805-08, 1997/08/01 (1997).
35- Rayan Fayad, Houssein Hajj Hassan, and Mohamad Hajj-Hassan, Transparent ITO-based Heater for Prevention of Laparoscopic Lens Fogging. (2019), pp. 1-4.
36- Ceana Nezhat and Vadim Morozov, "A Simple Solution to Lens Fogging during Robotic and Laparoscopic Surgery." *JSLS : Journal of the Society of Laparoendoscopic Surgeons / Society of Laparoendoscopic Surgeons,* Vol. 12p. 431, 11/30 (2007).
37- Y. Fisher, "Retractable wipe for cleaning endoscopic surgical devices." Patent US5514084A, (1994).
38- Miller EC and Gatos L, "Endoscope Lens Cleaner." Patent US20090105543A1, (2008).
39- Guru K and Chowriappa A, "Lens cleaning instrument for surgical procedures performed in an enclosed cavity." Patent WO2014145063, (2014).
40- Josh Kessler and Marc Rd, "Light source and lens cleaner for laparoscopic surgery." Patent US20090240111, (2009).
41- C. A. Clark, A. I. Fleming, and C. O'Prey, "Endoscope wiper blade cleaner." Patent AU2011236022, (2011).
42- H Zarate, "Endoscopic lens cleaner." Patent US8460180, (2013).
43- R. J. Cercone, M. K. Adams, D. L. Gatto, and D. R. Valentine, "Endoscope cleaning and defogging apparatus." Patent US5274874, (1994).
44- R. A. Gomez and S. L. Heck, "Minimally invasive apparatus and method for cleaning endoscope lenses." (2014).
45- R. Hurst, "System and method for cleaning a scope during a surgical procedure." Patent US20140246051, (2014).
46- C. O'Prey, V. A. Scott, and A. I. Fleming, "Thoracic scope port cleaner." Patent US20130150670, (2013).
47- U. Gordin, G. Heftman, M. Sobol, A. Schvartzer, and A. Szold, "Lens cleaning device, system and method for surgical procedures." Patent US20090250081, (2009).
48- S. A. Swallert, "Rotable lens cleaning device." Patent US6258025, (2001).
49- B. E. Wiita, M. J. Teets, and G. D. Wiita, "Lens cleaning apparatus." Patent EP0664101, (1995).
50- A. C. Smith and G. F. Peters, "Method and apparatus for cleaning an endoscope lens." Patent US6447446, (2002).
51- G. Grice and J. Miles, "Disposable scope cleaner and method of using same." Patent US20060293559, (2006).
52- D. T. Kato, "Automated laparoscopic lens cleaner." Patent US6354992, (2002).
53- W. L. Poll, M. J. Huddleston, C. M. Crisafulli, A. Landis, and G. P. Drach, "Patent Application Publication." Patent US20150005582, (2015).
54- L. Sasaki, "Laparoscopic lens cleaner." Patent US8047215, (2011).
55- T. Kawanishi, "Observation window cleaning device for endoscope." Patent US20070225566, (2007).
56- R. Fujimoto, "Endoscope cleaning sheath, and endoscope apparatus and endoscope comprising the cleaning sheath." Patent US20080188715, (2011).
57- S. Miyamoto and A. Suzuki, "Endoscope, distal end cap-equipped endoscope and endoscope cleaning sheath." Patent US20130204088, (2013).
58- M. Shalman, "Endoscope with cleaning optics." Patent US20040220452, (2008).
59- A. G. James, J. Chen, and A. A. Wills, "Flow guide for an endoscope." Patent GB2481727, (2009).
60- H. Kawano, "Cleaning device for cleaning view window of endoscope." Patent US6409657, (2002).
61- I. I. William B. Weisenburgh, C. J. Hess, R. H. Nobis, D. B. Griffith, and R. M. Trusty, "Apparatus and methods for cleaning the lens of an endoscope." Patent US20130217970, (2013).
62- M. D. Maguire, "Endoscope cleansing catheter and method of use." Patent US5337730, (1992).
63- D. L. Emmons, III, "Dental mirror with mirror cleaning suction." Patent US8133052, (2012).
64- N. J. McCaffrey, "Electromechanical in-situ cleaning of optical elements." Patent US20080188714, (2008).
65- T. Peterson and D. Pal, "Method and apparatus for cleaning medical instruments and the like." Patent WO0053341, (2000).
66- Jp Iv Newton, "Method and apparatus for cleaning the field of view of an endoscopic lens." Patent US20120178995, (2012).
67- T. Bahls and F. A. Froehlich, "Camera system and method for cleaning a camera." Patent US20150216401, (2015).
68- P. H. Kwon, J. L. Levinsohn, and J. R. Swift, "APPARATUS AND METHOD FOR IN VIVO CLEANING OF AN OPTICAL LENS OF A SURGICAL VISUALIZATION DEVICE." Patent US20220061646, (2022).

69- C Rylander, C Idelson, and J Uecker, "Devices, systems and methods for cleaning of elongated instrument surface." Patent US11058291B2, (2021).
70- C. Rylander, C. Idelson, and J. Uecker, "Devices, systems and methods for cleaning of elongated instrument surface." Patent *WO2019226855A1*, (2019).
71- J. Williams, "Endoscope cleaning device." Patent US20220047354A1, (2022).
72- J. J. Thomas *et al.*, "Endoscope cleaning device." Patent US20220039912A1, (2022).
73- J. L. Gilkey and M. R. Gilkey, "Imaging element cleaning apparatus." Patent US20210100444A1, (2021).
74- M. Syed Ahmed, A. H. Mujawar, J. S. S. Maddur, and Y. K. Vikharankar, "Intraoperative lens cleaning device." Patent US20190231183A1, (2019).
75- J. L. Rosenbaum *et al.*, "SCOPE WITH INTEGRAL CLEANING ELEMENT FOR USE DURING A LAPAROSCOPIC PROCEDURE." Patent US20180344141A1, (2018).
76- D. P. Allen and R. M. Evans, "Surgical access device incorporating scope cleaner." Patent 20190110674A1, (2019).
77- C. Idelson, C. Rylander, M. R. Gilkey, and J. L. Gilkey, "Wiper assembly for imaging element-cleaning apparatus." Patent US20190110674A1, (2021).
78- J. L. Gilkey and M. R. Gilkey, "Imaging element-cleaning device with imaging device fitment adjustability." Patent US10993609B1, (2021).
79- X. Liu, "Surgical Lens Cleaning Device." Patent US2021033854A1, (2021).
80- E. C. Leuthardt, G. Genin, C. Yarbrough, T. Somers, and D. Margolis, "Self-cleaning endoscope." Patent US10709321B2, (2020).
81- LM, Faria, D, Gaidos, NH, and Marshall, "Apparatus for cleaning an imaging system used during a medical procedure." Patent US20190110675A1, (2019).
82- A. N. Anki and S. K. Al Sabah, "Cleaning device for surgical tool." Patent US11123152B2, (2021).
83- S. Retailleau, R. C. Reid, and E. Brennan, "Cleaning devices for instruments, and related methods." Patent US20210219832A1, (2021).
84- T and Watanabe, "Endoscope." Patent US20210177249A1, (2021).
85- T. Watanabe, H. Okano, and T. Ito, "Endoscope having observation window with circumferential side surface and cleaning nozzles directed to circumferential side surface." Patent US11042020B2, (2021).
86- R. Yan and S. Takeuchi, "Endoscope observation window cleaning." Patent US 20220104696A1, (2022).
87- D. B. Roppenecker, G. W. Schütz, and N. R. Tobies, "Endoscope with improved viewing window cleaning nozzle." Patent WO2021219826A1, (2021).
88- R. Yan and S. Takeuchi, "Endoscope observation window cleaning." Patent US20200367736A1, (2020).
89- A. Mowlai-Ashtiani and P. Berman, "Lavage and Cleansing System and Method." Patent US20220125288A1, (2022).
90- W. Ding, S. Ahamed, K. Huang, and K. Zhang, "Methods and systems for realtime monitoring and cleaning of a laparoscopic lens." Patent WO2021179249A1, (2021).
91- C. Wright, E. C. Close, and K. H. Lipkin, "Optical entry trocar camera." Patent WO2019227018A1, (2019).
92- K. Matsumoto, K. Takagi, T. Nagayasu, and H. Takezaki, "Rigid endoscope cover and endoscope unit." Patent US20210228069A1, (2021).
93- J. Coffeen, T. Leclere, and E. Huynh, "Systems and methods for intraoperative surgical scope cleaning." Patent US20200375444A1, (2020).
94- H. E. Holsten, P. D. Richard, G. P. Ebersole, and S. P. Budhabhatti, "Endoscope including a cleaning assembly." Patent US20210369098A1, (2021).
95- K. Arcot, W. Johnston, Z. Zohny, and S. Ravi, "Endoscope lens cleaning device." Patent US010806337B2, (2017).
96- T. Hsu and S. Hsu, "Devices and methods for removal of debris from the objective lens of an endoscope." Patent US9241610B2, (2016).
97- D. M. Pattison and H. E. Holsten, "Hydrophobic finish for medical devices." Patent US20210315441A1, (2021).
98- National Institute of Biomedical Imaging and Bioengineering. (2020). Mini wiper blade enables clear view through minimally invasive surgical scope. [Online]. Available: https://www.nibib.nih.gov/news-events/newsroom/mini-wiper-blade-enables-clear-view-through-minimally-invasive-surgical-scope.
99- Mitsubishi Medical. (2014). FloShield. [Online]. Available: https://www.novuslight.com/mitsubishi-medical-to-distribute-floshield-in-japan_N2935.html.
100- INC FloShield. (2024). FloShield Air. [Online]. Available: https://floshield.com/floshield-air.
101- Inc Medeon Biodesign. (2020). ClickClean. [Online]. Available: https://clickclean-medeon.com/].
102- S. Bendifallah *et al.*, "Prospective, randomized comparison of the use of FloShield Air System((R)) versus the reference technique (water + povidone-iodine solution) during gynecologic endoscopic surgery to evaluate the operative lens vision quality." *Surg Endosc,* Vol. 32 (No. 3), pp. 1593-99, Mar (2018).
103- S. Golestani, C. Hill, J. Ali, C. Idelson, C. Rylander, and J. Uecker, "A Clean Sweep: Initial Experience with a Novel Intracavity Laparoscopic Cleaning Device." *JSLS,* Vol. 26 (No. 4), Oct-Dec (2022).
104- M. B. Martin, "Improved visibility during bariatric surgery with in situ laparoscopic lens cleaning." in *Surgical endoscopy*, (2021), Vol. 35: *NLM (Medline)*, pp. 104-330.

105- Z. A. Khan *et al.*, "Towards a Video Quality Assessment based Framework for Enhancement of Laparoscopic Videos." 2020/3// (2020).
106- P. Sánchez-González *et al.*, "Laparoscopic video analysis for training and image-guided surgery." in *Minimally Invasive Therapy and Allied Technologies* Vol. 20, ed, (2011), pp. 311-20.
107- J. Cartucho, S. Tukra, Y. Li, D. S. Elson, and S. Giannarou, "VisionBlender: a tool to efficiently generate computer vision datasets for robotic surgery." *Computer Methods in Biomechanics and Biomedical Engineering: Imaging and Visualization,* Vol. 9 (No. 4), pp. 331-38, (2021).
108- S. Voros, J.A. Long, and P. Cinquin, "Automatic detection of instruments in laparoscopic images: A first step towards high-level command of robotic endoscopic holders." in *International Journal of Robotics Research*, (2007), Vol. 26, pp. 1173-90.
109- D. Owen, M. Grammatikopoulou, I. Luengo, and D. Stoyanov, "Automated identification of critical structures in laparoscopic cholecystectomy." *International Journal of Computer Assisted Radiology and Surgery,* Vol. 17 (No. 12), pp. 2173-81, 2022/12// (2022).
110- E. Padovan *et al.*, "A deep learning framework for real-time 3D model registration in robot-assisted laparoscopic surgery." *International Journal of Medical Robotics and Computer Assisted Surgery,* Vol. 18 (No. 3), 2022/6// (2022).
111- M. Carstens *et al.*, "The Dresden Surgical Anatomy Dataset for Abdominal Organ Segmentation in Surgical Data Science." *Scientific Data,* Vol. 10 (No. 1), pp. 3-3, 2023/1// (2023).
112- B.F. Allen, F. Kasper, G. Nataneli, E. Dutson, and P. Faloutsos, "Visual tracking of laparoscopic instruments in standard training environments." in *Studies in Health Technology and Informatics*, (2011), Vol. 163: *IOS Press*, pp. 11-17.
113- D. Bouget, M. Allan, D. Stoyanov, and P. Jannin, "Vision-based and marker-less surgical tool detection and tracking: a review of the literature." in *Medical Image Analysis* Vol. 35, ed: *Elsevier B.V.*, (2017), pp. 633-54.
114- Mansoor Ali, Gilberto Ochoa-Ruiz, and Sharib Ali, "A semi-supervised Teacher-Student framework for surgical tool detection and localization." 2022/8// (2022).
115- J. Cartucho, C. Wang, B. Huang, D. S. Elson, A. Darzi, and S. Giannarou, "An enhanced marker pattern that achieves improved accuracy in surgical tool tracking." *Computer Methods in Biomechanics and Biomedical Engineering: Imaging and Visualization,* Vol. 10 (No. 4), pp. 400-08, (2022).
116- S. Bernhardt, S.A. Nicolau, L. Soler, and C. Doignon, "The status of augmented reality in laparoscopic surgery as of 2016." in *Medical Image Analysis* Vol. 37, ed: *Elsevier B.V.*, (2017), pp. 66-90.
117- F. Joeres, F. Heinrich, D. Schott, and C. Hansen, "Towards natural 3D interaction for laparoscopic augmented reality registration." *Computer Methods in Biomechanics and Biomedical Engineering: Imaging and Visualization,* Vol. 9 (No. 4), pp. 384-91, (2021).
118- J.R. Abbing, F.J. Voskens, B.G. A. Gerats, R.M. Egging, F. Milletari, and I.A. M. J. Broeders, "Towards an AI-based assessment model of surgical difficulty during early phase laparoscopic cholecystectomy." *Computer Methods in Biomechanics and Biomedical Engineering: Imaging and Visualization,* (2023).
119- T.A. Alshirbaji, N.A. Jalal, L. Mündermann, and K. Möller, "Classifying smoke in laparoscopic videos using SVM." *Current Directions in Biomedical Engineering,* Vol. 3 (No. 2), pp. 191-94, 2017/9// (2017).
120- A. Leibetseder, M.J. Primus, S. Petscharnig, and K. Schoeffmann, "Real-time image-based smoke detection in endoscopic videos." in *Thematic Workshops 2017 - Proceedings of the Thematic Workshops of ACM Multimedia 2017, co-located with MM 2017*, (2017): *Association for Computing Machinery, Inc*, pp. 296-304.
121- A. Leibetseder, M.J. Primus, and K. Schoeffmann, "Automatic smoke classification in endoscopic video." in *Lecture Notes in Computer Science (including subseries Lecture Notes in Artificial Intelligence and Lecture Notes in Bioinformatics)*, (2018), Vol. 10705 LNCS: *Springer Verlag*, pp. 362-66.
122- W. Reiter, "Improving endoscopic smoke detection with semi-supervised noisy student models." *Current Directions in Biomedical Engineering,* Vol. 6 (No. 1), 2020/5// (2020).
123- S. Salazar-Colores, H. M. Jiménez, C.J. Ortiz-Echeverri, and G. Flores, "Desmoking Laparoscopy Surgery Images Using an Image-to-Image Translation Guided by an Embedded Dark Channel." *IEEE Access,* Vol. 8pp. 208898-909, (2020).
124- N.A. Jalal, T.A. Alshirbaji, L. Mündermann, and K. Möller, "Features for detecting smoke in laparoscopic videos." *Current Directions in Biomedical Engineering,* Vol. 3 (No. 2), pp. 521-24, 2017/9// (2017).
125- J. Immerkaer, "NOTE: Fast Noise Variance Estimation." in "COMPUTER VISION AND IMAGE UNDERSTANDING," (1996), Vol. 64.
126- A. Chetouani, A. Beghdadi, and M. Deriche, "A new reference-free image quality index for blur estimation in the frequency domain." in *IEEE International Symposium on Signal Processing and Information Technology, ISSPIT 2009*, (2009), pp. 155-59.
127- R. Bansal, G. Raj, and T. Choudhury, "Blur image detection using Laplacian operator and Open-CV." in *Proceedings of the 5th International Conference on System Modeling and Advancement in Research Trends, SMART 2016*, (2017): *Institute of Electrical and Electronics Engineers Inc.*, pp. 63-67.
128- U. Ali and M.T. Mahmood, "Analysis of blur measure operators for single image blur segmentation." *Applied Sciences (Switzerland),* Vol. 8 (No. 5), 2018/5// (2018).
129- Shun Zhang *et al.*, "Concerns of quality, utility, and reliability of laparoscopic gastrectomy for gastric cancer in public video sharing platform." *Annals of Translational Medicine,* Vol. 8pp. 196-96, 03/01 (2020).

130- Xiwen Liu, Xiaoming Tao, Mai Xu, Yafeng Zhan, and Jianhua Lu, "An EEG-Based Study on Perception of Video Distortion Under Various Content Motion Conditions." *IEEE Transactions on Multimedia,* Vol. PPpp. 1-1, 08/09 (2019).
131- A. Onan, "Bidirectional convolutional recurrent neural network architecture with group-wise enhancement mechanism for text sentiment classification." *Journal of King Saud University - Computer and Information Sciences,* Vol. 34 (No. 5), pp. 2098-117, 2022/5// (2022).
132- Z.A. Khan, A. Beghdadi, M. Kaaniche, and F.A. Cheikh, "RESIDUAL NETWORKS BASED DISTORTION CLASSIFICATION AND RANKING FOR LAPAROSCOPIC IMAGE QUALITY ASSESSMENT." in "2020 IEEE International Conference on Image Processing (ICIP)," (2020).
133- N. Aldahoul, H.A. Karim, M.J.T Tan, and J.L. Fermin, "Transfer Learning and Decision Fusion for Real Time Distortion Classification in Laparoscopic Videos." *IEEE Access,* Vol. 9pp. 115006-18, (2021).
134- Z.A. Khan, A. Beghdadi, M. Kaaniche, F.A. Cheikh, and O. Gharbi, "A Neural Network based Framework for Effective Laparoscopic Video Quality Assessment." 2022/2// (2022).
135- M. Siddaiah-Subramanya, M. Nyandowe, and K.W. Tiang, "Technical problems during laparoscopy: A systematic method of troubleshooting for surgeons." *Innovative Surgical Sciences,* Vol. 2 (No. 4), pp. 233-37, 2017/12// (2017).
136- A. Beghdadi, "Real-Time Distortion Classification inLaparoscopic Videos ICIP." ed, (2020).
137- Aytuğ Onan, "Consensus Clustering-Based Undersampling Approach to Imbalanced Learning." *Scientific Programming,* Vol. 2019(2019).
138- Mahak Gupta and Jaspreet Kaur, "Automation in Blur Image Detection with Segmentation using Machine learning."
139- S. Lakshmi Bhavani, "Detection and Classification of Blur Images using Multi-Class Support Vector Machine; Detection and Classification of Blur Images using Multi-Class Support Vector Machine." [Online]. Available: www.ijert.org.
140- Andreas Leibetseder, Manfred Jürgen Primus, Stefan Petscharnig, and Klaus Schoeffmann, "Image-Based Smoke Detection in Laparoscopic Videos." in *Lecture Notes in Computer Science (including subseries Lecture Notes in Artificial Intelligence and Lecture Notes in Bioinformatics)*, (2017), Vol. 10550 LNCS: *Springer Verlag*, pp. 70-87.
141- G. T. Reddy *et al.*, "Analysis of Dimensionality Reduction Techniques on Big Data." *IEEE Access,* Vol. 8pp. 54776-88, (2020).
142- B. Schölkopf, "SVMs - A practical consequence of learning theory." *IEEE Intelligent Systems and Their Applications,* Vol. 13 (No. 4), pp. 18-21, 1998/7// (1998).
143- A. Onan, "An ensemble scheme based on language function analysis and feature engineering for text genre classification." *Journal of Information Science,* Vol. 44 (No. 1), pp. 28-47, 2018/2// (2018).
144- Z.A. Khan, "Learning based quality assessment for medical imaging in the context of liver cancer treatment." PhD thesis, *Sorbonne Paris Nord University Paris XIII*, 2021PA131004, (2021).
145- Praveen Konduri and G. Rao, "A transfer learning coupled framework for distortion classification in laparoscopic videos." *Multimedia Tools and Applications,* pp. 1-22, 10/18 (2023).
146- A.P. Twinanda, S. Shehata, D. Mutter, J. Marescaux, M. De Mathelin, and N. Padoy, "EndoNet: A Deep Architecture for Recognition Tasks on Laparoscopic Videos." *IEEE Transactions on Medical Imaging,* Vol. 36 (No. 1), pp. 86-97, 2017/1// (2017).
147- K. He, X. Zhang, S. Ren, and J. Sun, "Deep Residual Learning for Image Recognition." in *2016 IEEE Conference on Computer Vision and Pattern Recognition (CVPR)*, (2016), pp. 770-78.
148- Luqman Ali, Fady Alnajjar, Hamad Jassmi, Munkhjargal Gochoo, Wasif Khan, and Mohamed Serhani, "Performance Evaluation of Deep CNN-Based Crack Detection and Localization Techniques for Concrete Structures." *Sensors,* Vol. 21p. 1688, 03/01 (2021).
149- Bernd Münzer, Klaus Schoeffmann, and Laszlo Böszörmenyi, "Content-based processing and analysis of endoscopic images and videos: A survey." *Multimedia Tools and Applications,* Vol. 77 (No. 1), pp. 1323-62, 2018/01/01 (2018).
150- BOLA spol s.r.o. (2024). What are solenoid valves? [Online]. Available: https://www.bolasystems.com/help-advice/what-are-solenoid-valves.
151- Dassault Systèmes SolidWorks Corporation. Solidworks. [Online]. Available: https://www.solidworks.com.
152- GeeksforGeeks. (2023). Internal working of Python. [Online]. Available: https://www.geeksforgeeks.org/internal-working-of-python.
153- George Robotics. (2023). MicroPython. [Online]. Available: https://micropython.org/.
154- Configr Technologies. MicroPython. [Online]. Available: https://configr.medium.com/micropython-2c7c8dae1e1d.

Annex

Python framework used in the third chapter

```
import os
import numpy as np
import cv2
import matplotlib.pyplot as plt
import pickle
import random
from sklearn import svm
from sklearn.model_selection import train_test_split
from sklearn.svm import SVC
from skimage.transform import resize
from skimage.io import imread
import time
from scipy.ndimage import variance
from skimage.filters import laplace
from skimage import filters
#categories = ['BlurredImage', 'GoodImage']
#categories2 = ['DefocusBlurImage', 'MotionBlurImage']
categories = ['DegradedImage', 'GoodImage']
categories2 = ['BlurredImage', 'SmokedImage']
categories3 = ['DefocusBlurImage', 'MotionBlurImage']
featuresImg = []
def histo(imgi):

    hsvt = cv2.cvtColor(imgi, cv2.COLOR_BGR2HSV)
    hist = cv2.calcHist([hsvt], 1, None, [256], [0, 256])
    ps = 0
    i = 0
    while (i <= 89.6):
        ps += i * hist[i]
        i += 1
    k = 90
    pnos = 0
    while (k < 256):
        pnos += k * hist[k]
        k += 1

    return ps / (ps + pnos)
pick = open('model1.sav', 'rb')
classifier = pickle.load(pick)
pick.close()
# read all videos found in the folder test_data1
dir = 'C:/Users/DELL/Downloads/Compressed'
path = 'C:/Users/DELL/Downloads/Compressed/test_data1'
cptBlurredVideo=0
compteur=0
stTotal= time.process_time()
for video in os.listdir(path):
    vidpath = os.path.join(path,video)
    vid = cv2.VideoCapture(vidpath)
    count = vid.get(cv2.CAP_PROP_FRAME_COUNT)
    position = vid.get(cv2.CAP_PROP_POS_AVI_RATIO)
    currentframe = 0
    blr = 0
    smokeDetec=''
    blurDetect=''
```

```
    #print('nbrframe',count)
    nbr=0
    #si le dossier nexiste pas
    if not os.path.exists('C:/videoTest'):
        os.mkdir('C:/videoTest')
    st=0
    st = time.process_time()
    while (nbr<count):

        sucess, frame = vid.read()
        #cv2.imshow("output", frame)
        cv2.imwrite('C:/videoTest/frame' + str(currentframe) + '.jpg', frame)
        images = cv2.imread("C:/videoTest/frame0.jpg", 1)
        images = cv2.resize(images, (224, 224))
        psmoke = histo(images)
        gryscale_image = cv2.cvtColor(images, cv2.COLOR_RGB2GRAY)
        edge_laplace = laplace(gryscale_image, ksize=3)
        variancelaplace = variance(edge_laplace)
        maxlaplace = np.amax(edge_laplace)
        edge_sobel = filters.sobel(gryscale_image)
        variancesobel = variance(edge_sobel)
        maxsobel = np.amax(edge_sobel)
        featuresImg.append(variancelaplace)
        featuresImg.append(maxlaplace)
        featuresImg.append(maxsobel)
        featuresImg.append(variancesobel)
        featuresBlur = np.array(featuresImg, dtype="object").flatten().reshape(1, -
1)
        featuresImg.append(psmoke)
        imageTH = np.array(featuresImg,dtype="object").flatten().reshape(1,-1)
        #print('features image', imageTH)
        #st = time.process_time()
        prediction = classifier.predict(imageTH)

        if cv2.waitKey(1) & prediction[0] == 0:
            #print('Blurred video detected')
            #print('name of degraded video',video)
            pick2 = open('model2.sav', 'rb')
            classifier2 = pickle.load(pick2)
            pick2.close()
            prediction2 = classifier2.predict(imageTH)
            if prediction2[0] == 1:
                smokeDetec = categories2[prediction2[0]]

            if cv2.waitKey(1) & prediction2[0] == 0:
                pick3 = open('model3.sav', 'rb')
                classifier3 = pickle.load(pick3)
                pick3.close()
                prediction3 = classifier3.predict(featuresBlur)
                # print('Prediction is: ', categories3[prediction3[0]])
                blurDetect = categories3[prediction3[0]]
            # get the  time
            #et = time.process_time()
            #get execution time
            #res = et - st
            #print('CPU Execution time:', res, 'seconds')
            # break
            #print('Type of distortion is: ', categories2[prediction2[0]])
        blr = 1
        cptBlurredVideo +=1
        featuresImg.clear()
```

```
            #print('Position of blurred frame',nbr)
        # get the  time
        #et = time.process_time()
         # get execution time
        # = et - st
        #print('CPU Execution time:', res, 'seconds')
            #break
        nbr +=1
        featuresImg.clear()

    #if blr == 1:
       # print('name of video', video,'Distortions detected: ',smokeDetec,'-',
blurDetect)
        #print('Distortion detected: ', smokeDetec,'-', blurDetect)
    # get the  time
    et = time.process_time()
    # get execution time
    res = et - st
    #print('CPU Execution time:', res, 'seconds')
    print(' ', res)
    vid.release()
    #print('nbr blurred video',cptBlurredVideo)
    compteur +=1
etTotal = time.process_time()
    # get execution time
resTotal = etTotal - stTotal
print('Total CPU Execution time:', resTotal, 'seconds')
print('total number of video',compteur)
# cv2.destroyWindow()
```

```
import os
import numpy as np
import cv2
import matplotlib.pyplot as plt
import pickle
from scipy.ndimage import variance
from skimage.filters import laplace
from skimage import filters
dir = "C:/Users/DELL/laparoscopyImg/defogmotion"
#categories = ['DegradedImage', 'GoodImage']
#categories = ['BlurredImage', 'SmokedImage']
categories= ['DefocusBlurImage', 'MotionBlurImage']
data = []


def histo(imgi):

    hsvt = cv2.cvtColor(imgi, cv2.COLOR_BGR2HSV)
    hist = cv2.calcHist([hsvt], 1, None, [256], [0, 256])
    ps = 0
    i = 0
    while (i <= 89.6):
        ps += i * hist[i]
        i += 1
    k = 90
```

```
    pnos = 0
    while (k < 256):
        pnos += k * hist[k]
        k += 1

    return ps / (ps + pnos)


for category in categories:
    path = os.path.join(dir,category)
    label = categories.index(category)
    for img in os.listdir(path):
        imgpath = os.path.join(path,img)
        pet_img =cv2.imread(imgpath,1)
        if cv2.waitKey(1) & 0xFF == ord('q'):
           break
        try:

           pet_img2= cv2.resize(pet_img,(224,224))
           psmoke = histo(pe_img2)
           #psmoke is the SAN classifier of smoke
           gryscale_image = cv2.cvtColor(pe_img2, cv2.COLOR_RGB2GRAY)
           edge_laplace = laplace(gryscale_image, ksize=3)
           variancelaplace=variance(edge_laplace)
           maxlaplace=np.amax(edge_laplace)
           edge_sobel = filters.sobel(gryscale_image)
           variancesobel = variance(edge_sobel)
           maxsobel = np.amax(edge_sobel)
           #featuresImg=[variancelaplace,maxlaplace,variancesobel,maxsobel,psmoke]
           featuresImg = [variancelaplace,maxlaplace,variancesobel,maxsobel]
           imageT = np.array(featuresImg,dtype="object").flatten()
           # image 2d vers img sur une liste 1d
           #mettre dans une liste les images avec leurs labels
           data.append([imageT,label])
           #print('donnee',data)
        except Exception as e:
            pass
print(len(data))
#ouvrir un fichier en ecriture
pick_in = open('data3.pickle','wb')
#remplir le fichier par les donnees
pickle.dump(data,pick_in)
pick_in.close()
```

Python framework used in the fourth chapter (using Resnet50)

```
import torch
import torch.nn as nn
from torch.utils.data import Dataset, DataLoader
from torchvision import transforms
from torchvision.datasets import ImageFolder
import torchvision.models as models
import matplotlib.pyplot as plt
from torch.utils.data import DataLoader, Subset, random_split
from sklearn.metrics import confusion_matrix
import seaborn as sns
import os
batch_size=100
num_epochs=5
losses = []
# Define the file path where you want to save the model
model_save_path = 'D:/belmokeddem_classes_extLVQ/tenClass/modelRs50.pth'
# Lists to store accuracy history for plotting
train_accuracy_history = []
train_correct_predictions = 0
train_total_samples = 0
validation_total_samples = 0
validation_accuracy_history = []
validation_correct_predictions = 0
train_loss_history = []
validation_loss_history = []
true_labels = []
predicted_labels = []
# Define your class labels
class_labels = ['WN', 'DB_UI','DB','MB','WN_SM_UI','WN_SM','WN_UI','SM_UI','SM','UI']
```

```
# Define a custom dataset class
class CustomDataset(Dataset):
    def __init__(self, data_dir, transform=None):
        self.data = ImageFolder(data_dir, transform=transform)
    def __len__(self):
        return len(self.data)
    def __getitem__(self, idx):
        img, label = self.data[idx]
        return img, label
# Define data transformations
transform = transforms.Compose([
    transforms.Resize((224, 224)),
    transforms.ToTensor(),
    transforms.Normalize(mean=[0.485, 0.456, 0.406], std=[0.229, 0.224, 0.225]),
])
 #Load the pre-trained ResNet-50 model
resnet50 = models.resnet50(pretrained=True)
# Modify the final fully connected layer for classification with 6 classes
num_ftrs = resnet50.fc.in_features
resnet50.fc = nn.Linear(num_ftrs,10)  # Change  to the number of  classes(10)
#'/content/gdrive/My Drive/extanded_LVQ'
# Create instances of custom datasets and dataloaders
train_dataset = CustomDataset(data_dir='D:/belmokeddem_classes_extLVQ/tenClass', transform=transform)
train_dataloader = DataLoader(train_dataset, batch_size=batch_size, shuffle=True)
# Specify the size of the validation set (e.g., 20% of the total dataset)
validation_size = 0.2
# Calculate the sizes of the training and validation sets
total_size = len(train_dataloader.dataset)
validation_size = int(validation_size * total_size)
train_size = total_size - validation_size
```

```
# Use random_split to split the dataset into training and validation subsets
train_subset, validation_subset = random_split(train_dataloader.dataset, [train_size, validation_size])


# Create DataLoader instances for the training and validation subsets
train_dataloader = DataLoader(train_subset, batch_size=batch_size, shuffle=True)
validation_dataloader = DataLoader(validation_subset, batch_size=batch_size, shuffle=False)
# Define your loss function and optimizer
criterion = torch.nn.CrossEntropyLoss()
optimizer = torch.optim.Adam(resnet50.parameters(), lr=0.0001)


# Now, we can use the provided code snippet within a training loop
for epoch in range(num_epochs):
  # Training phase
  train_loss = 0.0  # Initialize training loss
  resnet50.train() # Set the model to training mode
  for inputs, labels in train_dataloader:
    outputs = resnet50(inputs)
    loss = criterion(outputs, labels)
    train_loss += loss.item()
     # Backward pass and optimize
    optimizer.zero_grad()
    loss.backward()
    optimizer.step()
    # Calculate predicted labels by taking the argmax of the model outputs
    _, predicted = torch.max(outputs, 1)

  # Calculate training accuracy for the current epoch
  train_correct_predictions += (predicted == labels).sum().item()
  train_total_samples += labels.size(0)
# Calculate training accuracy for the current epoch
```

```
  train_accuracy = train_correct_predictions / train_total_samples
  train_accuracy_history.append(train_accuracy)
# Calculate average training loss for the epoch
  average_train_loss = train_loss / len(train_dataloader)
  train_loss_history.append(average_train_loss)
   # Validation phase
  resnet50.eval()  # Set the model to evaluation mode
  validation_loss = 0.0  # Initialize validation loss

  for inputs, labels in validation_dataloader:
    outputs = resnet50(inputs)
    _, predicted = torch.max(outputs, 1)
    validation_correct_predictions += (predicted == labels).sum().item()
    validation_total_samples += labels.size(0)
    loss = criterion(outputs, labels)
    validation_loss += loss.item()

    # Append true and predicted labels to the lists
    true_labels.extend(labels.cpu().numpy())
    predicted_labels.extend(predicted.cpu().numpy())
  # Calculate validation accuracy for the current epoch
  validation_accuracy = validation_correct_predictions / validation_total_samples
  validation_accuracy_history.append(validation_accuracy)

  # Calculate average validation loss for the epoch
  average_validation_loss = validation_loss / len(validation_dataloader)
  validation_loss_history.append(average_validation_loss)
  # Calculate the confusion matrix
  confusion = confusion_matrix(true_labels, predicted_labels)
  # Print and update the accuracy for the current epoch
```

```
  print(f'Epoch [{epoch + 1}/{num_epochs}] Training Accuracy: {train_accuracy * 100:.2f}%, Validation Accuracy: {validation_accuracy * 100:.2f}%')

  # Print and update losses for the current epoch

  print(f'Epoch [{epoch + 1}/{num_epochs}] Training Loss: {average_train_loss:.4f}, Validation Loss: {average_validation_loss:.4f}')


# Plot the training and validation loss graphs

plt.figure(figsize=(10, 5))

plt.plot(range(1, num_epochs + 1), train_loss_history, marker='o', linestyle='-', color='b', label='Training Loss')

plt.plot(range(1, num_epochs + 1), validation_loss_history, marker='o', linestyle='-', color='r', label='Validation Loss')

plt.xlabel('Epoch')

plt.ylabel('Loss')

plt.title('Training and Validation Loss Over Epochs')

plt.legend()

plt.grid(True)

plt.savefig('D:/belmokeddem_5classes_extLVQ/Loss.png')

plt.show()



#Save the trained model if needed

torch.save(resnet50.state_dict(), model_save_path)

# Plot the training and validation accuracy graphs

plt.figure(figsize=(10, 5))

plt.plot(range(1, num_epochs + 1), train_accuracy_history, marker='o', linestyle='-', color='b', label='Training Accuracy')

plt.plot(range(1, num_epochs + 1), validation_accuracy_history, marker='o', linestyle='-', color='r', label='Validation Accuracy')

plt.xlabel('Epoch')

plt.ylabel('Accuracy')

plt.title('Training and Validation Accuracy Over Epochs')

plt.legend()

plt.grid(True)
```

```
plt.savefig('D:/belmokeddem_classes_extLVQ/Accuracy.png')
plt.show()


# Plot the confusion matrix
plt.figure(figsize=(8, 6))
sns.heatmap(confusion, annot=True, fmt='d', cmap='Blues', xticklabels=class_labels, yticklabels=class_labels)
plt.xlabel('Predicted')
plt.ylabel('True')
plt.title('Confusion Matrix')
plt.savefig('D:/belmokeddem_classes_extLVQ/Confusion_Matrix.png')
plt.show()
```